

***PRELIMINARY DESIGN OF A MEDIUM RANGE HYBRID TRANSPORT
JET***

A Project Presented to
The Faculty of The Department of Aerospace Engineering
San Jose State University

In Fulfillment of Requirements of the Degree
Master of Science

By
Esuyawkal Engdaw

Faculty Advisor
Dr. Nikos J. Mourtos

©May 2020

Contents

<i>CHAPTER 1—MISSION SPECIFICATION & COMPARATIVE STUDY</i>	1
1.1 INTRODUCTION.....	1
1.2 MISSION SPECIFICATION.....	1
1.2.1 Mission Specification	1
1.2.2 Mission Profile.....	2
1.2.3 Market Analysis.....	2
1.2.4 Technical Feasibility	2
1.2.5 Critical Mission Requirements	2
1.3 COMPARATIVE STUDY OF SIMILAR AIRPLANES.....	3
1.3.2 Comparison of Important Design Parameters	3
1.3.3 Discussion.....	4
1.4 CONCLUSIONS AND RECOMMENDATIONS.....	5
1.4.1 Conclusions.....	5
1.4.2 Recommendations	5
<i>CHAPTER 2-- CONFIGURATION SELECTION</i>	6
2.1 INTRODUCTION	6
2.2 COMPARATIVE STUDY OF AIRPLANES WITH SIMILAR MISSION PERFORMANCE.....	6
2.2.1 Comparison of Weights, Performance, and Geometry of Similar Airplanes.....	6
2.2.2 Configuration Comparison of Similar Airplanes	7
2.3 CONFIGURATION SELECTION	14
2.3.1 Overall Configuration	14
2.3.2 Wing Configuration	14
2.3.3 Empennage Configuration	15
2.3.4 Integration of the Propulsion System.....	15
2.3.5 Landing Gear Disposition	15
2.4 Conclusion	15
<i>CHAPTER 3 - WEIGHT SIZING & WEIGHT SENSITIVITIES</i>	16
3.1 INTRODUCTION.....	16
3.2 MISSION WEIGHT ESTIMATES	16
3.2.1 Data Base for Takeoff Weights and Empty Weights of Similar Airplanes	16
3.2.2 Determination of Regression Coefficients A and	17

3.3 Determination of Mission Weights.....	19
3.3.1 Manual Calculation of Mission Weights.....	19
3.3.2 Calculation of Mission Weights Using the AAA Program	21
3.4 TAKEOFF WEIGHT SENSITIVITIES	22
3.4.1 Manual Calculation of Takeoff Weight Sensitivities	22
3.4.2 Calculation of Takeoff Weight Sensitivities Using the AAA Program.....	23
3.5 Trade Studies	24
3.5.1 Trading Lift to Drag Ratio for Takeoff Weight	24
3.5.2 Trading Range for Payload Weight.....	25
3.5.3 Trading Cruise Lift to Drag Ratio for Payload Weight	27
3.6 DISCUSSION	28
3.7 Conclusion	29
<i>CHAPTER 4---PERFORMANCE CONSTRAINT ANALYSIS</i>	<i>30</i>
4.1 INTRODUCTION.....	30
4.2 MANUAL CALCULATION OF PERFORMANCE CONSTRAINTS	30
4.2.1 Sizing to Takeoff Distance Requirements	30
4.2.2 Sizing to Landing Distance Requirements.....	31
4.2.3 Drag Polar Estimation	32
4.2.4 Climb Constraints.....	33
4.2.4.1 Sizing to FAR 25.111 One engine Inoperative (OEI) Requirement	33
4.2.4.2 Sizing to FAR 25.121 One Engine Inoperative Requirements.....	33
4.2.4.3 Sizing to FAR 25.121 One engine Inoperative Requirement	33
4.2.4.4 Sizing to FAR 25.121 One Engine Inoperative CGR>0.012 Requirement	34
4.2.4.5 Sizing to FAR 25.119 All Engines Operating (AEO) CGR>0.032 Requirement...	34
4.2.4.6 Sizing to FAR 25.121 One Engine Inoperative Condition CGR>0.021	34
4.2.5 Sizing to Cruise Speed Requirements.....	35
4.3. CALCULATION OF PERFORMANCE CONSTRAINTS WITH THE AAA PROGRAM.....	35
4.3.1 Takeoff Distance	35
4.3.2 Landing Distance	36
4.3.3 Climb Constraints.....	36
4.3.4 Speed Constraints	36
4.3.5 Summary of Performance Constraints.....	37
4.4. SELECTION OF PROPULSION SYSTEM	38

4.4.1 Selection of the Propulsion System Type.....	38
4.4.2 Selection of the Number of Engines	38
4.5. DISCUSSION	38
<i>CHAPTER 5--FUSELAGE DESIGN</i>	41
5.1 INTRODUCTION.....	41
5.2 LAYOUT DESIGN OF THE COCKPIT	41
5.3 LAYOUT DESIGN OF THE FUSELAGE.....	42
5.4 DISCUSSION	45
<i>CHAPTER 6--Wing Planform Design</i>	46
6.1 INTRODUCTION.....	46
6.2 Wing Planform Design	46
6.2.1 Sweep Angle - Thickness Ratio Combination.....	47
6.3 AIRFOIL SELECTION.....	49
6.4 WING DESIGN EVALUATION.....	50
6.5 DESIGN OF THE HIGH-LIFT DEVICES	51
6.5.1 Design of the Lateral Control Surfaces.....	54
6.6 DRAWINGS.....	55
6.7 DISCUSSION.....	56
6.8 CONCLUSIONS	56
<i>CHAPTER 7---DESIGN OF THE EMPENNAGE & THE LONGITUDINAL AND DIRECTIONAL CONTROLS</i>	58
7.1 Introduction	58
7.2 Overall Empennage Design	58
7.3 Design of the Horizontal Stabilizer	60
7.4 Design of the Vertical Stabilizer.....	61
7.5 Empennage Design Evaluation.....	62
7.6 DESIGN OF THE LONGITUDINAL AND DIRECTIONAL CONTROLS	63
7.7 DRAWINGS.....	64
7.8 DISCUSSION.....	66
7.8 CONCLUSIONS	66

<i>Chapter 8--Landing Gear Design; Weight and Balance Analysis</i>	67
8.1 Introduction	67
8.2 Component Weight and Balance Analysis	67
8.3 Landing Gear Design.....	74
8.4 Discussion.....	76
8.5 Conclusion	76
<i>CHAPTER 9---STABILITY AND CONTRL ANALYSIS /WEIGHT AND BALANCE- STABILITY AND CONTROL CHECK</i>	78
9.1 Introduction	78
9.2 Static Longitudinal Stability	78
9.3 Static Directional Stability.....	83
9.4 Rudder Deflection to Hold One Engine Inoperative Condition	85
9.5 Empennage Design- Weight and Balance- Landing Gear Design- Longitudinal Static Stability and Control Check.....	86
9.6 Discussion.....	86
9.7 Conclusion	86
<i>CHAPTER 10---DRAG POLAR ESTIMATION</i>	87
10.1 Introduction	87
10.2 Airplane Zero-Lift Drag	87
10.3 Low Speed Drag Increments	89
10.4 Compressibility Drag.....	90
10.5 Airplane Drag Polar.....	91
10.6 Discussion.....	92
10.7 Conclusion	93
<i>Chapter 11---Construction of V-n Diagram</i>	94
11.1 Introduction	94
11.2 Background.....	94
11.3 Method of V-n Diagram Construction.....	96
11.3.1 V-n Diagrams for FAR 25 Certified Airplanes.....	96
11.3.2 Determination of Parameters and Critical Points	96

11.3.2.1 Determination of +1g Stall Speed.....	96
11.3.2.2 Determination of Design Limit Load Factor (<i>n_{lim}</i>).....	97
11.3.2.3 Determination of Design Maneuvering Speed.....	97
11.3.2.4 Construction of Gust Load Factor Lines.....	98
11.3.2.5 Determination Design Speed for Maximum Gust Intensity (<i>V_B</i>).....	99
11.3.2.6 Determination of Design Cruising Speed.....	100
11.3.2.7 Determination of Design Diving Speed.....	100
11.3.2.8 Determination of Negative Stall Speed Line.....	100
11.3.2.9 V-n Diagram.....	101
11.4 Discussion.....	102
11.5 Conclusion.....	104
<i>Chapter 12----- Class II Method for Estimating Airplane Component Weights.....</i>	<i>105</i>
12.1 Introduction.....	105
12.2 Structural Weight Estimation.....	105
12.2.1 Wing Weight Estimation.....	105
12.2.2 Empennage Weight Estimation.....	106
12.2.3 Fuselage Weight Estimation.....	106
12.2.4 Nacelle Weight Estimation.....	107
12.2.5 Landing Gear Weight Estimation.....	107
12.3 Class II Method for estimating Powerplant Weight.....	108
12.3.1 Weight of Engines.....	108
12.3.2 Fuel System Weight Estimation.....	109
12.3.3 Estimation of Propulsion System Weight.....	110
12.4 Class II Method for Estimating Fixed Equipment Weight.....	111
12.4.1 Flight Control System Weight Estimation.....	112
12.4.2 Hydraulic and/or Pneumatic System Weight Estimation.....	112
12.4.3 Electrical System Weight Estimation.....	112
12.4.4 Instrumentation, Avionics, and Electronics Weight.....	112
12.4.5 Weight Estimation for Air-conditioning, Pressurization, Anti&Deicing Systems.....	112
12.4.6 Oxygen System Weight Estimation.....	113
12.4.7 Auxiliary Power Unit Weight Estimation.....	113
12.4.8 Furnishings Weight Estimation.....	113
12.4.9 Weight Estimation of Baggage and Cargo Handling Equipment.....	113

12.4 10 Paint Weight Estimation.....	113
12.5 Class II Empty Weight Calculation	114
12.6 Weight and Balance.....	114
12.7 Discussion	117
<i>CHAPTER 13---Final Design Report-Environmental/Economic Tradeoffs; Safety/Economic Tradeoffs.</i>	<i>119</i>
13.1 Introduction	119
13.2 Summary of Most Important Design Parameters	119
13.3 Recommendations	120
13.4 Environmental/Economic Tradeoffs.....	121
13.5 Safety/Economic Tradeoffs	123
13.6 Conclusions	124
References	125
Appendix A	a
Appendix B.....	c
Appendix C	c

List of Symbols

Symbol	Definition	Units
<i>AR</i>	<i>Aspect Ratio</i>	
<i>B</i>	<i>Regression slope</i>	
<i>c_t</i>	<i>Fuel consumption</i>	
<i>c_r</i>	<i>Root chord</i>	<i>ft</i>
<i>c_t</i>	<i>Tip chord</i>	
<i>d</i>	<i>Depth</i>	<i>ft</i>
<i>L/D</i>		
<i>E*</i>	<i>Energy density</i>	<i>Wh/kg</i>
<i>e</i>	<i>Oswald Efficiency</i>	
<i>h</i>	<i>Altitude</i>	<i>ft</i>
<i>i_w</i>	<i>Wing incidence</i>	<i>degrees</i>
<i>L/D</i>	<i>Lift to drag</i>	
<i>l</i>	<i>Length of fuselage</i>	<i>ft</i>
<i>R</i>	<i>Range</i>	<i>ft</i>
<i>S</i>	<i>Wing area</i>	<i>ft²</i>
<i>T</i>	<i>Thrust</i>	<i>lb</i>
<i>V</i>	<i>Speed</i>	<i>ft/s</i>
<i>W</i>	<i>Weight</i>	<i>lb</i>
Greek Symbols		
<i>ε_t</i>	<i>Wing twist</i>	<i>degrees</i>
<i>η</i>	<i>Efficiency</i>	
<i>Λ</i>	<i>Wing sweep</i>	<i>degrees</i>
<i>λ</i>	<i>Taper ratio</i>	
<i>θ</i>	<i>Fuselage elevation</i>	<i>degrees</i>
Constants		
<i>a</i>	<i>Length constant</i>	
<i>c</i>	<i>Length constant</i>	
<i>g</i>	<i>Gravity</i>	<i>ft/s²</i>
Subscripts		
<i>A</i>	<i>Approach</i>	
<i>E</i>	<i>Empty</i>	
<i>f</i>	<i>fuselage</i>	
<i>fc</i>	<i>fuselage cone</i>	
<i>FL</i>	<i>Field length</i>	
<i>PL</i>	<i>payload</i>	
<i>tent</i>	<i>Tentative</i>	
<i>TO</i>	<i>takeoff</i>	
<i>max</i>	<i>maximum</i>	

CHAPTER 1—MISSION SPECIFICATION & COMPARATIVE STUDY

1.1 INTRODUCTION

The science of flight has reached its climax in a little over a century. However, the dependence on fossil fuel to operate air vehicles is a little concerning. This is because of the scarcity of fossil fuel, pollution of the environment due to emission of Carbon, and reduced efficiency of fuel driven propulsion systems. To resolve these issues the design of hybrid air vehicle (aircraft in this case) is invaluable. On the road to achieving this purpose, the mission specification of a small hybrid transport jet is proposed.

1.2 MISSION SPECIFICATION

1.2.1 Mission Specification

Below are given the mission specifications of a mid-range hybrid transport jet.

- Payload=4000lb
- Passengers=40
- Number of crew members=3
- Range=700 miles
- Cruise speed=400mi/hr
- Cruise altitude=20,000 feet
- Take-off field length=2000 feet
- Landing field length=2000 feet
- Approach speed=90miles/hr

1.2.2 Mission Profile

The hybrid transport jet is proposed to transport 40 passengers at a low cost of flight by combining fossil fuel with electricity. Figure 1.1 below shows the mission profile of the proposed aircraft.



Figure 1.1 Mission Profile of the Hybrid-Electric Aircraft.

1.2.3 Market Analysis

The major cost of an airline is operating cost. Among operating costs is cost of fuel. Every Airline would appreciate to have an aircraft that consumes less fuel. The proposed aircraft will be designed to consume fuel during the beginning of the flight and then switch to a battery after takeoff, which means less fuel, is consumed. Aircraft operated with fossil fuel must be refueled every time. However, aircraft run by battery only need to charge battery, which is less costly. As a result, the market will prefer this hybrid aircraft.

1.2.4 Technical Feasibility

Designing a hybrid aircraft is not structurally different from fossil fuel dependent aircraft. For this reason, the manufacturing cost of the proposed aircraft is not any different from other aircraft that are around. The proposed aircraft might have a less fuel container, which makes it lighter and smaller than current airplanes. However, the main challenge in designing the proposed aircraft is the unavailability of energy storage mechanism that can supply the amount of power needed to get 40 people in the air.

1.2.5 Critical Mission Requirements

Mission requirements that are very hard to achieve are called critical mission requirements. Among the mission requirements of the proposed aircraft the following are critical in the design.

- Cruise speed
- Range

1.3 COMPARATIVE STUDY OF SIMILAR AIRPLANES

1.3.1 Mission Capabilities and Configuration Selection

Several hybrid aircraft are prototyped while some others are under development.

Table 1 below lists these aircraft along with their capabilities and configurations.

Table 1.1: List of Hybrid aircraft

Type	Capabilities	Configurations
Aerovironment	Very high flexibility	High wing configuration and propeller at the nose
MIT Monarch	2 seat aircraft	Low wing configuration
Siemens FlyEco (Mangus eFusion)	Provides upset recovery and aerobatic training	Low wing configuration Symmetric along the fuselage
Volta Volare GT4	4 seat private aircraft	Swept mid wing
Parallel Hybrid Engine	Single seat, uses 30% less fuel	Low wing configuration
Esu hybrid	40 passengers +crew	Low wing

1.3.2 Comparison of Important Design Parameters

Table 1.2: Parameters of hybrid aircraft listed in table 1.1.

Type	W_{TO} (lbs)	W_E (lbs)	h (ft)	S (ft ²)	V (ft/s)
1	100	14	500	9.2	6
2	150	92	400	5.2	8.2
3	300	204	12,000	89	182
4	3000	2,600	24,000	95	269
5	992	309	1,5000	64	150

1.3.3 Discussion

As mentioned before, hybrid aircraft have two major advantages. These are greater efficiency and low gas emission to the environment. However, due to the lack of battery technology, hybrid aircraft are not being used significantly. The ones that are currently in use are not efficient enough in terms of addressing the problems that fuel driven aircraft cause. As we see from the comparison table (Table 2) above, the capabilities of the hybrid aircraft mentioned are nowhere near the aircraft that are around. Almost all of them do not carry that much load and cruise at a speed that current aircraft can.

Aiming to make a hybrid-electric transport jet feasible, this short to medium range hybrid aircraft is proposed. This aircraft will be designed to transport 40 passengers plus 3 crews in a short to medium distance. The aircraft will conduct warm up, taxi, takeoff, and climb on fossil fuel and the rest of the mission on battery. The energy density of the battery will be assumed to be higher than what is available now because the aircraft will be feasible as the battery technology progresses. The aircraft that are compared to the proposed one are small and most of them are prototypes.

1.4 CONCLUSIONS AND RECOMMENDATIONS

1.4.1 Conclusions

Most aircraft we see around are run by fossil fuel. However, fossil fuel might be scarce and the level of pollution we have gotten is so concerning. Due to this the design of aircraft run by both batteries and fuel is crucial. The proposed airplane is one of such type.

1.4.2 Recommendations

Many hybrid-electric aircraft have been designed and produced. However, the capacities of these aircraft are not anywhere near to the aircraft that are currently flying. This is due to battery technology. At the moment the battery technology that is available is not powerful enough to get 40 people up in the sky. Predicting a value for the energy density of a battery is crucial in designing a hybrid aircraft. This is because when the battery technology gets there the design of the aircraft is already done and it will be easy to produce the aircraft.

CHAPTER 2-- CONFIGURATION SELECTION

2.1 INTRODUCTION

Aircraft design involves a tremendous number of tradeoffs. It is almost possible to correct every single problem in the design independently. However, it is quite challenging to put all the components of a given aircraft and meet every single mission requirement. For this and other reasons components of an aircraft must be configured in a way that the integrated components are at their best functioning configuration. This process of integrating aircraft components is called configuration design. The purpose of this work is to select configurations of different parts of a hybrid-electric aircraft. This work outlines the advantages and disadvantages of the selected configuration by comparing the proposed configuration with configurations of other aircraft of the same propulsion system and capacity. There is always more than one design that can meet the same mission specifications. However, designs can be ranked based on some design merits. This work is also intended to magnify the need for the proposed aircraft based on some design merits.

2.2 COMPARATIVE STUDY OF AIRPLANES WITH SIMILAR MISSION PERFORMANCE

2.2.1 Comparison of Weights, Performance, and Geometry of Similar Airplanes

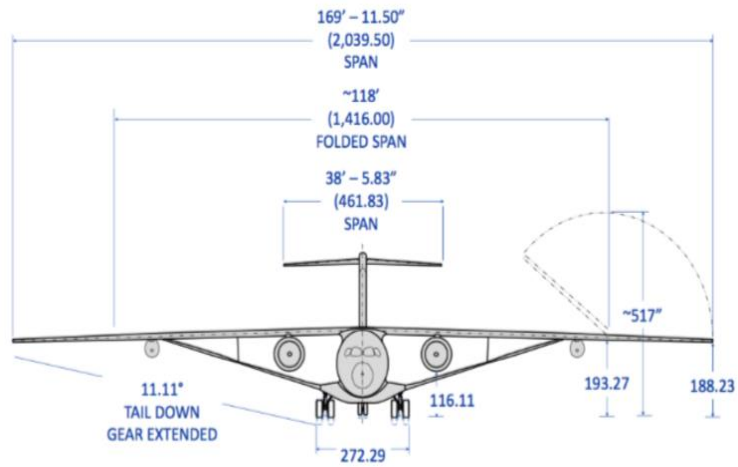
Different people working on a design to meet a given mission specification can come up with different designs that can all meet the mission requirements. However, an aircraft is better if it is simple, and it has a better performance than other designed aircraft. Table 2.1 below compares different parameters of different designs of hybrid aircraft.

Table 2.1: Dimensions of different hybrid airplanes.

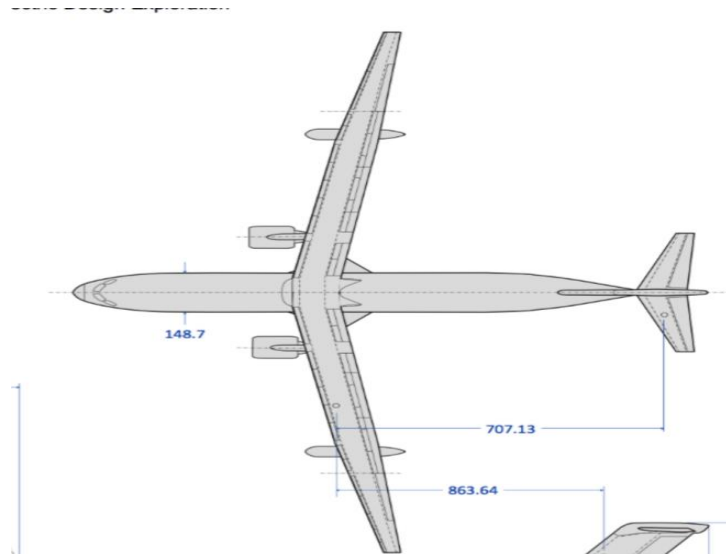
Type	W_{TO}	W_E	h	b	V_{cruise}
Aerovironment	240lb	140lb	500ft	9.2ft	6ft/s
SUGAR	150,000lb	135,300lb	30,000ft	2039in	490mi/hr
Mangus eFusion	600kg	410kg	12000ft	8.3m	200km/hr
Volta Volare GT4	3000lb	2600lb	24000ft	8ft	200km/hr
Parallel Hybrid engine	992lb	309lb	1500ft	6m	130ft/s

2.2.2 Configuration Comparison of Similar Airplanes

Even though aircraft of different designs have their own advantages and disadvantages, they can be compared and contrasted based on various configurations integrated in them. Figures 2.1 below presents different views of the five different aircraft that are compared and contrasted in table 2.1 above based on performance, weight and geometry.



a)



b)

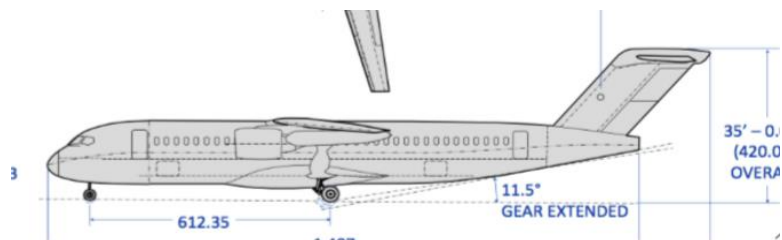
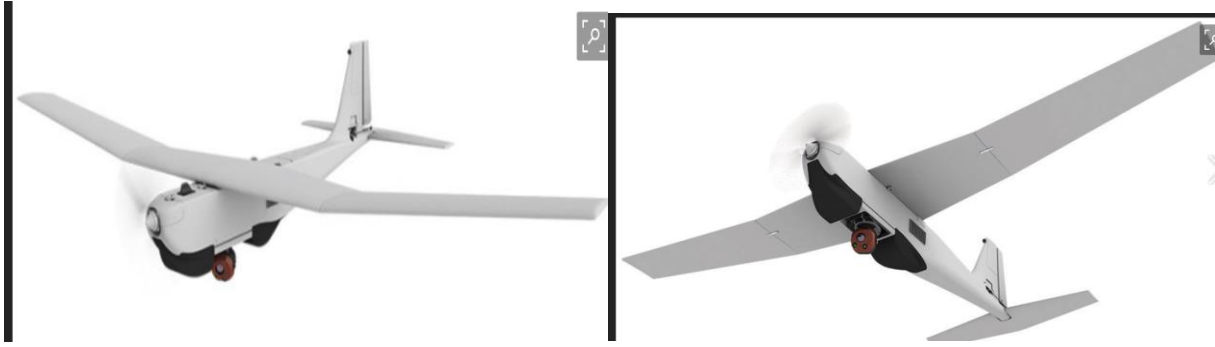


Figure 2.1: SUGAR: a) Front view of the aircraft. b) Top view of the aircraft. c) Left side view of the aircraft.



a



b



c

Figure 2.2: Aerovironment. a) Top view of the aircraft. b) Bottom view of the aircraft. c) left side view of the aircraft.



a



b



c

Figure 2.3: Mangus efusion a) top view of the aircraft. b) side view of the aircraft. c) Front view of the aircraft.



a



b



c

Figure 2.4: Volta Volare GT4 a) Top view of the aircraft. b) Side view of the aircraft. c) Front view of the aircraft.



a



b



c

Figure 2.5: Parallel hybrid engine. a) Front view of the aircraft. b) Side view of the aircraft. c) Top view of the aircraft.

2.2.3 Discussion

Figures 2.1 present different aircraft that are configured differently up to their mission requirements. Even though each aircraft is good enough for its own mission requirements, there still exist tradeoffs due to configuration of wing, fuselage, landing gear and engine. The major advantages and disadvantages of each configuration are discussed here.

As depicted in figure 2.1 SUGAR has a strut supported high wing, landing gears placed at the struts, engines attached under the wings, and a T tail. The advantages of having a high wing are quick loading and unloading, lighter weight wing due to the strut support, safe landing and takeoff, less chance of catching fire during landing, and less ground effect. However, the high wing configuration eliminates under floor cargo and does not prevent the fuselage from sinking during water landing. The disposition of the landing gear at the roots of the struts makes them shorter which in turn makes the overall structure lighter. Integrating the engines under the wings reduces drag since it is not sticking out by itself. However, this engine placement produces a noisy cabin since it is over the fuselage.

The Aerovironment in figure 2.2 has a high wing, a landing gear attached to the fuselage, and engine along the fuselage centerline. The high wing configuration is safe during landing. The disadvantages are mentioned in the discussion of SUGAR. In this case the high wing is not supported, and it produces greater bending moment thus a heavier structure. Mounting the engine along the fuselage centerline is advantageous because there is no thrust asymmetry in the event of engine failure. However, the propeller driven engine disturbs the air before it gets to the wing, so the flow is disturbed in this case.

The Mangus eFusion in figure 2.3 has a low wing configuration. The low wing configuration in this case provides efficient use of under-floor space and decreased takeoff distance. It also gives better maneuverability than a corresponding high wing configuration. However, this configuration is unsafe because there is a potential of fire hazard in an even of forced landing. This configuration must also be accompanied by long landing gear to provide tip clearance, which, on the other hand, results a heavier structure. The aircraft is

driven by propeller engine mounted along the centerline of the fuselage with the aforementioned advantages and disadvantages in figure 2.2.

The mid-wing configuration in figure 2.4 provides better maneuverability even though it reduces cargo space. The canard configuration increases the lift to drag ratio, and it also improves stability and control. However, the canard must be designed carefully to produce the required lift to drag ratio. The center of gravity must also be moved forward due to the canard configuration.

The Parallel hybrid engine aircraft in figure 2.5 mainly has a mid-wing and engine in the back configuration. The mid wing provides better maneuverability at the cost of under-floor fuselage space. The placement of the engine in the back creates a quiet cabin. However, the engine opening must be raised higher above the fuselage to avoid boundary layer ingestion at large angle of attack.

2.3 CONFIGURATION SELECTION

2.3.1 Overall Configuration

The proposed aircraft is a land-based hybrid electric aircraft. The aircraft will have a conventional configuration with the tail after the wing. The conventional configuration is convenient because so much work has been done on conventional configurations that information is greatly handy. However, with conventional configuration, a lot has to be done to meet the mission requirements.

2.3.2 Wing Configuration

This hybrid-electric aircraft will have a low wing configuration simply because it is a transport jet and the under-floor fuselage space is needed. However, this configuration is effective at the cost of making the landing gear longer for tip clearance, which tends to make the structure heavier.

2.3.3 Empennage Configuration

The Empennage configuration of the proposed aircraft is a conventional tail with horizontal stabilizers and a rudder. The stabilizers provide stability and control. However, the downward lifting effect might counteract the upward lifting effect of the wing.

2.3.4 Integration of the Propulsion System

The propulsion system for the proposed aircraft is a combination of a turbojet engine run by fuel and a battery. Both will be integrated under the wing simply because this method reduces drag. However, the potential of catching fire is very high if the fuel run engines hit the ground during landing.

2.3.5 Landing Gear Disposition

The landing gear for the hybrid-electric aircraft is placed under the fuselage. It is obvious that the landing gear cannot be positioned under the wing since the wing is low. Landing gear in this case must be longer than a corresponding high wing configuration in order to achieve tip clearance. This placement, however, will need more landing gear material, which adds weight to the overall structure.

2.4 Conclusion

To summarize the proposed aircraft is a land-based aircraft with conventional Configuration. The only improvement in this design is fuel consumption. The aircraft is intended to run on fuel for several profiles of the flight and on battery for the rest of the mission. This will greatly reduce the amount of fossil fuel consumed and the amount of carbon released to the atmosphere. The conventional configuration is chosen to reduce drag and minimize structural weight of the proposed aircraft. In general, this project seems possible compared to the other similar projects implemented in the past.

CHAPTER 3 - WEIGHT SIZING & WEIGHT SENSITIVITIES

3.1 INTRODUCTION

Aircraft cruise in the air with different types of load. For instance, a transport jet accommodates passengers, passengers' baggage, fuel, crew, and crew baggage to mention some. It is well known that one cannot have indefinite amount of passengers and cargo in an aircraft for there is a takeoff weight limit for a given aircraft. The takeoff weight is a very important parameter that sizes the aircraft. It also is the very first parameter to be determined in the design process. Weight sizing is a critical step in the process where the designer has to reiterate to compromise among different design parameters. This work is intended to estimate the takeoff weight of medium range hybrid-electric aircraft. This is accomplished by estimating a takeoff weight value close to sample aircraft. Then a feasible point is achieved by reiterating until the estimated value matches a calculated value from a data of similar aircraft.

3.2 MISSION WEIGHT ESTIMATES

3.2.1 Data Base for Takeoff Weights and Empty Weights of Similar Airplanes

The process of weight sizing begins with collecting different aircraft having similar capacity to the proposed aircraft. Ten different aircraft with almost similar capacities are listed in table 3.1 below to aid the weight-sizing task.

Table 3.1: List of different aircraft similar to the proposed aircraft with their takeoff and empty weights.

Types of aircraft	W_{TO} (lb)	W_E lb	References
Whitworth Ensign	66,000	35,075	List_of_aircraft
Antonov An---140	47,350	28,240	List_of_aircraft
Antonov An---24	46,300	29,321	List_of_aircraft
ATR---42	37,257	22,680	List_of_aircraft

ATR---72	50,706	29,346	List_of_aircraft
Embraer 120	26,433	15,586	List_of_aircraft
Fairchild	30,843	20,062	List_of_aircraft
Martin 2---0---2	39,900	25,086	List_of_aircraft
Martin 4---0---4	44,900	29,126	List_of_aircraft
Saab 2000	50,265	30,424	List_of_aircraft

3.2.2 Determination of Regression Coefficients A and B

The mathematical relationship between takeoff weight and the empty weight is

given by:

$$\log_{10} W_{TO} = A + B \log_{10} W_E \quad (3.1)$$

Where A is the y intercept and B is the slope of the log-log plot of W_E versus W_{TO} . The data for the similar aircraft given in table 1 is plotted in log-log plot given in figure 1 below. The important coefficients in equation (3.1) above are called regression coefficients and are given with the plot.

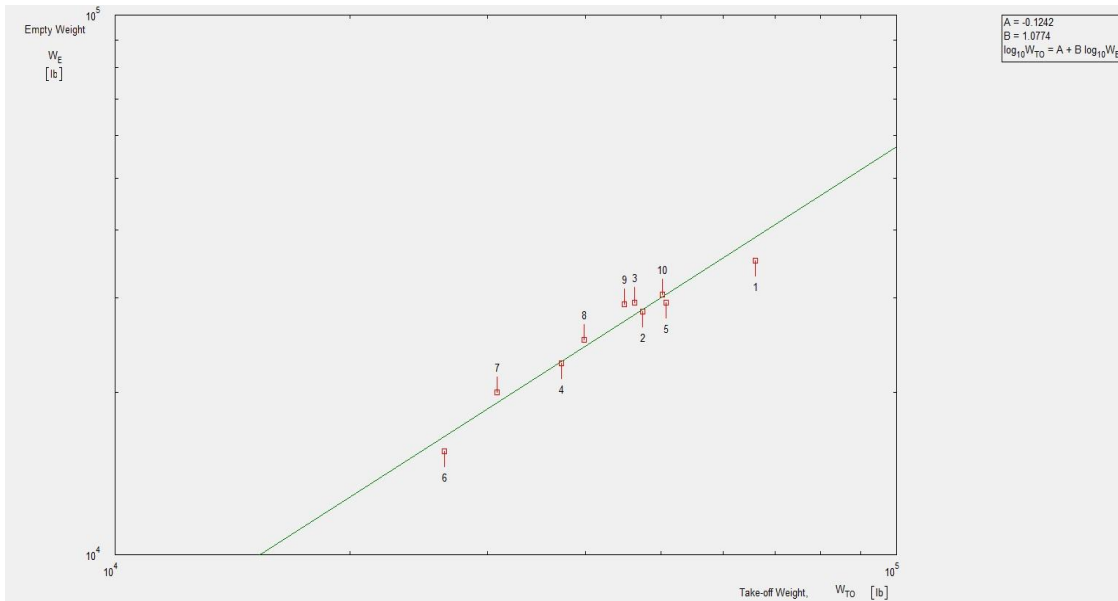


Figure 3.1: Regression coefficients of the log-log plot of the similar aircraft.

3.3 Determination of Mission Weights

3.3.1 Manual Calculation of Mission Weights

Determination of takeoff weight of an aircraft involves a series of processes and iterations. The process begins with estimating a takeoff weight value followed by determining payload (W_{PL}) from the capacity of the proposed aircraft. For the hybrid aircraft the payload is calculated in table 3.2 below.

Table 3.2: Payload weight of the hybrid aircraft.

Load	Weight per element	Total weight (lb.)
40 Passengers	175	7,000
40 Passenger baggage	40	1600
3 Crews	175	525
3 Crew baggage	30	90
Grand total		9215

From the similar aircraft data 50,000lb is a likely takeoff weight for the proposed hybrid transport jet. The following missions are accomplished by burning fuel.

- Warm up
- Taxi
- Takeoff and
- Climb.

Since the takeoff weight also includes the weight of the fuel, the mission fuel weight must be determined by defining the beginning and end weight ratio for each mission profile as follow.

$$\frac{W_1}{W_{TO}} \frac{W_2}{W_1} \frac{W_3}{W_2} \frac{W_4}{W_3} = (0.990)(0.990)(0.995)(0.980) = 0.955 \quad (3.2)$$

From equation (3.2) the weight of the fuel used can be calculated as

$$W_{fuel} = (1 - 0.955) W_{TO} = 0.044 W_{TO} \quad (3.3)$$

For the estimated weight, $W_{fuel} = 2,200lb$.

A battery power completes the rest of the mission and the weight of the battery needed is given by Hepperle's Range equation as follows.

$$R = E^* \frac{1}{g} \frac{L}{D} \frac{W_{battery}}{W_{TO}} \quad (3.4)$$

Substituting $R = 3,600,000ft$ and assuming $\eta = 0.8, E^* = 1400 Wh/kg$, equation (3.4) can be simplified to give the relationship between battery weight and takeoff weight.

$$\frac{W_{battery}}{W_{TO}} = 0.2 \quad (3.5)$$

For the estimated weight, $W_{battery} = 10,000lb$.

The tentative empty weight of the aircraft can be calculated as

$$W_{E_{tent}} = W_{TO} - W_{battery} - W_{fuel} - W_{PL} \quad (3.6)$$

Using the results from table 1 and equations (3.3) and (3.5), the tentative empty weight of the aircraft is

$$W_{E_{tent}} = 50,000 - 10,000 - 2,200 - 9,215 = 28,585lb$$

The actual empty weight using the regression coefficients from the log-log plot of the data of similar aircraft is

$$W_E = \text{invlog} \left(\frac{\log 50,000 + 0.1242}{1.0774} \right) = 29,969 \text{ lb.}$$

However, W_E and $W_{E_{tent}}$ are not within 0.5% to each other. As a result, reiteration is needed. The reiteration along with the Matlab code in Appendix A gives an approximate takeoff weight of 56,800 lb.

3.3.2 Calculation of Mission Weights Using the AAA Program

Inputting the regression coefficients and other parameters, AAA program calculates the takeoff weight and other parameters given in the screenshots below.

Input Parameters									
A	-0.1242	$W_{TO_{est}}$	50000.0 lb	$W_{\Sigma_{crew}}$	525.0 lb	M_{tfo}	0.005 %	$W_{TO_{min}}$	5000.0 lb
B	1.0774	$W_{\Sigma_{pax}}$	7000 lb	$W_{\Sigma_{cargo}}$	16050.0 lb	M_{res}	0.500 %	$W_{TO_{max}}$	100000.0 lb
Output Parameters									
M_{ff}	0.9659	W_F	2149.7 lb	$W_{F_{res}}$	10.7 lb	W_{PL}	23050.0 lb	W_E	36965.9 lb
$W_{F_{used}}$	2139.0 lb	$W_{F_{max}}$	2149.7 lb	W_{tfo}	3.1 lb	W_{useful}	25724.7 lb	W_{TO}	62693.7 lb

Mission Profile Table: Output

	Mission Profile	W_{begin} lb	$\Delta W_{F_{used}}$ lb	$W_{F_{begin}}$ lb
1	Warmup	62693.7	626.9	2149.7
2	Taxi	62066.8	620.7	1522.7
3	Take-off	61446.1	307.2	902.1
4	Climb	61138.9	584.1	594.8
5	Cruise	60554.8	0.0	10.7
6	Loiter			
7	Descent			
8	Land/Taxi			

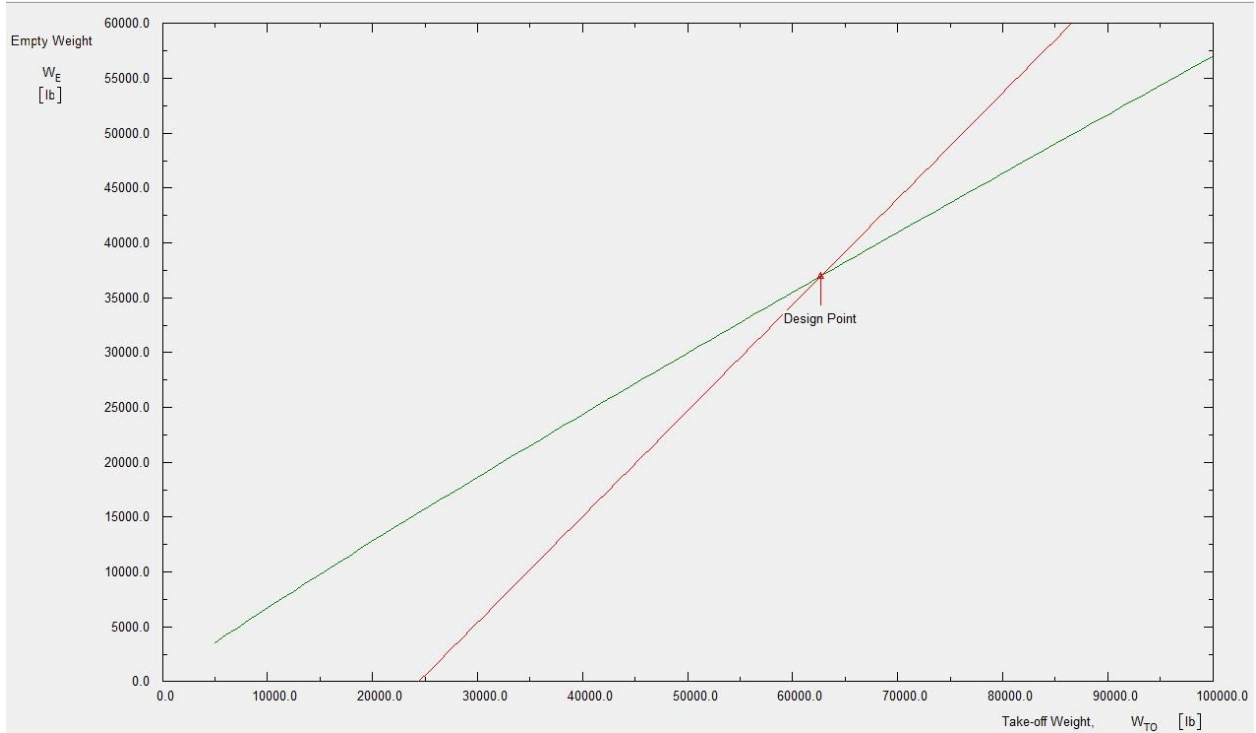


Figure 3.2: Screenshots of mission weight calculations from AA program.

3.4 TAKEOFF WEIGHT SENSITIVITIES

3.4.1 Manual Calculation of Takeoff Weight Sensitivities

From the way it was determined W_{TO} varies with different design parameters such as payload and empty weight. The amount by which takeoff weight varies with respect to a given variable indicates how sensitive takeoff weight is to a change in the given variable. To calculate the sensitivity of takeoff weight with respect to a given parameter the regression coefficients must be defined as follows.

$$A = -0.1242$$

$$B = 1.0774$$

$$C = 1 - (1 + M_{res})(1 - M_{ff}) - M_{tfo} = 0.963$$

$$D = 25,021lb$$

(3.7)

The sensitivity of W_{TO} with respect to W_{PL} is given by

$$\frac{\partial W_{TO}}{\partial W_{PL}} = \frac{BW_{TO}}{B-C(1-B)W_{TO}} = 2.4 \quad (3.8)$$

The left hand side in equation (3.8) is the growth factor of the airplane due to payload. In this case, the weight of the airplane grows 2.4 times for an increase in payload.

Takeoff weight sensitivity to empty weight can also be calculated as

$$\frac{\partial W_{TO}}{\partial W_E} = BW_{TO} \left[\text{invlog} \left(\frac{\log W_{TO} - A}{B} \right) \right]^{-1} = 1.63 \quad (3.9)$$

The growth factor of the takeoff weight due to an increase in empty weight is 1.63. Other sensitivity studies are documented in Appendix B.

3.4.2 Calculation of Takeoff Weight Sensitivities Using the AAA Program

In the design process takeoff weight of the aircraft is influenced by different design parameters. The change in the size of the aircraft due to these parameters is called sensitivity. Sensitivity can both be calculated by hand and by the AAA program. Below is a figure that shows the sensitivity values from the AAA program. It is succinct that the sensitivities calculated by hand and by the AAA program are close enough.

Input Parameters							
B	1.0774	W_{PL}	23050.0 lb	M_{tfo}	0.005 %	W_{TO}	62693.7 lb
M_{ff}	0.9556	$W_{\Sigma crew}$	525.0 lb	M_{res}	0.500 %	W_E	36965.9 lb
Output Parameters							
$\partial W_{TO} / \partial W_{PL}$	2.39	$\partial W_{TO} / \partial W_{crew}$	2.39	$\partial W_{TO} / \partial W_E$	1.83		

Mission Sensitivity Table: Output								
	Mission Prctile	$\partial W_{TO} / \partial W_{FL_{exp}}$	$\partial W_{TO} / \partial W_{FL_{load}}$	$\partial W_{TO} / \partial W_{F_{refuel}}$	$\partial W_{TO} / \partial c_j$ lb-hr	$\partial W_{TO} / \partial R$ $\frac{lb}{nm}$	$\partial W_{TO} / \partial L/D$ lb	$\partial W_{TO} / \partial E$ $\frac{lb}{hr}$
1	Warmup							
2	Taxi							
3	Take-off							
4	Climb				2327.2		-139.6	8727.1
5	Cruise							
6	Loiter							
7	Descent							
8	Land/Taxi							

Figure 3.3: Screenshots of sensitivity calculation from the AAA program.

3.5 Trade Studies

3.5.1 Trading Lift to Drag Ratio for Takeoff Weight

Aircraft design involves a tremendous amount of tradeoff. One parameter can be traded for another parameter in the design to find the best design point. In this work, lift to drag ratio for climb can be traded for W_{TO} which means $\frac{L}{D}$ can be varied over a range of values to observe how W_{TO} changes. In the AAA program L/D can be varied to give varying values for W_{TO} . Table 3.3 below is a record of the output of the AAA program for W_{TO} when climb $\frac{L}{D}$ is varied.

Table 3.3: Trading $\frac{L}{D}$ for W_{TO} .

L/D	10	13	15	17
W_{TO}	62,693	62,372	62,230	62,122

The result of trading lift to drag ratio for takeoff weight can be graphed to see the design point.

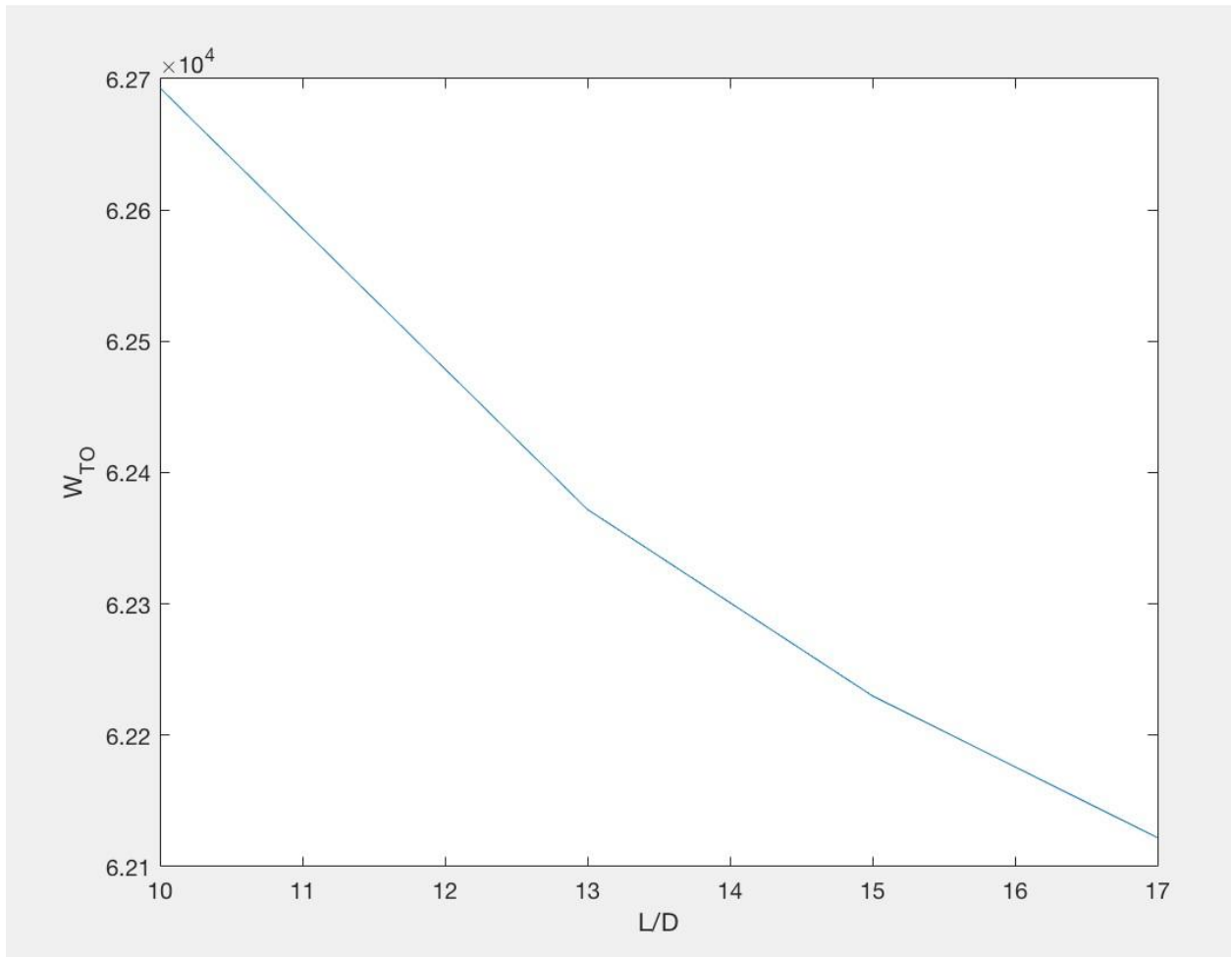


Figure 3.4: Trading L/D for takeoff weight.

Figure 3.4 shows minimizing the lift to drag ratio can maximize the takeoff weight of the aircraft. The lift to drag ratio, however, cannot be reduced indefinitely, so there is a saturation point.

3.5.2 Trading Range for Payload Weight

Furthermore, reducing payload can maximize range and vice versa. By keeping the takeoff weight constant, a trade off study between range and payload can be established. From Hepperle's range equation, battery weight values can be calculated which affects payload since takeoff weight is constant. To investigate the relationship between payloads and range the following equation can be used.

$$R = 5.348 * 10^6 \frac{W_{battery}}{W_{TO}} \quad (3.9)$$

Equation (3.9) above, gives $W_{battery}$ for any given range at a constant takeoff weight. Payload at a given range can then be retrieved from the following equation.

$$W_{PL} = W_{TO} - W_E - W_{fuel} - W_{battery} \quad (3.10)$$

Table 3.4: Results of trading R for W_{PL} .

$R(m)$	1,100,200	1,108,200	1,111,200	1,112,200	1,113,200	1,115,200	1,120,200
$W_{PL}(lb)$	8,891	8,806	9,215	8777	8,766	8,737	8,703

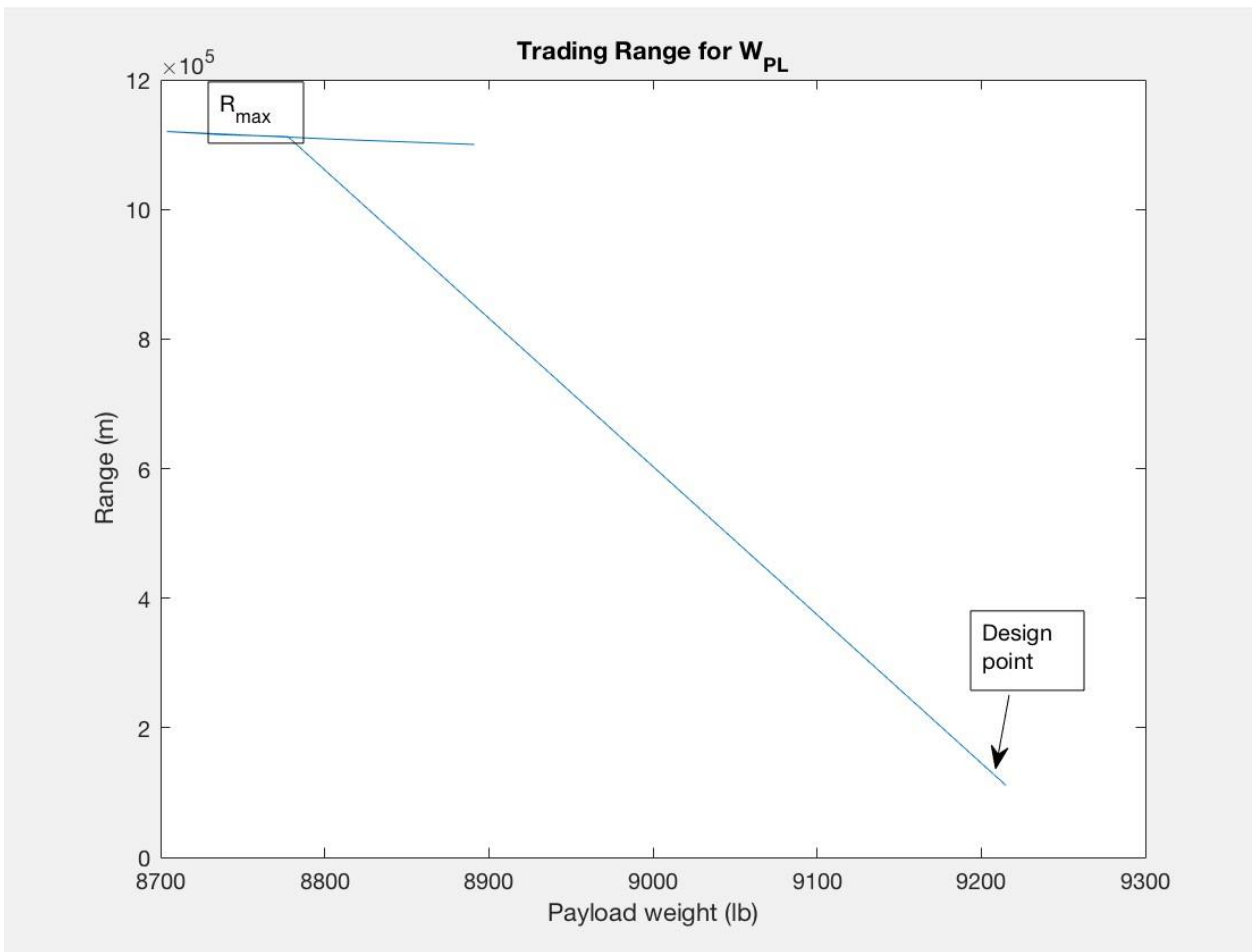


Figure 3.5: Trading Range for Payload Weight.

3.5.3 Trading Cruise Lift to Drag Ratio for Payload Weight

Hepperle's equation magnifies the relationship between lift to drag ratio and battery weight. A trade study can then be established between payload weight and lift to drag ratio by keeping takeoff weight and range constant as demonstrated below.

$$W_{battery} = 2.70083 \frac{W_{TO}}{L/D} \quad (3.11)$$

Table 3.5: Trading L/D for W_{PL} .

L/D	10	11	12	13	14	15	16	17	18
W_{PL} lb	5,234	6,626	7,791	8,774	9,617	10,348	10,987	11,551	12,052

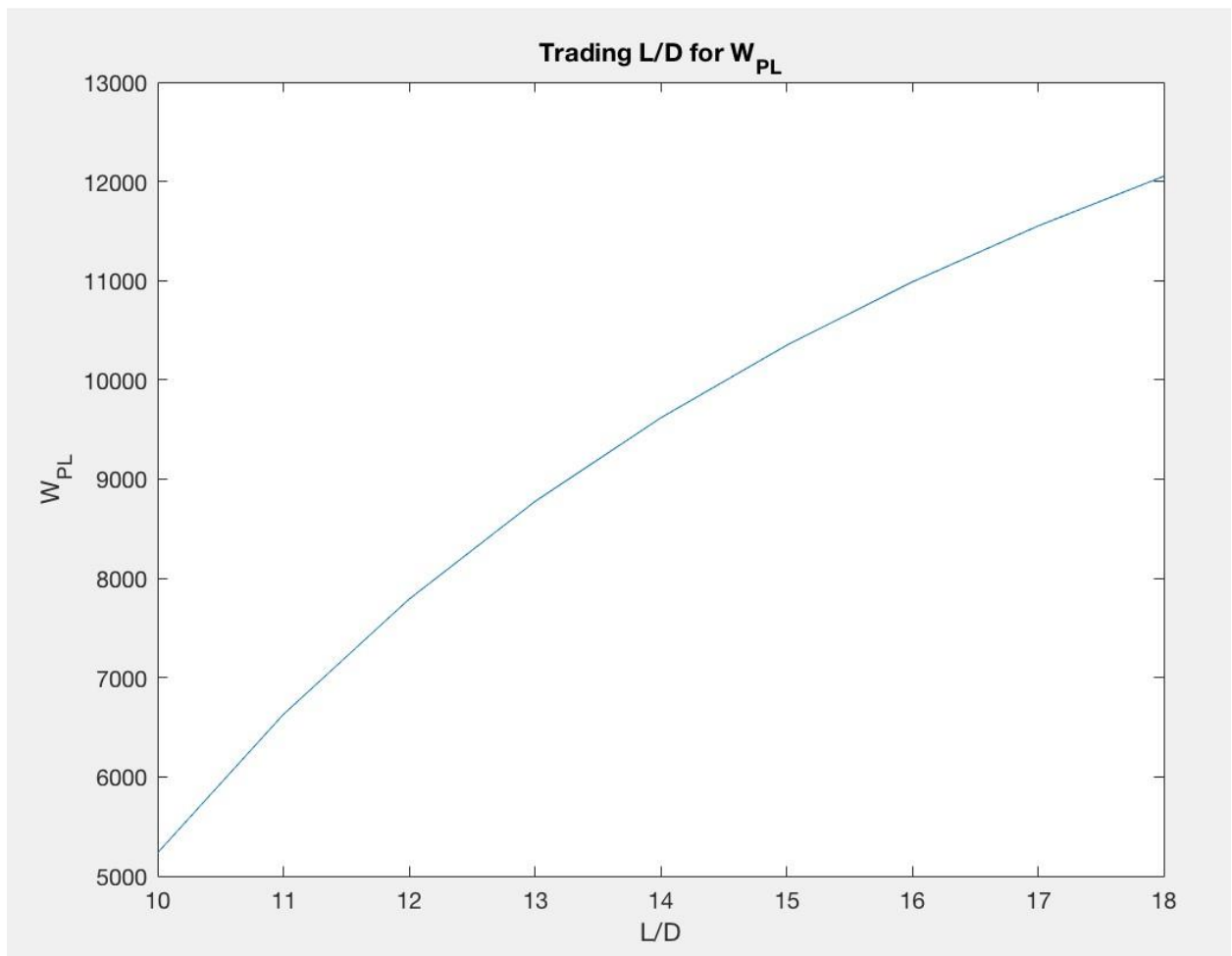


Figure 3.6: Trading L/D for W_{PL} .

3.6 DISCUSSION

In this work the takeoff weight a hybrid transport jet is calculated. To size the hybrid transport jet both a hand calculation and a software calculation are done. The calculation of takeoff weight is a function of different parameters meaning that is sensitive to different design parameters. The takeoff weight of the hybrid transport jet in proposal is an aggregate sum of the following parameters.

- Payload weight (Passengers and bags)
- Mission fuel weight
- Battery weight
- Empty weight

Takeoff weight can be calculated in two different ways. One way is by collecting aircraft of similar capacities to the proposed aircraft and finding the regression coefficients to be used in equation (3.1). The other way is to calculate each parameter in the list above and add them up to get the total takeoff weight which involves estimating a takeoff weight first and reiterating this estimate. If an agreement between the empty weight and tentative weight is reached, then the estimate is good enough. Otherwise, a similar reiteration given in Appendix A should be done.

The AAA software is also used to calculate the takeoff weight. Takeoff weight from hand calculation is $W_{TO} = 56,800lb$ and the value from the AAA software is $W_{TO} = 62,000lb$ as it is designated by 'design point' in figure 2. The hand calculated and the software-calculated values are within 8% to each other.

Takeoff weight is also sensitive to other design parameters such as lift to drag ratio, specific fuel consumption, and range. Sensitivity predicts how takeoff weight is affected by changing a given design parameter. Trade off, on the other hand, is varying a given parameter to maximize or minimize a design parameter to reach a

design point. In sensitivity study of takeoff weight to lift to drag ratio is investigated. In trade studies (figure 3.4), it is confirmed that the slope of W_{TO} versus L/D is negative. This implies that increasing lift to drag ratio decreases the takeoff weight of the aircraft. In this sense the sensitivity and trade studies match.

Different design parameters can be traded for takeoff weight one example being $\frac{L}{D}$. It is also possible to trade R for payload weight since they are relation via equation (3.4). Figure (3.5) clearly shows that when $R = 0$, W_{PL} is maximum and vice versa. At the point where R_{max} is labeled, range is maximum and a change in W_{PL} cannot make a difference in R which means W_{PL} cannot be traded for range.

There is also a point where W_{PL} saturates and changing R does not change it. At this point trade cannot be made between the two parameters. Between these two saturation points there is a linear portion where changing one parameter affects the other. The design point is where the trade is at its best for the design, and that point is marked on the graph.

3.7 Conclusion

Sizing the hybrid transport jet is the main purpose of this work. Estimating different parameters and validating them accomplishes the sizing process. The proposed hybrid-electric aircraft accomplishes certain parts of its mission by burning fuel and the rest with a battery it carries. As a result, the sizing process is somehow involved because of the two parts must be dealt with separately. In the first part of the mission weight change must be considered since fuel being burned. For there rest of the mission where battery is used as a means of propulsion, weight does not change anymore since there is no fuel to burn. As a result, Hepperle's range equation is used to predict the battery weight that the aircraft should carry around to accomplish the electric part of the flight. Adding the battery weight to the payload, fuel, and empty weights, the aircraft weighs 56,000lb. It is beneficial to see how various parameters affect the size of the aircraft and use that information for trade study. The most important parameters for tradeoff are payload and range.

CHAPTER 4---PERFORMANCE CONSTRAINT ANALYSIS

4.1 INTRODUCTION

The aircraft under design is a hybrid FAR 25 transport jet. As per by FAA regulations, FAR25 jets must be sized to landing distance, takeoff distance, climb constraints, and cruise speed requirements. The proposed aircraft, in its mission specification, had a landing distance, takeoff distance, cruise speed, and climb requirements. From previous works, the aircraft's weight including the battery weight is also known. By using the parameters that have already been determined and the parameters that are listed as requirements in the mission specification, the performance of the aircraft can be analyzed. This specifically means that the wing loading for different flight conditions such as takeoff, climb, cruise, and landing can be determined. The thrust required to keep the aircraft moving forward can also be determined. A better design point for the proposed aircraft can be found by trading one parameter for the other from thrust to weight ratio versus the wing loading graph. The requirements that the aircraft must adhere to will be calculated and plotted and a design point will be picked based on the mission requirements and the availability of propulsion systems.

4.2 MANUAL CALCULATION OF PERFORMANCE CONSTRAINTS

4.2.1 Sizing to Takeoff Distance Requirements

Since it is required to size a passenger airplane so that the FAR 25, field length is given by $S_{TOFL} < 5000ft$ at $8000ft$ standard atmosphere. Using this requirement

$$TOP_{25} = \frac{5000ft}{37.5} = 133.3 lb/ft^2 \quad (4.1)$$

The relationship between thrust to weight ratio and TOP_{25} is given by

$$\frac{(W/S)_{TO}}{C_{Lmax_{TO}}(T/W)_{TO}} = 0.786TOP_{25} = 104.8 lb/ft^2 \quad (4.2)$$

From this relationship the required $(T/W)_{TO}$ can be calculated and tabulated as follow.

Table 4.1: Thrust to Weight Ratio Required at Take-off by Varying Wing Loading and Lift Coefficient.

$C_{Lmax_{TO}}$	1.2	1.4	1.6	1.8	2.0	2.2
$(W/S)_{TO}$	$(T/W)_{TO}$	$(T/W)_{TO}$	$(T/W)_{TO}$	$(T/W)_{TO}$	$(T/W)_{TO}$	$(T/W)_{TO}$
30	0.24	0.20	0.18	0.16	0.14	0.13
40	0.32	0.27	0.24	0.21	0.20	0.17
50	0.39	0.34	0.30	0.30	0.24	0.22
60	0.47	0.41	0.36	0.32	0.29	0.26
70	0.56	0.48	0.42	0.37	0.33	0.30
80	0.64	0.55	0.48	0.42	0.38	0.35
90	0.72	0.61	0.54	0.48	0.43	0.39
100	0.78	0.68	0.60	0.53	0.48	0.43

4.2.2 Sizing to Landing Distance Requirements

The FAR landing field length is the total landing distance divided by 0.6.

Approach speed and stall speed at landing can be related by

$$V_A = 1.3V_{SL} \quad (4.3)$$

Landing field length and approach speed can also be related as

$$S_{FL} = 0.3V_A^2 \quad (4.4)$$

where landing field length is in feet and approach speed is in knots.

It is required to size a transport jet for a landing field length of 5000ft at sea level on a standard day. For the proposed transport jet $W_{TO} = 56,800lb$ and $W_L = 0.95W_{TO}$. From equation (4.4) $V_A = 129kts$ and from equation (4.3) $V_{SL} = 99.3kts$.

Wing loading at landing and take-off can be related as

$$(W/S)_{TO} = 33.2C_{Lmax_L} \quad (4.5)$$

Using equation (4.5) above, the following table of values can be generated.

Table 4.2: Landing and Take-off Relationship

C_{Lmax_L}	1.8	2.0	2.2	2.6	2.8
$(W/S)_{TO}$	60	66.4	73	86	93

4.2.3 Drag Polar Estimation

Coefficient of drag of a subsonic airplane can be written as

$$C_D = C_{D0} + C_L^2/\pi A e \quad (4.6)$$

where the profile drag $C_{D0} = \frac{S_{wet}}{S} = \frac{f}{S}$. The wetted area can be calculated using

$$\log S_{wet} = c + d \log W_{TO} \quad (4.7)$$

For a jet aircraft $c = 0.0199$ and $d = 0.7531$ are reasonable. For the proposed aircraft, equation (8) gives $S_{wet} = 3984 ft^2$. The equivalent parasite area f can be calculated as

$\log f = a + b \log^{3.984} = 16 ft^2$. Assuming average wing loading of $85 psf$ for this aircraft, the following table of values can be generated.

Table 4.3: Parameters Needed for Drag Polar Estimation.

W_{TO}	$\left(\frac{W}{S}\right)_{TO}$	S	S_{wet}	f	C_{D0}
56,800lb	85psf	668ft ²	3984ft ²	16ft ²	0.02395

If we assume an aspect ratio of 10 and efficiency factor of 0.85, low speed clean drag polar is given by

$$C_D = 0.02395 + 0.03747 C_L^2 \quad (4.8)$$

Flaps and landing gear also contribute to the profile drag. These additions of profile drag from flaps and gear are

- Take-off flaps: 0.015 with $e=0.8$
- Landing flaps: 0.060 with $e=0.75$
- Landing gear: 0.017 with $e=0.75$

To summarize, the airplane drag polar is:

- Low speed clean: $C_D = 0.02395 + 0.03747 C_L^2$
- Take-off gear up: $C_D = 0.03895 + 0.0398 C_L^2$
- Take-off gear down: $C_D = 0.05595 + 0.0398 C_L^2$
- Landing gear up: $C_D = 0.08395 + 0.04246 C_L^2$
- Landing gear down: $C_D = 0.10095 + 0.04246 C_L^2$

4.2.4 Climb Constraints

It is required to size a twin-engine jet transport to FAR 25 climb requirements at take-off and landing.

4.2.4.1 Sizing to FAR 25.111 One engine Inoperative (OEI) Requirement

This is the case where $CGR > 0.012$ and the following configurations are taken into consideration.

- Gear up
- Take-off flaps
- Take-off thrust on the remaining engine
- Ground effect and $1.2V_{STO}$

The thrust to weight ratio at take-off is then

$$(T/W)_{TO} = 2 \left(\frac{1}{L/D} + 0.012 \right) \quad (4.9)$$

Assuming $C_{L_{max_{TO}}} = 2$, actual $C_L = \frac{2.0}{1.44} = 1.38$. Lift to drag ratio and the actual drag ratio can also be calculated and the values are $\frac{L}{D} = 12$ and $C_D = 0.1157$. Plugging in the lift to drag ratio in equation (4.9), $(T/W)_{TO} = 0.191$ and taking the the 50°F effect $(T/W)_{TO} = \frac{0.191}{0.8} = 0.238$.

4.2.4.2 Sizing to FAR 25.121 One Engine Inoperative Requirements

For this requirement $CGR > 0$ and the following configurations are considered.

- Gear down
- Take-off flaps
- Take-off thrust on remaining engines
- Ground effect
- Speed between V_{LOF} and $1.2V_{STO}$

Following similar procedures as before, $(T/W)_{TO} = 0.24$ after correcting for 50°F.

4.2.4.3 Sizing to FAR 25.121 One engine Inoperative Requirement

For this requirement $CGR > 0.024$ and the following configurations are considered.

- Gear up

- Take-off flaps
- No ground effect
- Take-off thrust on remaining engines
- $1.2V_{S_{TO}}$

Following the procedures outlined before $(T/W)_{TO} = 0.268$.

4.2.4.4 Sizing to FAR 25.121 One Engine Inoperative CGR>0.012 Requirement

The following configurations are required.

- Gear up
- Flaps up
- Enroute climb altitude
- Maximum continuous thrust on remaining engines
- $1.25V_S$

Following the procedures and correcting for the ratio of maximum continuous thrust to maximum take-off thrust being 0.94, $(T/W)_{TO} = 0.24$

4.2.4.5 Sizing to FAR 25.119 All Engines Operating (AEO) CGR>0.032 Requirement

The following configurations are desired in this requirement.

- Gear down
- Landing flaps
- Take-off thrust on all engines
- Maximum design landing weight

Following all the procedures $(T/W)_{TO} = 0.245$

4.2.4.6 Sizing to FAR 25.121 One Engine Inoperative Condition CGR>0.021

The following configuration is required.

- Gear down
- Approach flaps
- Take-off thrust on remaining engines

This gives $(T/W)_{TO} = 0.345$

4.2.5 Sizing to Cruise Speed Requirements

It is required to size an airplane with $W_{TO} = 56,800\text{lbs}$ so that it has a maximum speed of $M = 0.92$ at sealevel. Compressibility drag increment is assumed to be 0.0040. Assuming $A=10$ and $e=0.85$, allowable values of wing loading and thrust to weight ratio to meet a given maximum speed at sealevel can be calculated.

$$(T/W)_{req} = \frac{35.69}{(W/S)_{TO}} + \frac{(W/S)_{TO}}{34,081} \quad (4.10)$$

By selecting and plugging in different values for wing loading in equation (11), table 4 below can be generated.

Table 4: Allowable wing loading and thrust to weight ratio to meet a given maximum speed.

$(\frac{W}{S})_{TO}$	40	60	80	100
$(\frac{T}{W})_{req}$	0.893	0.5965	0.4485	0.3598

4.3. CALCULATION OF PERFORMANCE CONSTRAINTS WITH THE AAA PROGRAM

4.3.1 Takeoff Distance

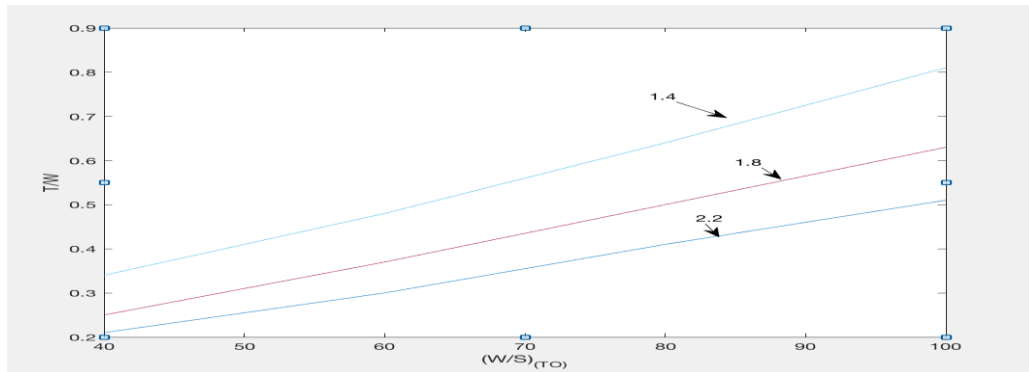
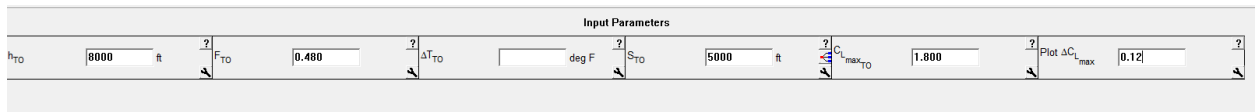


Figure 4.1: T/W versus W/S for Three Different C_{LmaxTO}



4.3.2 Landing Distance

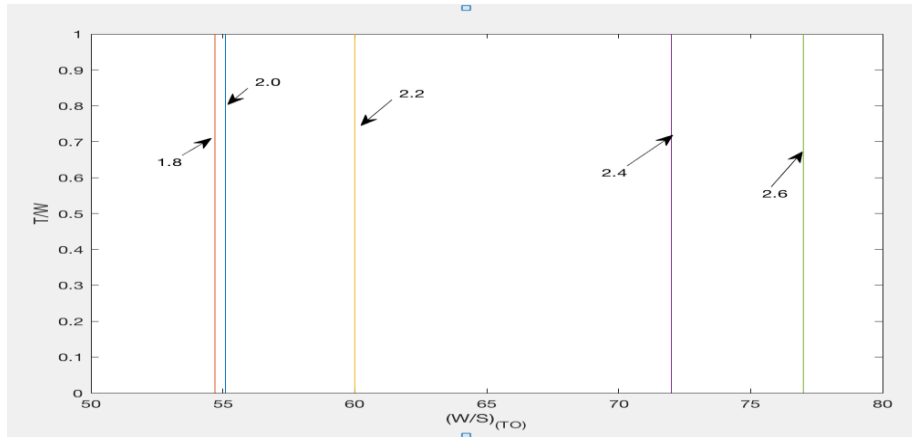


Figure 4.2: T/W versus W/S for Four Different C_{LmaxL}

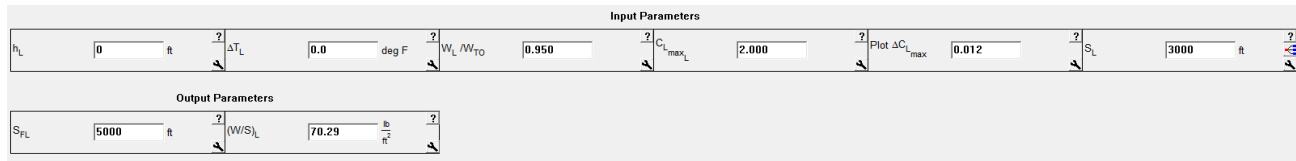


Figure 4.3: AAA Output for Landing Distance Requirement.

4.3.3 Climb Constraints

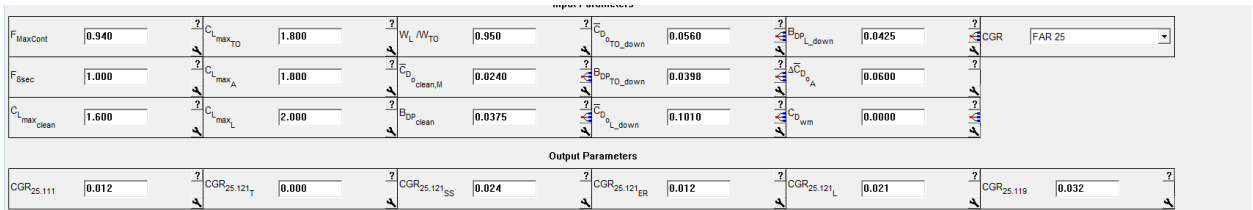


Figure 4.5: AAA Outputs for Climb requirements.

4.3.4 Speed Constraints

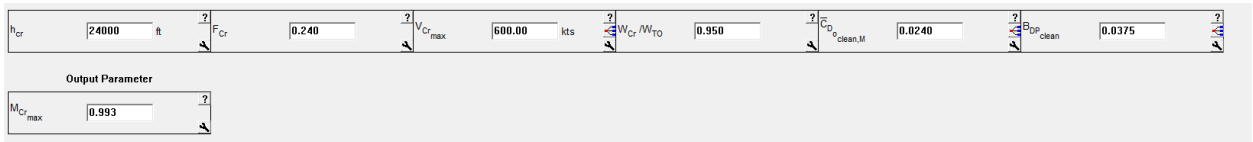


Figure 4.6: Speed Constraint outputs of AAA program.

4.3.5 Summary of Performance Constraints

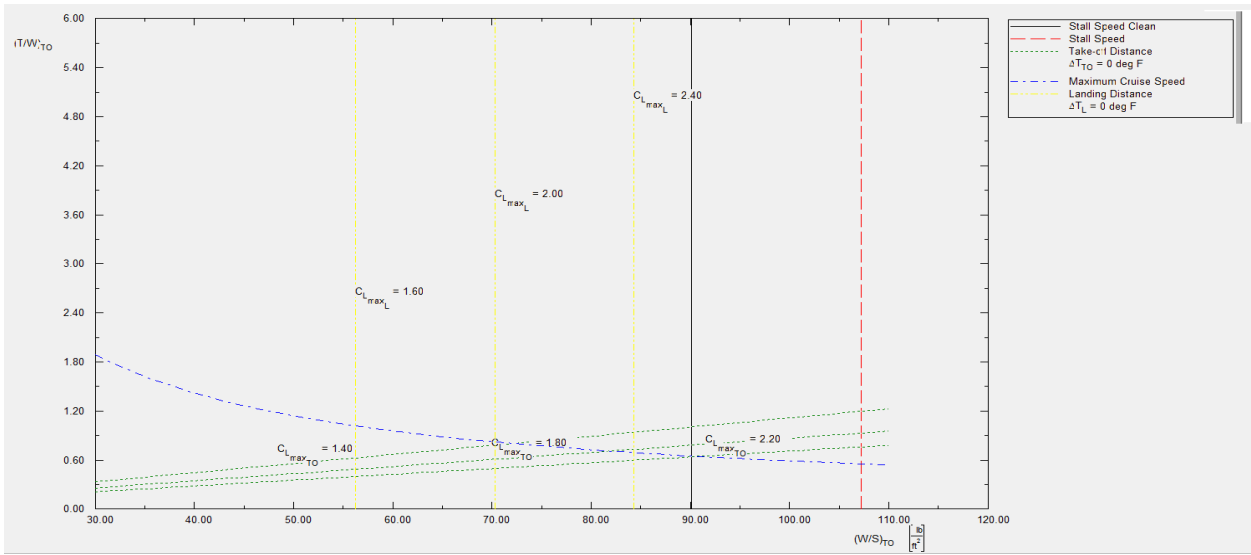


Figure 4.7: Matching graph from AAA program

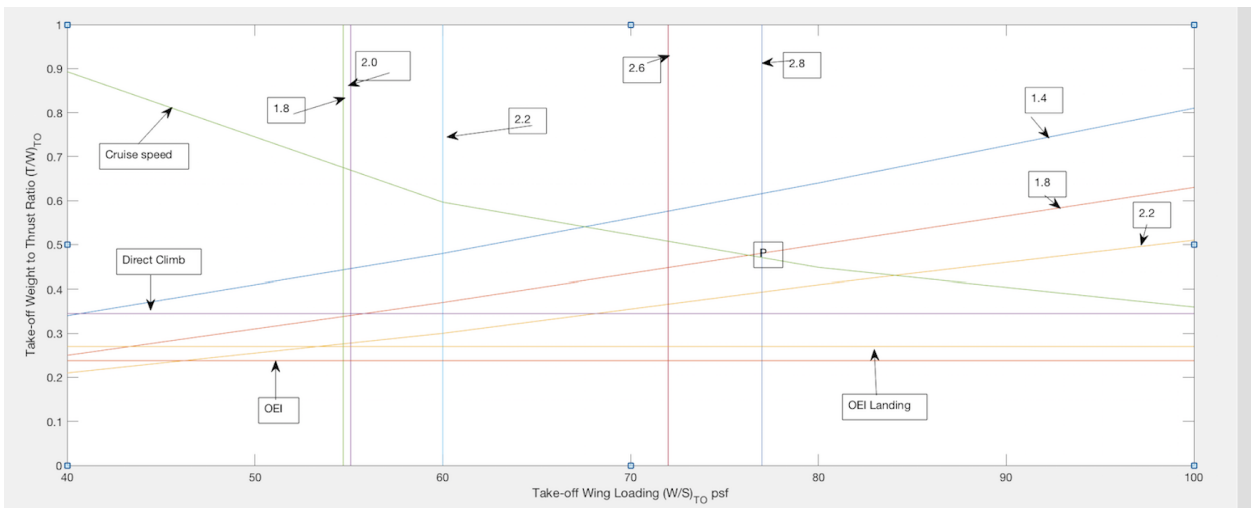


Figure 4.8: Matching Graph from Matlab with the Design Point.

From the design point chosen above, the following values can be read.

- $(T/W)_{TO}=0.49$
- $(W/S)_{TO}=78\text{psf}$
- $C_{Lmax} \text{ (clean)}=1.6$
- $C_{LmaxTO}= 1.8$
- $C_{LmaxL}=2.8$

- A (wing aspect ratio)=10

From these values, the T_{TO} required is 27,832lb and a reasonable wing area is 728ft².

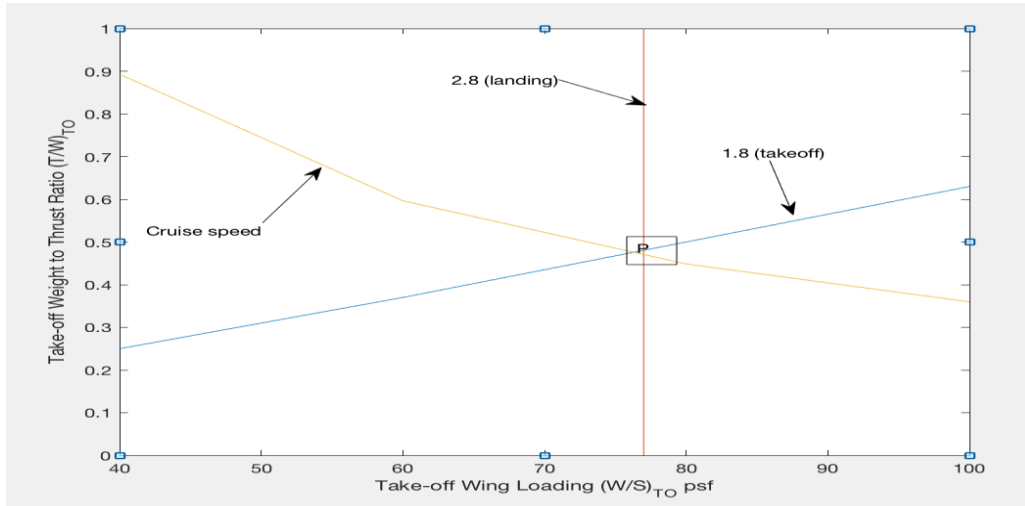


Figure 4.9: Cleaned Up Version of Matching Graph with Cruise Speed, Landing Requirement, and Takeoff Requirement Which are Critical Requirements.

4.4. SELECTION OF PROPULSION SYSTEM

4.4.1 Selection of the Propulsion System Type

In the mission specification of this aircraft, it is mentioned that the aircraft will be driven by a turbofan engine. From the weight sizing it is also determined that a battery that weighs 12,000lb will drive the turbofan engines starting from cruise to landing. From the matching plot of performance sizing it is determined that the engines must be able to supply a thrust of about 28,000lb.

4.4.2 Selection of the Number of Engines

The mission specification clearly states that the aircraft must have two turbofan engines. From performance sizing a thrust of about 28,000lbs is needed. As a result, each engine must be able to produce a thrust greater than 14,000lbs so satisfy the one engine out condition.

4.5. DISCUSSION

The purpose of this chapter is to explore the operating conditions of the proposed aircraft in terms of design parameters. As it is well articulated design is a tradeoff which

means parameters can be traded. In this chapter the most important parameters are the thrust required and the size of the wing. The thrust required and the wing size can be affected by takeoff, climb, cruise, and landing. In each case the thrust required, and the wing loading were calculated by varying the maximum lift coefficient. Figure 4.8 clearly shows the landing (vertical), takeoff (right slanting), cruise speed, and climb requirements. The thrust required versus the wing size is plotted. Based on the plot a design point P is shown in the figure. This design point P is chosen because it is an optimal condition where cruise speed, landing and takeoff requirements are critical. At the design point the following values can be read.

- $\frac{T}{W} = 0.49$
- $\frac{W}{S} = 78psf$
- $C_{LmaxTO} = 1.8$
- $C_{LmaxL} = 2.8$

From previous works, the takeoff weight is 56,800lbs. Using the takeoff weight, the above values give $T = 28,000lbs$ and $S = 728ft^2$.

From the design point cruise speed, landing, and takeoff are all critical. It is possible to move away from the design point in the following ways.

- Moving right on the same takeoff lift coefficient requires both a powerful engine and a bigger wing which is desirable for takeoff and landing to generate more lift. However, bigger wing means more drag, and this is not desired for cruise.
- Moving up on the same landing condition and towards less takeoff lift coefficients will require a powerful engine by keeping the wing size the same. However, since this is a hybrid aircraft battery technology will be a limitation.
- Moving left of the design point results less wing size. Even though a small wing means less drag and it is beneficial during cruise, it is not desired for both takeoff and landing.
- Moving down on the same landing condition by increasing the takeoff lift coefficient requires a less powerful engine which is not desired.

From previous works ten comparable aircraft were chosen to determine the takeoff weight of the proposed aircraft. Even though most of them have different propulsion system the wing area range is $200ft^2 - 2000ft^2$. The wing area of the proposed aircraft is then reasonable compared to those aircraft.

As a result, the following items affect the design greatly.

- Cruise speed
- Takeoff
- Landing.

4.6. CONCLUSIONS AND RECOMMENDATIONS

4.6.1 Conclusions

Performance analysis is an important step in aircraft design. In performance analysis thrust and wing size are determined. The thrust is the force that pushes the aircraft overcoming the drag force. The wing is part of the aircraft that lifts the aircraft up to balance the weight. These parameters are very important and they must be determined in the process of designing an aircraft. In this work these two parameters are determined. To determine the two important parameters takeoff, landing, cruise, and climb conditions were considered. Having done these steps, the thrust required is determined to be $28,000\text{lbs}$ and $S = 728\text{ft}^2$.

4.6.2 Recommendations

This aircraft is FAR25 certified. As a result, the FAR25 requirements and conditions are applied. The reader is recommended to check what these requirements are. It is the designer's recommendation that the determination of thrust take temperature difference (hot day condition) into account. That is why a scaling to thrust is made in climb requirement calculations.

CHAPTER 5--FUSELAGE DESIGN

5.1 INTRODUCTION

The proposed aircraft is starting to take a shape! The purpose of this chapter is to design a fuselage and a cockpit to meet mission requirements regarding passengers, crew, and payload. It is required that the cockpit crew has a desired vision and access to control knobs without any difficulty. As a result, the cockpit must be designed to serve these purposes. In addition, the fuselage must be designed to accommodate the desired number of passengers with FAR25 requirements of comfort. Consequently, the fuselage must also be designed to meet certain requirements. In general, the fuselage of the aircraft will be designed to accommodate all the weights that were determined in the weight sizing work.

5.2 LAYOUT DESIGN OF THE COCKPIT

The hybrid electric transport jet under design has 2 cockpit crewmembers. As a result, the cockpit must be designed so that the pilot and the copilot have vision and ability to access every control key without any difficulty. The seats must be positioned in a way so that vision to control conflicting traffic enroute and during takeoff and landing are achieved. There are 2 seats for the cockpit crewmembers. The dimensions of the seats and vision angles are sketched as follow.

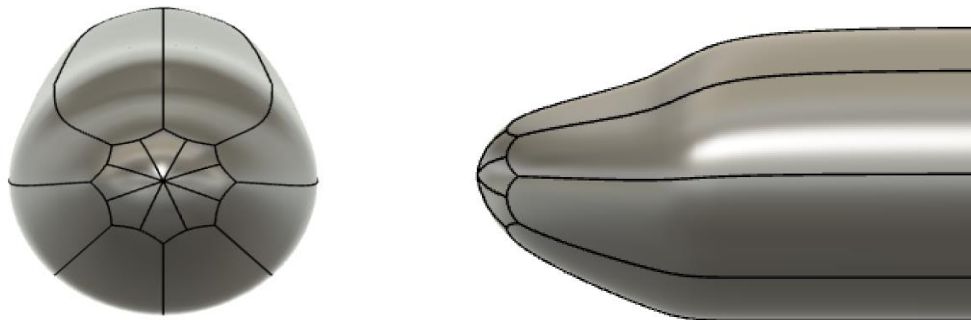


Figure 5.1: Different views of the cockpit

5.3 LAYOUT DESIGN OF THE FUSELAGE

The length of fuselage of an aircraft depends heavily on the amount of weight it has to carry. From previous works the takeoff weight of the hybrid electric aircraft under design is was determined to be 56,800lbs. The length of a fuselage needed to carry a takeoff weight of W_{TO} is given by

$$l_f = aW_{TO}^c \quad (5.1)$$

where a and c are constants given in table 5.1 below.

Table 5.1: Relationship between types of aircrafts and fuselage length

Types of Aircrafts	a	c
Sailplane -unpowered	0.86	0.48
Sailplane-powered	0.71	0.48
Homebuilt-metal/wood	3.68	0.23
Homebuilt-composite	3.50	0.23
General aviation-single engine	4.37	0.23
General aviation-twin engine	0.86	0.42
Agricultural aircraft	4.04	0.23
Jet transport	0.67	0.43
Twin turboprop	0.37	0.51
Jet fighter	0.93	0.39

Using the constants given in table 5.1 above in equation 5.1 the fuselage length of the proposed aircraft is 74ft. From comparable aircrafts a depth of 9.8ft is reasonable. Taking the ratios of dimensions from figure 5.3;

$$\frac{l_f}{d_f} = 7.5 \quad (5.2)$$

$$\frac{l_{fc}}{d_f} = \frac{27}{9.8} = 2.75$$

The results from equation 5.2 are in the range given for jet transport in table 5.2 below which is important because the range in the table must not be exceeded.

Table 5.2: Desirable fuselage dimension ratios [ref 2, p110].

Airplane Type	l_f/d_f	l_{fc}/d_f	θ_{fc} (deg)
Homebuilts	4 - 8	3*	2 - 9
Single Engine	5 - 8	3 - 4	3 - 9
Twins	3.6** - 8	2.6 - 4	6 - 13
Agricultural	5 - 8	3 - 4	1 - 7
Business Jets	7 - 9.5	2.5 - 5	6 - 11
Regionals	5.6 - 10	2 - 4	15 - 19****
Jet Transports	6.8 - 11.5	2.6 - 4	11 - 16
Mil. Trainers	5.4 - 7.5	3*	up to 14
Fighters	7 - 11	3 - 5*	0 - 8
Mil. Transports, Bombers and Patrol Airplanes	6 - 13	2.5 - 6	7 - 25*****
Flying Boats	6 - 11	3 - 6	8 - 14
Supersonics	12 - 25	6 - 8	2 - 9

From Range of angles for the tail cone elevation 13° is appropriate for this aircraft. From this information a preliminary sketch of the aircraft can be given as follow.



Figure 5.2: Side view of the fuselage.

The number of passengers, crew, and the weight of the baggage can be used to determine the shape of fuselage cross-section to be use and the location of cabin floor in that cross-section. Given below are all the components of the fuselage cross section.

- Number of persons abreast= 2
- One aisle 20in wide and 76in high
- All the seats are economy class (40)
- 2 toilets (one in the front and one in the back)

- 1 galley
- 1 cabin crew seat.

The following figure clearly shows the cross-section of the fuselage where the outer shell is $9ft$ and the inner shell is $8ft$ in diameter.

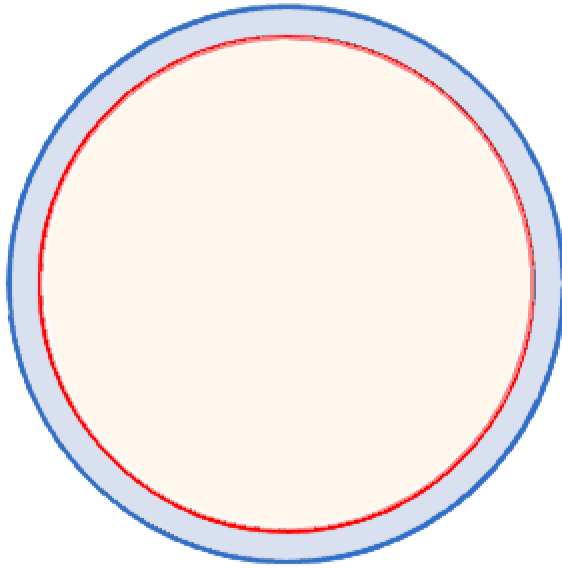


Figure 5.3: Cross-section of the Fuselage

The following overall top view of the aircraft can be made.



Figure 5.4: Overall interior view of the aircraft.

The interior design of the aircraft is now completed. The aircraft can be drawn from different perspectives. The figure below shows the different views of the 3D aircraft.

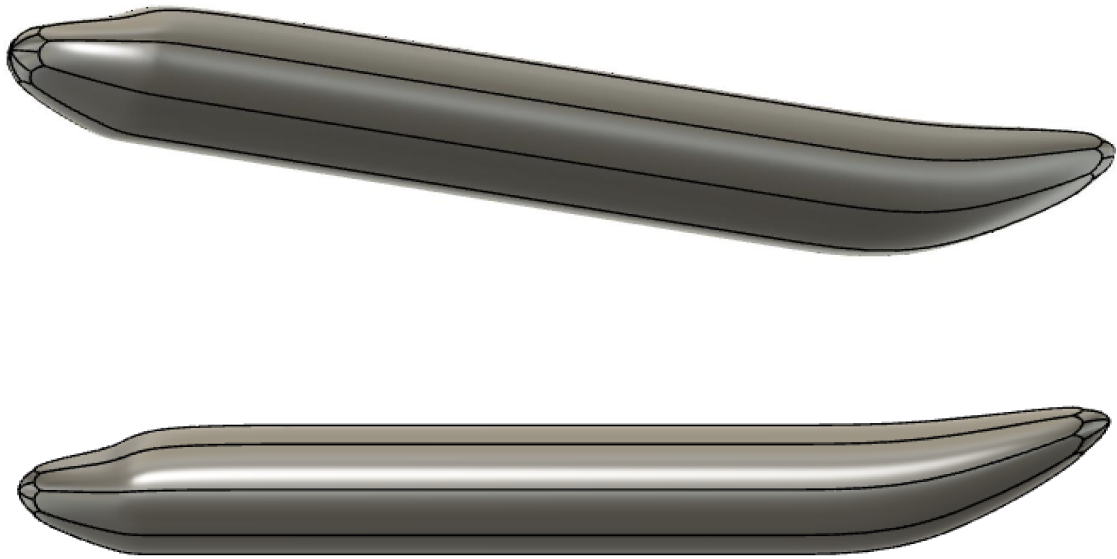


Figure 5.5: Two different views of the proposed aircraft.

5.4 DISCUSSION

In the design process of an aircraft, after the mission requirements are set and the mission weight is determined, the fuselage and the cockpit must be designed to satisfy all the requirements. At this step the aircraft starts to take a shape. In cockpit and fuselage design crew seats and passengers seats must be designed. In designing the pilot seats appropriate view and positioning so that the pilot is able to reach all controls must be taken into account. In designing the fuselage passenger comfort, aisle size, attendant seat, galley and lavatories must be considered. The mission requirement of this aircraft states that 2 pilots are needed and as such the cockpit is designed. The mission requirement also states that there are 40 passengers and 10 rows with 2 passengers abreast are required. As such the fuselage is designed. The aircraft, all parts given above combined, looks like what is given in the figure below momentarily.

CHAPTER 6--Wing Planform Design

6.1 INTRODUCTION

In previous works the area of the wing was determined. The purpose of this chapter is to determine the structure of the wing with its parameters. The lift coefficients needed for takeoff, cruise, and landing were determined during preliminary performance sizing. In this chapter, the airfoil will be picked so that the lift requirements are satisfied. If the lift coefficients are not satisfied with plain wing high lift devices will be designed. From previous works the wing is configured low so that the cargo space can be available for payload. However, since the aircraft has a mission requirement of higher subsonic speed, the wing must be swept. The sweeping of the wing means higher structural weight. As a result the wing sweep must be determined so that wing alone is not structurally heavier than the takeoff weight. The sweep of the wing helps to increase critical Mach number. However, sweeping also affects other parameters and it should be done carefully. In this work, the parameters related to the wing will be determined along with the sweep.

6.2 Wing Planform Design

From preliminary performance sizing the following wing parameters were determined.

- Gross area of the wing: $S = 728ft^2$
- Aspect ratio of the wing: $AR = 10$
- Span of the wing: $b = \sqrt{SAR} = 85ft$

These are not the only parameters that describe the wing. For the wing to have lateral stability a dihedral angle must be chosen since the wing is configured low. The taper ratio must also be selected from similar aircraft. The following values are appropriate based on similar aircraft.

- Taper ratio=0.25
- Dihedral angle=2.5°

6.2.1 Sweep Angle - Thickness Ratio Combination

The proposed hybrid electric aircraft is required to fly at $M = 0.93$ (high subsonic speed). As a result, the trade between thickness ratio and sweep angle turns out to be a deciding factor in the design of the wing. The relationship between thickness ratio and sweep angle is given by:

$$\begin{aligned} & \frac{0.8649 \cos^2(y)}{\sqrt{1 - 0.8649 \cos^2(y)}} \left(\frac{3.168 x}{\cos(y)} + 1.616 \times \frac{x}{\cos^3(y)} \right) + \\ & \frac{0.8649 \cos^2(y)}{1 - 0.8649 \cos^2(y)} \left(2.091 \times \frac{x^2}{\cos^2(y)} \right) + \\ & 0.8649 \cos^2(y) \left(1 + \frac{1.224}{\cos^2(y)} + \frac{0.3121}{\cos^4(y)} \right) = 1 \quad w \end{aligned} \tag{6.1}$$

Where $y = \Lambda_c$ and t/c .

Since the critical lift coefficient of the proposed aircraft is 0.2, the following graph from [1] can be used for the relationship between sweep angle and thickness ratio.

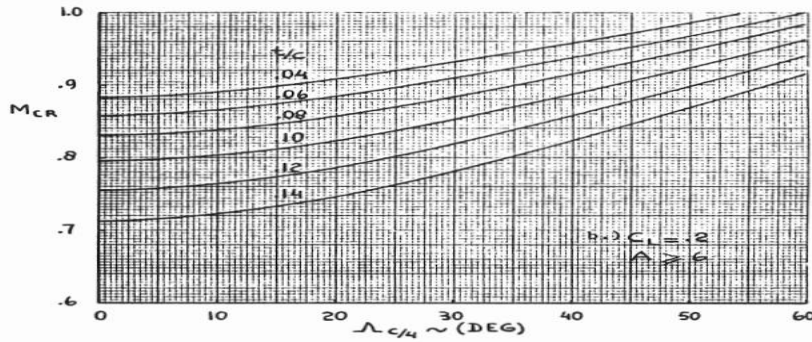


Figure 6.1: Relationship between thickness ratio and sweep angle.

From figure 6.1 a thickness of wing root 0.12 and thickness of wing tip 0.10 is appropriate with the corresponding wing sweep of 32° . As stated before the wing weight also depends on the sweep angle of the wing. It must be verified that this sweep angle is appropriate by studying the trade between wing sweep and wing weight. The dependence of wing weight on wing sweep is given by:

$$y = 92.2828 \left(\frac{85}{\cos(x)} \right)^{0.75} \left(1 + \sqrt{0.074 \cos(x)} \right) \left(3.5 \left(\frac{1.117}{\cos(x)} \right)^{0.3} \right) \quad (6.2)$$

where $y = w_w$ and $\frac{\Lambda_c}{2}$. By substituting a range of half chord sweep angles the following table of values can be produced.

Table 6.1: Half-chord sweep angle versus wing weight.

$\frac{\Lambda_c}{2}$	0	10	20	30	40	50	60	70	80
w_w	11,889	12,062	12,608	13,622	15,309	18,108	23,075	33,421	65,410

The half-chord sweep angles and wing weights given in table 6.1 can be plotted as follow.

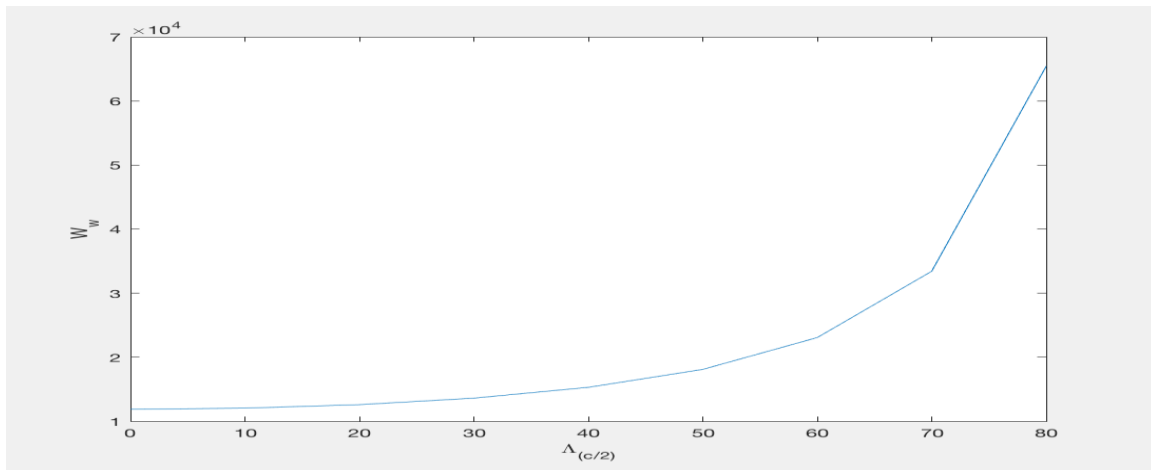


Figure 6.2: Relationship between half-chord sweep and wing weight.

Low subsonic speed flights prefer wing that is not swept. However, since the hybrid electric aircraft is required to fly at high subsonic speed, the wing must be swept. The wing is swept at the cost of gaining structural weight. Sweeping the wing also causes low performance at low subsonic speeds. In figure 6.2 above it is clear that the wing sweep greatly affects the weight of the wing. What is interesting is that the weight of the wing is greater than the empty weight of the proposed aircraft at 60° . This implies that the wing sweep must be chosen carefully and the wing sweep for this aircraft is chosen to be 32° which is reasonable according to figure 6.2.

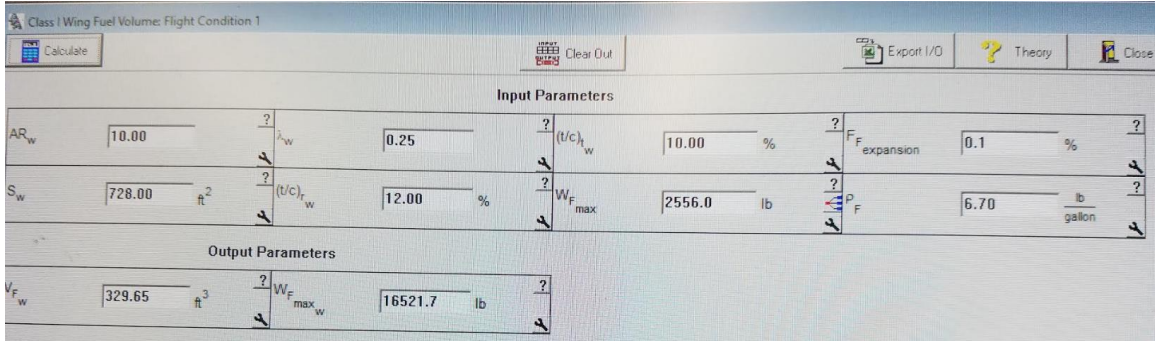
6.3 AIRFOIL SELECTION

One very important task in designing the wing of an aircraft is selecting the airfoil. Selection of airfoil mainly depends on section drag coefficient, section lift coefficient, section critical Mach number, and section moment coefficient. For the sweep angle and thickness ratio selected in the previous section a supercritical derivative of NACA64A410 is appropriate. The following parameters are also reasonable for the hybrid electric aircraft.

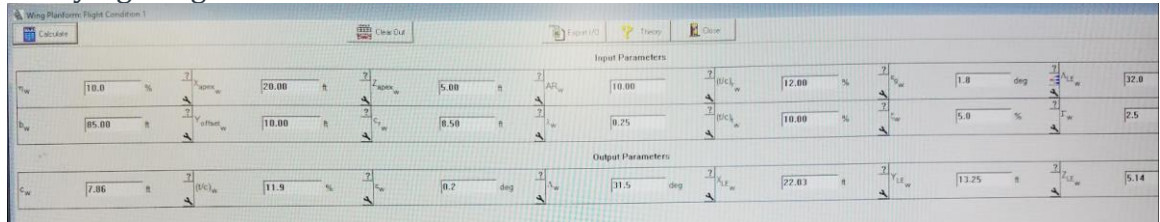
- Incidence angle: $i_w = 1.4^\circ$

- Twist angle at the tip: $\epsilon_t = -1.8^\circ$

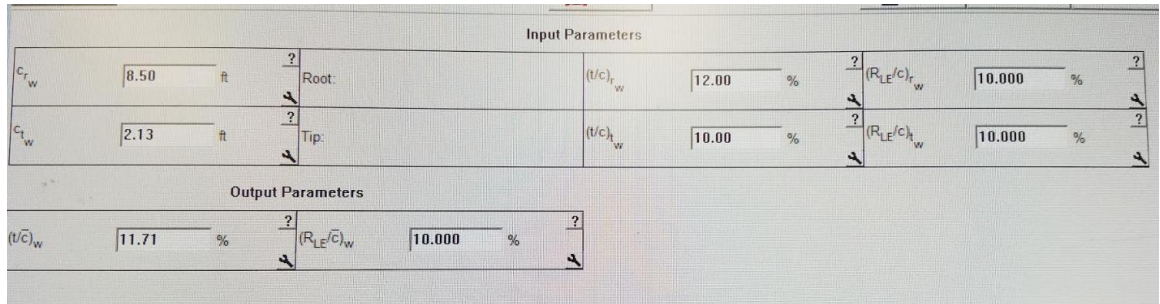
6.4 WING DESIGN EVALUATION



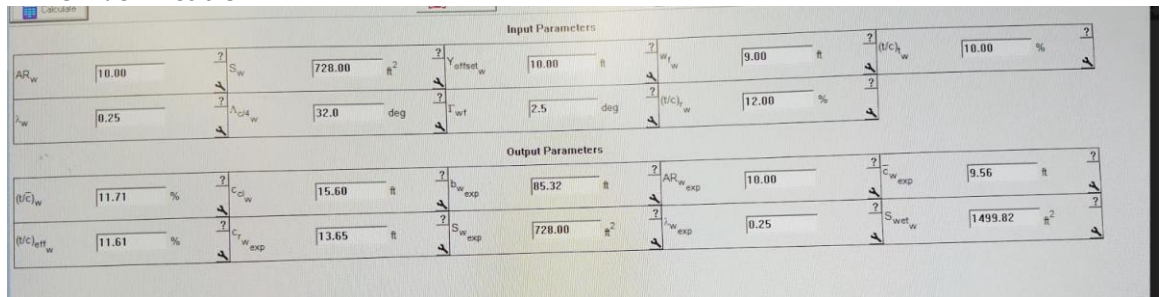
a) Verifying wing fuel volume



b) Chord thickness verification



c) Airfoil verification



d) Wing exposed verification

Figure 6.3: AAA Wing Design Evaluation

6.5 DESIGN OF THE HIGH-LIFT DEVICES

From preliminary performance sizing:

- $C_{L_{max_{TO}}} = 1.8$
- $C_{L_{max_L}} = 2.8$
- $C_{L_{max}} = 1.5$

In this work it is necessary to verify whether or not the wing geometry selected is consistent with the required lift. If the wing is not able to provide the required lift, high lift devices must be added. To summarize the following set of wing parameters are determined so far.

$$\Rightarrow A = 10, S = 728ft^2, b = 85ft, \Lambda_c = 32^\circ$$

$$\Rightarrow \lambda = 0.25, c_r = 8.5ft, c_t = 2.125ft$$

To calculate the maximum lift coefficient of the aircraft, Reynold's number s of the root and the tip should be calculated as follow.

$$R_{nr} = \frac{(0.002378)(209)(8.5)}{3.737 * 10^{-7}} = 10.3 * 10^6$$

$$R_{nt} = 2.83 * 10^6$$

Note that a speed of $\frac{209f}{s}$ is used to calculate Reynold's number.

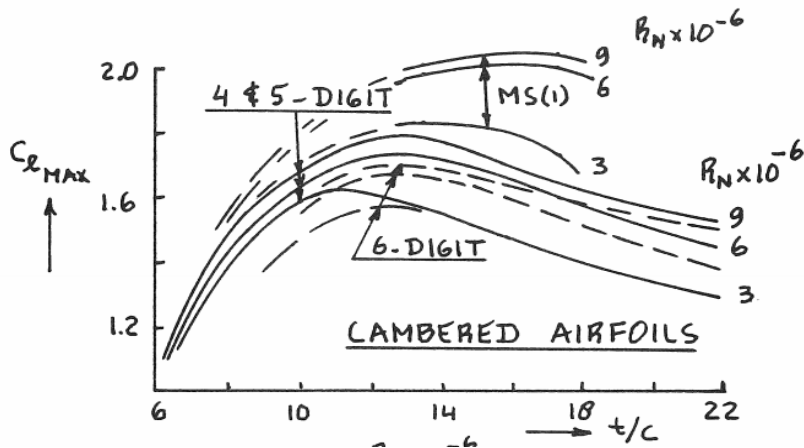


Figure 6.4: Effect of Reynold's number on section maximum lift curve of a cambered airfoil (Roskam Vol II)

From figure 6.3 it is clear that a root airfoil with $\frac{t}{c} = 0.12$ produces $C_{L_{max}} = 2.0$. A tip airfoil of thickness $\frac{t}{c} = 0.1$ produces $C_{L_{max}} = 1.8$. From these two values the lift coefficient of the whole wing can be calculated as

$$C_{L_{max_w}} = \frac{0.95(2.0+1.8)}{2} = 1.805 \quad (6.3)$$

Since the wing has aft sweep of 32° the effect of sweeping must be taken into consideration as:

$$C_{L_{max_w}} = 1.805 \cos(32^\circ) = 1.44 \quad (6.4)$$

The lift coefficient of the wing after the wing sweep is taken into consideration is very close to $C_{L_{max}} = 1.5$ which was determined from previous works.

Even though the lift coefficient calculated with the wing sweep is close to the cruise lift coefficient, the wing alone is not sufficient to provide the required lift during landing and takeoff. As a result, a high lift device system must be designed on the wing. The high lift device (flaps in this case) lift increments can be calculated as:

$$\Delta C_{L_{max_{TO}}} = 1.05(1.8 - 1.5) = 0.315 \quad (6.5)$$

$$\Delta C_{L_{max_L}} = 1.05(2.8 - 1.5) = 1.370 \quad (6.6)$$

From equation (6.6) above it is clear that the required flap lift during landing is large. Therefore, there might be a need for Fowler flaps.

Now it is possible to compute the required incremental section maximum lift coefficient with the flaps down using:

$$\Delta C_{l_{max}} = \frac{\Delta C_{L_{max}} \left(\frac{S}{S_{wf}} \right)}{k_A} \quad (6.7)$$

where

$$k_A = \left(1 - 0.08 \cos^2 \Lambda_c \right) \cos^{\frac{3}{4}} \left(\Lambda_c \right) = 0.824 \quad (6.8)$$

At this stage it is appropriate work with $\frac{S_{wf}}{S}$ values of 0.6 and 0.8.

Table 6.2: Takeoff Flaps

$\frac{S_{wf}}{S}$	0.6	0.8
$\Delta C_{l_{max}}$	0.64	0.48

Table 6.3: Landing Flaps

$\frac{S_{wf}}{S}$	0.6	0.8
$\Delta C_{l_{max}}$	2.77	2.08

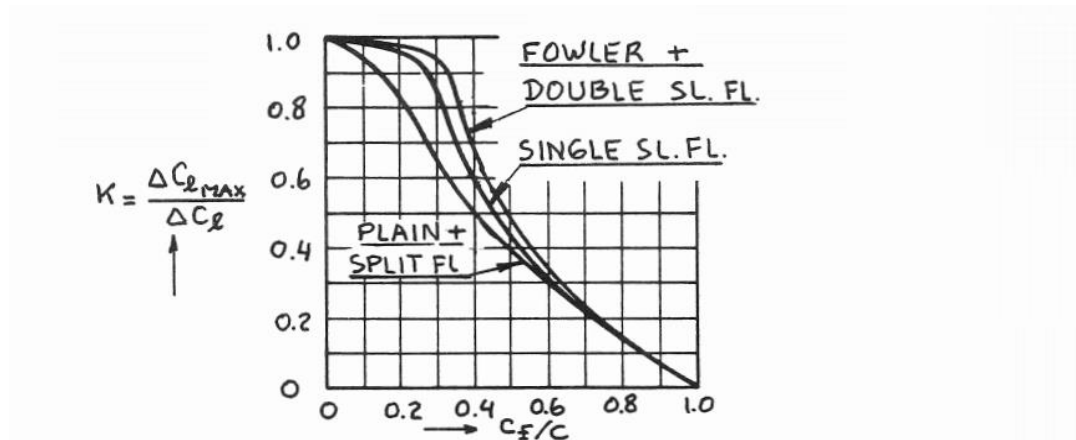


Figure 6.5: Relationship between lift coefficient ratio and chord ratio.

From figure 6.4 above for $k = 0.9, \frac{c_f}{c} = 0.3$. Deflection of flaps at takeoff and landing can be guessed to be 30° and 35° respectively. Now we can find Δc_l at landing and takeoff as follow.

Table 6.4: Takeoff flaps.

$\frac{S_{wf}}{S}$	0.6	0.8
$\Delta C_{l_{max}}$	0.67	0.53

Table 6.5: Landing flaps.

$\frac{S_{wf}}{S}$	0.6	0.8
$\Delta C_{l_{max}}$	3.07	2.31

The lift slope of the flaps is, therefore, $c_{l_{\alpha_f}} = 8$ and the lift increment is $\Delta c_l = 0.998$. The flaps run from root to tip so there is no need to leading edge high lift devices.

6.5.1 Design of the Lateral Control Surfaces

Ailerons and spoilers must be designed for lateral control purposes. Since flaps will be cut out because of the engine exhaust inboard ailerons will run from $\frac{0.2b}{2}$ to $\frac{0.3b}{2}$ along the wingspan. A chord ratio of 0.3 will be selected for the inboard ailerons, which are used for trim. Since flaps run full span, spoilers will also be needed. The positions of each control surface is as summarized below.

- ⇒ Inboard span fraction: 0.40
- ⇒ Inboard chord fraction: 0.20

- ⇒ Outboard span fraction: 0.70
- ⇒ Outboard chord fraction: 0.20
- ⇒ Hinge line: $0.70c$

Using aileron and flap chord ratio of 0.3, the rear spar will be at;

$$(1 - 0.30 - 0.005)c = 0.695c \quad (6.9)$$

while the front spar will be at $0.20c$.

6.6 DRAWINGS

From findings of previous sections, the following wing parameters are recorded and they are labeled on figure 6.5 below.

- ⇒ $b = 85ft, c_t = 2.125, c_r = 8.5$
- ⇒ Mean aerodynamic chord=5.95ft
- ⇒ Leading edge sweep angle= 32°
- ⇒ Trailing edge sweep angle= 15°
- ⇒ Coordinates of aerodynamic center= $(4.2,10)$

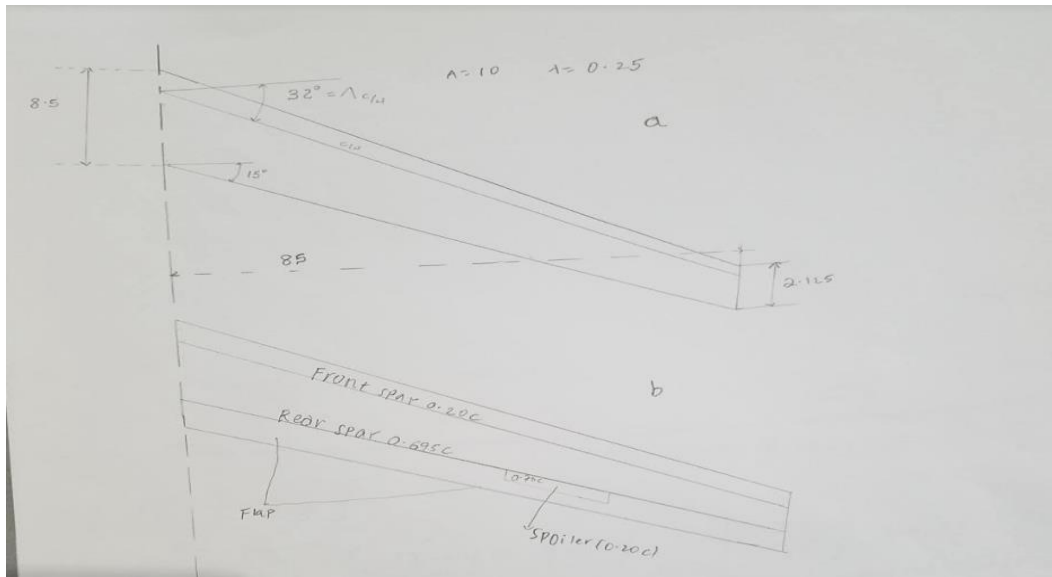


Figure 6.6: a) Wing Planform For the Hybrid Aircraft. B) Flap and Lateral Control Layout.

The wing fuel volume of this aircraft is $V_{wf} = 331ft^3$ which implies that the wing can carry 2,256lb of fuel that is required for taxi, takeoff, and climb.

6.7 DISCUSSION

In this work the wing is designed. The wing alone failed to give the required lift for landing and takeoff. As a result, high lift devices are added to it. Lateral control surfaces are also added on the wing. The complete airplane with the wing platform, the high lift devices, and the lateral control surfaces is shown in figure 6.6 below.

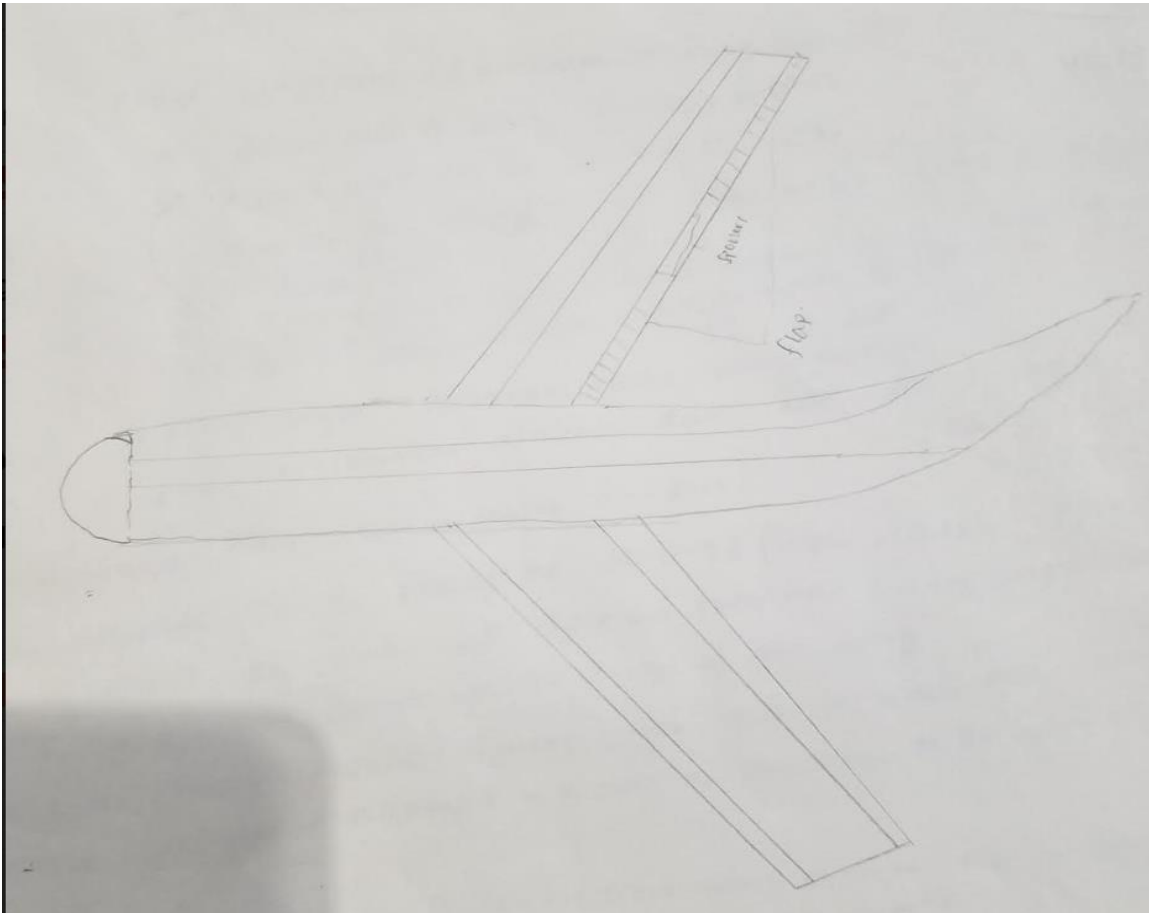


Figure 6.7: The Complete Airplane to Date.

6.8 CONCLUSIONS

The hybrid electric aircraft under design is required to fly at high subsonic speed per its mission requirements. As a result, the wing that was determined to have area of $728ft^2$ must be positioned to be effective at high subsonic speeds. The only way to suite it to high subsonic speeds is by sweeping the wing. However, sweeping the

wing increases the structural weight greatly. This aspect of the design was investigated and a reasonable sweep angle that minimizes the wing weight is selected. The wing itself is not able to provide the lift requirements for landing and takeoff. To compensate for the inability of the wing to provide enough lift a high lift device is designed and shown in the control surfaces layout. To date the aircraft is designed to provide enough lift and performance at high subsonic speeds.

CHAPTER 7---DESIGN OF THE EMPENNAGE & THE LONGITUDINAL AND DIRECTIONAL CONTROLS

7.1 Introduction

According to the configuration design of the hybrid electric aircraft under design, the aircraft has horizontal stabilizer and vertical tail. Having determined the size and the aerodynamic center of the wing along with other parameters, it is now time to determine the size and the disposition of the empennage along with the longitudinal and directional control surfaces. Most aircrafts depend on the tail for stability and control. This aircraft is not an exception to the fact that horizontal stabilizer balancing the moment from all other aerodynamic surfaces. In this work the sizes of the horizontal and vertical stabilizer along with other parameters will be determined.

7.2 Overall Empennage Design

From previous works it was determined that the aircraft has a conventional empennage configuration. That implies aft tail configuration. From general arrangement drawing of previous works the following moment arms of the horizontal stabilizer and the vertical tail can be estimated.

$$\Rightarrow x_h = 35ft$$

$$\Rightarrow x_v = 40ft$$

where x_h and x_v are moment arms of the horizontal and the vertical stabilizers measured from the center of mass (cm) of the aircraft. Estimating the moment arms of the horizontal and vertical stabilizers is not sufficient in sizing the empennage. Sizing the empennage is determining S_h and S_v , which are the area of the horizontal stabilizer and the vertical stabilizer respectively. The most efficient method of determining the size of the empennage is the \bar{V} method. This method is a process of selecting airplanes that are comparable to the aircraft under design and picking reasonable values of tail volume coefficient both for the horizontal and vertical

stabilizers. The tail volume coefficients for the horizontal and vertical tail are given by:

$$\bar{V}_h = \frac{x_h S_h}{S \bar{c}} \quad (7.1)$$

$$\bar{V}_v = \frac{x_v S_v}{S b} \quad (7.2)$$

In the equations above \bar{c} and b are the mean aerodynamic chord and the span of the wing.

To determine the tail volume coefficients of the horizontal and the vertical stabilizers the following comparable aircrafts best fit the hybrid electric aircraft.

Table 7.1: Empennage sizes of comparable aircrafts.

<i>Airplane Type</i>	\bar{V}_h	S_e/S_h	\bar{V}_v	S_r/S_v
<i>Fokker F – 28</i>	1.07	0.20	0.085	0.16
<i>Boeing 737</i>	1.28	0.27	0.100	0.24
<i>DC – 9 – 50</i>	1.32	0.38	0.079	0.41
<i>BA 146 – 200</i>	1.48	0.39	0.12	0.44
<i>Average</i>	1.29	0.31	0.096	0.31

For the hybrid electric aircraft under design the following values are reasonable in comparison with the table 7.1 above.

$$\Rightarrow V_h = 0.70, \frac{S_e}{S_h} = 0.30, \bar{V}_v = 0.05, \frac{S_r}{S_v} = 0.31$$

With the estimated values of the moment arms and the tail volume coefficients the sizes of the horizontal and vertical stabilizers can be calculated using equations (7.1) and (7.2) above.

$$S_h = \frac{\bar{V}_h S \bar{c}}{x_h} = \frac{(0.70)(728ft^2)(6ft)}{35ft} = 87.36ft^2 \quad (7.3)$$

$$S_v = \frac{\overline{V}_v S b}{x_v} = \frac{(0.050)(728ft^2)(85ft)}{40ft} = 77.35ft^2 \quad (7.4)$$

7.3 Design of the Horizontal Stabilizer

Based on the calculations in the previous section the following horizontal stabilizer parameters are selected.

- ⇒ Aspect ratio=3.5 from which $b_h = \sqrt{(3.5)(87.36)} = 17.47ft$
- ⇒ Taper ratio=0.30. This was selected so that the taper ratio is not very different from the taper ratio of the wing.
- ⇒ Sweep angle= 35° . The sweep angle of the horizontal stabilizer must be greater than the sweep angle of the wing. This is because the M_{crit} of the horizontal stabilizer must be greater than M_{crit} of the wing.
- ⇒ Thickness ratio=0.13.
- ⇒ Airfoil: NACA 0012, which is common for empennage.
- ⇒ Incidence angle is variable.
- ⇒ Dihedral angle= 1° .

These horizontal stabilizer parameters are in complete agreement with horizontal stabilizer data of jet transport data presented below.

F

Type	Dihedral Angle, Γ_h deg.	Incidence Angle, i_h deg.	Aspect Ratio, A_h	Sweep Angle, $\Delta C/4_h$ deg.	Taper Ratio, λ_h
Homebuilts	+5 - -10	0 fixed to variable	1.8 - 4.5	0 - 20	0.29 - 1.0
Single Engine Prop. Driven	0	-5 - 0 or variable	4.0 - 6.3	0 - 10	0.45 - 1.0
Twin Engine Prop Driven	0 - +12	0 fixed to variable	3.7 - 7.7	0 - 17	0.48 - 1.0
Agricultural	0 - +3	0	2.7 - 5.4	0 - 10	0.59 - 1.0
Business Jets	-4 - +9	-3.5 fixed	3.2 - 6.3	0 - 35	0.32 - 0.57
Regional Turbo-Props.	0 - +12	0 - 3 fixed to variable	3.4 - 7.7	0 - 35	0.39 - 1.0
Jet Transports	0 - +11	variable	3.4 - 6.1	18 - 37	0.27 - 0.62
Military Trainers	-11 - +6	0 fixed to variable	3.0 - 5.1	0 - 30	0.36 - 1.0
Fighters	-23 - +5	0 fixed to variable	2.3 - 5.8	0 - 55	0.16 - 1.0
Mil. Patrol, Bomb and Transports	-5 - +11	0 fixed to variable	1.3 - 6.9	5 - 35	0.31 - 0.8
Flying Boats, Amph. and Float Airplanes	0 - +25	0 fixed	2.2 - 5.1	0 - 17	0.33 - 1.0
Supersonic Cruise Airplanes	-15 - 0	0 fixed to variable	1.8 - 2.6	32 - 60	0.14 - 0.39

Figure 7.1: Horizontal Tail Parameter Range for Different airplanes.

7.4 Design of the Vertical Stabilizer

From the calculation in equation (7.4) and comparable aircraft data the following vertical stabilizer parameters are reasonable for the hybrid electric aircraft that is under design.

- ⇒ Aspect ratio=1.5 from which $b_v = \sqrt{(1.5)(77.35)} = 10.88ft.$
- ⇒ Taper ratio=0.30
- ⇒ Sweep angle= 40^0 . This is again to delay the formation of shock waves (so that Mach 1 is not reached here before the wing).
- ⇒ Thickness ratio=0.14
- ⇒ Airfoil is selected to be NACA 0015, which is common for vertical tail.
- ⇒ Incidence angle= 0^0
- ⇒ Dihedral angle= 90^0 which is why it is called vertical stabilizer.

This choice of parameters is in range with the jet transport data or vertical tail given in figure 7.2 below.

Type	Dihedral Angle, Γ_v deg.	Incidence Angle, i_v deg.	Aspect Ratio, A_v	Sweep Angle, $\Delta_c/4_v$ deg.	Taper Ratio, λ_v
Homebuilts	90	0	0.4 - 1.4	0 - 47	0.26 - 0.71
Single Engine Prop. Driven	90	0	0.9 - 2.2	12 - 42	0.32 - 0.58
Twin Engine Prop Driven	90	0	0.7 - 1.8	18 - 45	0.33 - 0.74
Agricultural	90	0	0.6 - 1.4	0 - 32	0.43 - 0.74
Business Jets	90	0	0.8 - 1.6	28 - 55	0.30 - 0.74
Regional Turbo-Props.	90	0	0.8 - 1.7	0 - 45	0.32 - 1.0
Jet Transports	90	0	0.7 - 2.0	33 - 53	0.26 - 0.73
Military Trainers	90	0	1.0 - 2.9	0 - 45	0.32 - 0.74
Fighters	75 - 90	0	0.4 - 2.0	9 - 60	0.19 - 0.57
Mil. Patrol, Bomb and Transports	90	0	0.9 - 1.9	0 - 37	0.28 - 1.0
Flying Boats, Amph. and Float Airplanes	90	0	1.2 - 2.4	0 - 32	0.37 - 1.0
Supersonic Cruise Airplanes	75 - 90	0	0.5 - 1.8	37 - 65	0.20 - 0.43

Figure 7.2: Vertical Tail Parameter Range for Different Group of Airplanes.

7.5 Empennage Design Evaluation

The following two figures are from AAA program. The output parameters from the program are very close to the calculated values.

Input Parameters							
b_h	17.47 ft	c_{r_h}	8.00 ft	c_{t_h}	2.00 ft	$\Delta_c/4_h$	35.0 deg
Output Parameters							
S_h	87.35 ft ²	λ_h	0.25	y_{mgc_h}	3.49 ft	Δ_{LE}_h	41.1 deg
AR_h	3.49	c_h	5.60 ft	x_{mgc_h}	3.05 ft	Δ_{TE}_h	10.5 deg
Straight Tapered Horizontal Tail Geometry: Output Parameters							
Panel	c_r ft	c_t ft	X_r ft	X_t ft	Y_r ft		
1	8.0000	2.0000	0.0000	7.6163	0.0000		

Figure 7.3: AAA Program Evaluation of the Horizontal Stabilizer

Input Parameters							
b_v	11.00 ft	c_{r_v}	11.00 ft	c_{t_v}	3.00 ft	$\Lambda_{cl}^4_v$	40.0 deg
Output Parameters							
S_v	77.00 ft ²	λ_v	0.27	z_{mgc_v}	4.45 ft	Λ_{LE}_v	45.6 deg
AR_v	1.57	\bar{c}_v	7.76 ft	x_{mgc_v}	4.55 ft	Λ_{TE}_v	16.4 deg
Straight Tapered Vertical Tail Geometry: Output Parameters							
Panel	c_r ft	c_t ft	X_r ft	X_t ft	Z_r ft		
1	11.0000	3.0000					

Figure 7.4: AAA Program Evaluation of the Vertical Stabilizer

7.6 DESIGN OF THE LONGITUDINAL AND DIRECTIONAL CONTROLS

On the horizontal stabilizer there are two elevators, which control longitudinal stability. The sizes of these elevators can be determined from the ratio of the areas of the horizontal stabilizer and the elevator selected based on similar aircraft data. It was determined that $\frac{S_e}{S_h} = 0.30$. It was also calculated that $S_h = 87.36ft^2$. From these values, $S_e = 26.27f$.

On the vertical stabilizer is a rudder that provides directional stability. The size of the rudder must be determined carefully for effective directional control during adverse yaw and crosswind landing. From the calculation in equation (7.4) and the selection of the ratio of control surfaces to lifting surfaces $S_r = 23.98ft^2$.

7.7 DRAWINGS

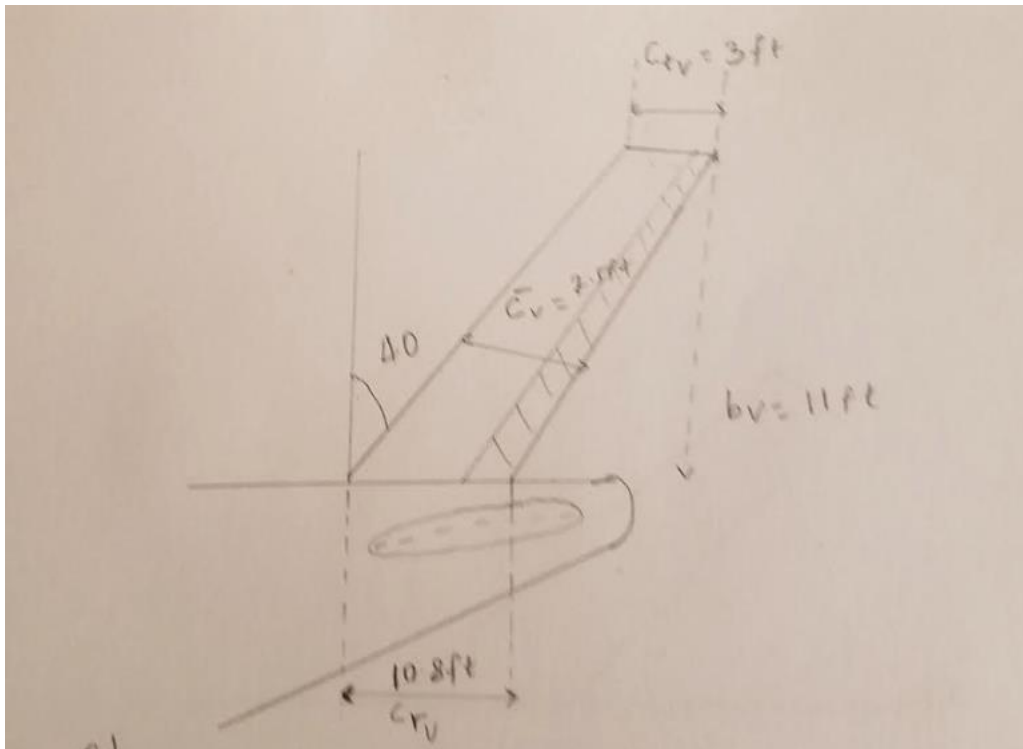


Figure 7.5: Vertical Stabilizer and the Rudder

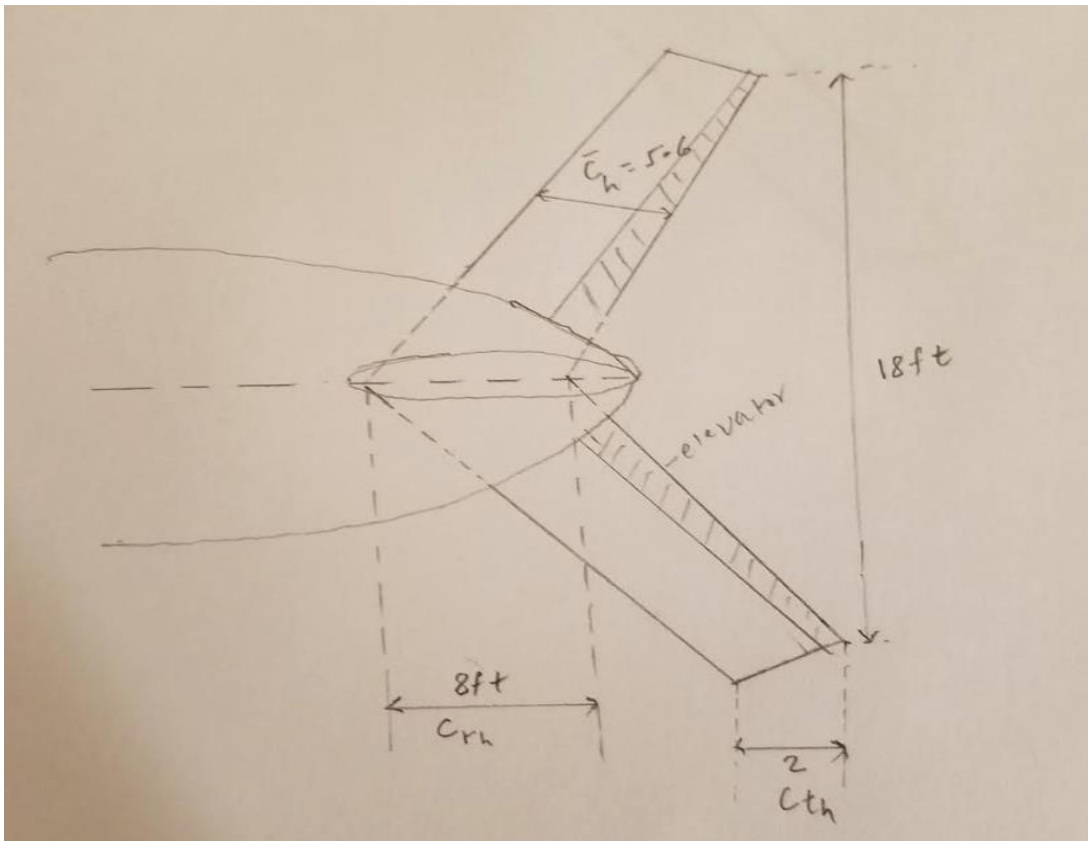


Figure 7.6: Planform of the Horizontal Stabilizer and the Elevator.

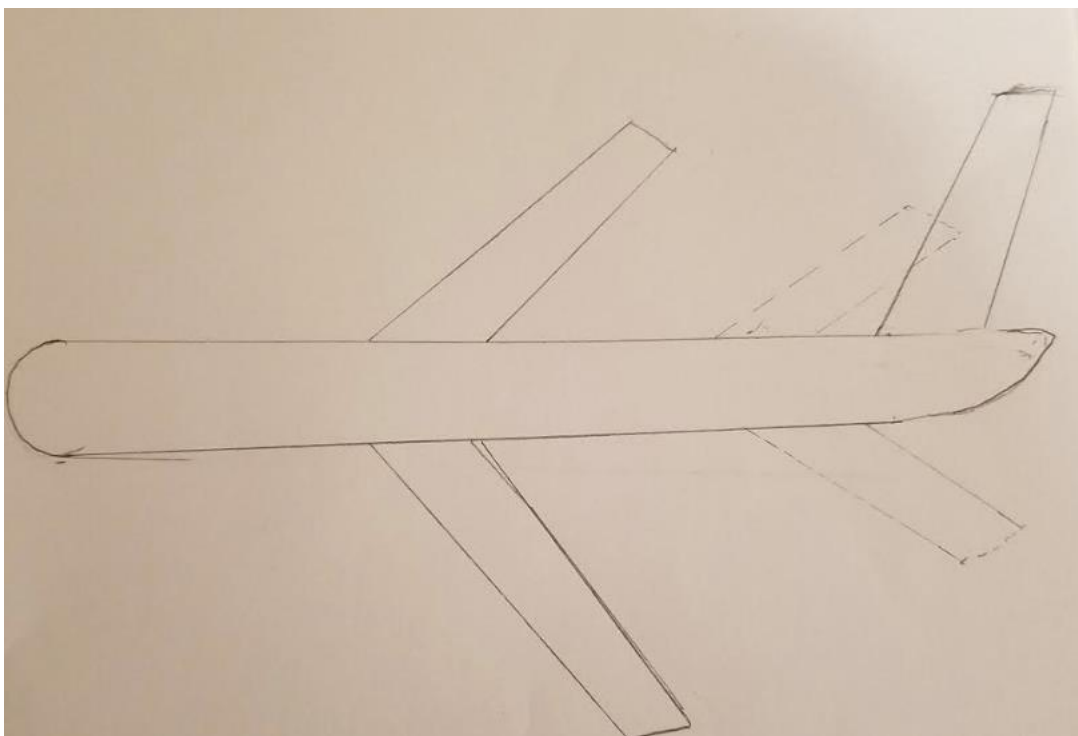


Figure 7.7: The Complete Drawing of the Aircraft to Date.

7.8 DISCUSSION

In configuration design, it was determined that the empennage would be a conventional one. However, the size of the empennage was not determined. In this work the size of the empennage is determined. The sizes of the control surfaces on the empennage are also determined. The area and other parameters of the horizontal stabilizer, the vertical stabilizer, the elevator, and the rudder are determined and summarized in table 7.2 below.

Table 7.2: Summary Empennage and Control Surfaces

Surface	<i>Area(ft²)</i>
Horizontal stabilize	87.36
Vertical stabilizer	77.35
Elevator	26.27
Rudder	23.98

7.8 CONCLUSIONS

In this work the sizes of horizontal stabilizer and the vertical stabilizer are determined. From preliminary sizing of the wing the directional control surface was determined. In empennage design the longitudinal and lateral control surfaces are determined. Now the aircraft has longitudinal, lateral, and directional control surfaces designed. The aircraft also has a stabilizing tail and the pitching moment coefficient is now negative and the aircraft is longitudinally stable.

Chapter 8--Landing Gear Design; Weight and Balance Analysis

8.1 Introduction

Designing the landing gear of an aircraft takes an immense part of the stability of the aircraft. From previous works weights of different components and the takeoff weight of the hybrid electric aircraft was determined. However, the determination takeoff weight and the weights of other components is not enough in the preliminary design process. It is necessary to determine the center of mass of the aircraft for different loading scenarios. That center of mass plays a great role in the disposition of the landing gear. If the landing gear is placed before the most aft center of mass position, then the aircraft will experience a longitudinal tip over. The most forward center of mass must also be place in such a way that the aircraft does not tip over. The landing must be designed to satisfy the tip over criteria, the ground clearance criteria, and the retraction criteria. The landing gear must also be designed to minimize the structural weight of the aircraft. In this work the landing gear of the hybrid electric aircraft will be designed to satisfy the weight and balance requirements.

8.2 Component Weight and Balance Analysis

From preliminary weight sizing the following weight data was found.

Table 8.1: Weight data of the hybrid electric aircraft under design.

Gross takeoff weight	56,840 <i>lb</i>
Empty weight	33,734 <i>lb</i>
Mission fuel weight	2,256 <i>lb</i>
Payload weight	9,215 <i>lb</i>
Crew weight	525 <i>lb</i>
Trapped fuel and oil weight	28 <i>lb</i>
Flight design gross weight (GW)	56,840 <i>lb</i>

Note that all measurements in table 1 are in lbs.

To study the component weight breakdown, the following components are considered.

- ⇒ Wing
- ⇒ Empennage
- ⇒ Fuselage
- ⇒ Landing gear
- ⇒ Nacelles
- ⇒ Power plant
- ⇒ Fixed equipment

Weight fractions of each component can be found from comparable aircraft data and by taking the average as presented in table 2 below.

Table 8.2

Types	Fokker 614	Sud AC	Fokker 28-1000	BAC 1-11/30	Average
Power plant/GW	0.107	0.079	0.083	---	0.095
Fixed equip/GW	0.161	0.145	0.145	0.149	0.152
Empty/GW	0.586	0.590	0.480	0.560	0.554
Wing/GW	0.141	0.134	0.113	0.111	0.125
Emp/GW	0.027	0.018	0.025	0.027	0.024
Fuselage/GW	0.128	0.105	0.108	0.112	0.113
Nace/GW	0.024	0.014	0.013	In fuse	0.017
Gear/GW	0.040	0.046	0.042	0.033	0.040

From preliminary weight sizing the empty weight of the hybrid electric aircraft was determined to be 33,734lb. We can take the ratio to verify that the

fraction in the table is accurate. The empty weight to design gross weight is 0.59, which is not drastically different from the fraction table 8.2, which is 0.55.

Using the average component weight fraction in table 8.2 above the following component weight summary can be determined.

Table 8.3: Component weight breakdown

Wing	7,100 <i>lb</i>
Empennage	1,363 <i>lb</i>
Nacelles	965 <i>lb</i>
Fuselage	6,418 <i>lb</i>
Landing gear	2,272 <i>lb</i>
Power plant	5,396 <i>lb</i>
Fixed equipment	8,633 <i>lb</i>
Empty weight	32,147 <i>lb</i>

The weight of each major component is listed in the table above. It is very crucial to determine the center of gravity of each major component. There is a convention as to where the center of gravity of major components should be placed and it is summarized below.

- ⇒ Wing: Since the aircraft under design has a swept wing the cg of the wing should be 70% of the distance between the front and rear spar behind the front spar at 35% of the semi span.
- ⇒ Horizontal tail: Regardless of sweep angle cg should be placed 42% chord from leading edge at 38% of the semi span
- ⇒ Vertical tail: 42% chord from leading edge at 38% vertical span
- ⇒ Fuselage: 0.42-0.45 times the fuselage length
- ⇒ Nacelles: 0.40 of nacelle length from nacelle nose
- ⇒ Landing gear: at 0.50 of the strut length

The following figure is taken from Roskam to summarize the summary above.

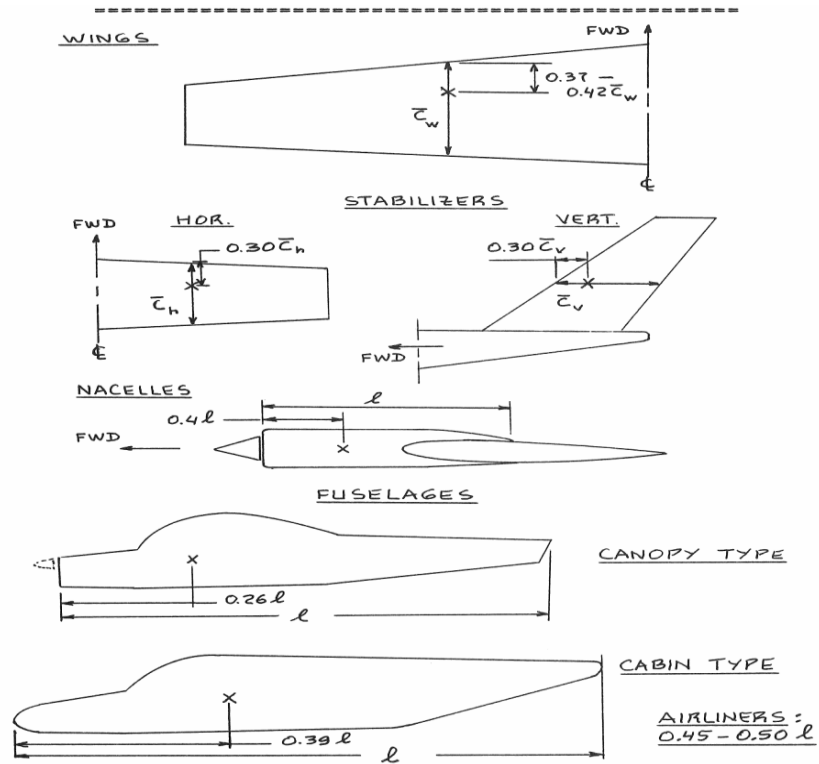


Figure 8.1: Approximate cg of different components (Taken from Roskam).

The placement of the cg of the main component for the hybrid electric aircraft under design is shown in figure 8.2 below.

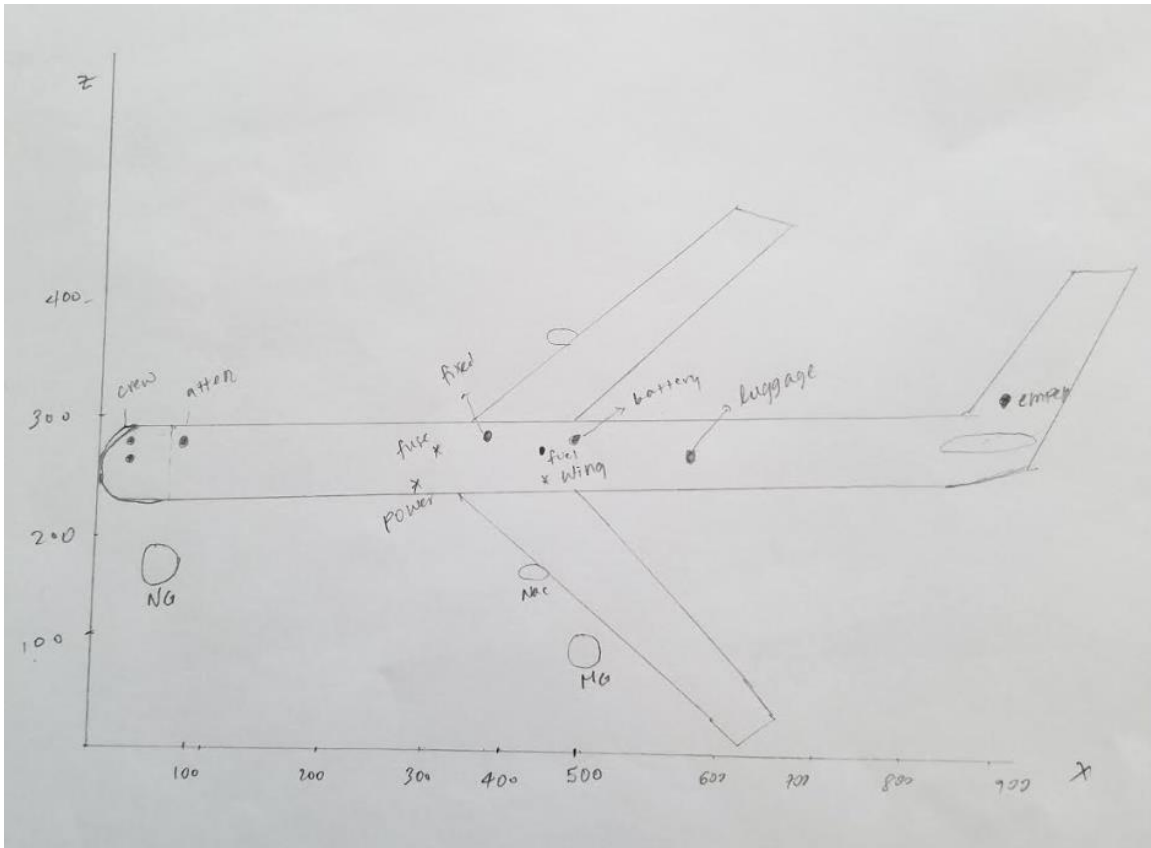


Figure 8.2: cg of major components (axes are labeled in inches).

From the component center of gravity figure above the following component weight and coordinate data can be extracted.

Table 8.3: Component weight and Coordinate Data.

	Weight (lb)	x(in)	Wx(lb-in)	y(in)	Wy(lb- in)	z(in)	Wz(lb-in)
Wing	7,100	500	355,000	0	0	220	1,562,000
Empennage	1,363	900	1,226,700	0	0	260	354,380
Fuselage	6,418	355	2,278,390	0	0	250	1,604,500
Nacelles	965	510	492,150	0	0	150	144,750
Landing NG	400	90	3,600	0	0	120	48,000
Landing MG	1,872	560	1,048,320	0	0	95	177,840
Power plant	5,396	400	2158400	0	0	205	1,106,180
Fixed equip	8,633	570	4,920,810	0	0	270	2,330,910
Empty weight	32,147	500	16,073,500	0	0	220	7,072,340
Fuel	2,256	510	1,128,000	0	0	200	451,200
Pilots	350	90	31,500	0	0	260	9,100
Attendant	175	120	21,000	0	0	260	45,500
Luggage	1,690	580	980,200	0	0	230	388,700
Battery	11,360	510	5,793,600	0	0	250	2,840,000
Takeoff weight	56,840	505	28,704,200	0	0	255	14,494,200

8.21 Determining Center of Gravity for different Loading Scenarios

From the weight component and coordinate data cg for different loading scenarios can be determined and plotted. A sample calculation is given below.

$$x_{cg_{W_E}} = \left(\sum_{i=1}^{i=6} W_i x_i \right) / W_E$$

8.1

Putting numbers in from table 8.3 $x_{(cg)_{W_E}} = 400in$

Center of gravity for other loading cases is listed in table 8.4 below.

Table 8.4: Center of gravity for different loading scenarios.

Loading Scenario	Cg (in)
Empty weight	400
Empty weight + crew	390
Empty weight +crew + fuel	395
Empty weight +crew+ battery	420
Empty weight +crew +battery	440
Takeoff weight	370

The cg data for different loading scenarios can be plotted as follow.

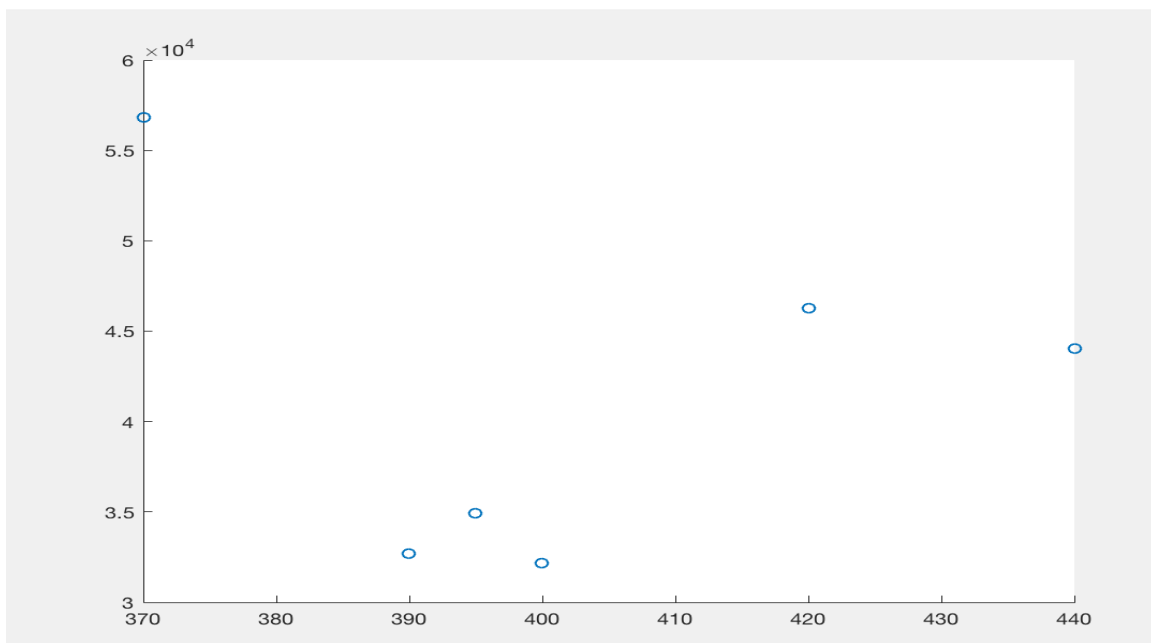


Figure 8.2: Center of Gravity for different loading scenarios (y label in lb and x label in inches).

The center of gravity range is 70in, which is in the range for the transport jet.

8.2 Estimating the Center of Gravity of the Airplane

The center of gravity of an aircraft shifts depending on the loading scenarios. This fact is shown in figure 8.2 above. However, the cg has the most forward and the most aft limit. For the longitudinal shift of the cg the most forward limit is at the takeoff weight and it is 370in. The most aft limit of the cg is 440in in the 5th loading scenarios in table 8.4 above. The z component of the center of gravity for each loading scenarios can also be calculated.

8.3 Landing Gear Design

In the previous sections, the center of gravity for different loading scenarios is determined. Most importantly, the most forward and aft limit of the center of gravity is determined. In this section the landing gear that fits the weight and balance must be designed.

Because of the high cruise speed requirement retractable landing gear is favored for the hybrid electric aircraft. For ground maneuvering and for the purpose of ground looping nose wheel configuration is preferred. A conventional tricycle landing gear is selected and it retracts to the fuselage.

The disposition of the landing gear must satisfy the tip over criteria. Figure 8.3 below shows the positions the most aft cg and the position of the main landing gear. This shows that the Main landing gear is behind the most aft cg. As a result, this disposition of the landing gear satisfies the longitudinal tip-over criteria.

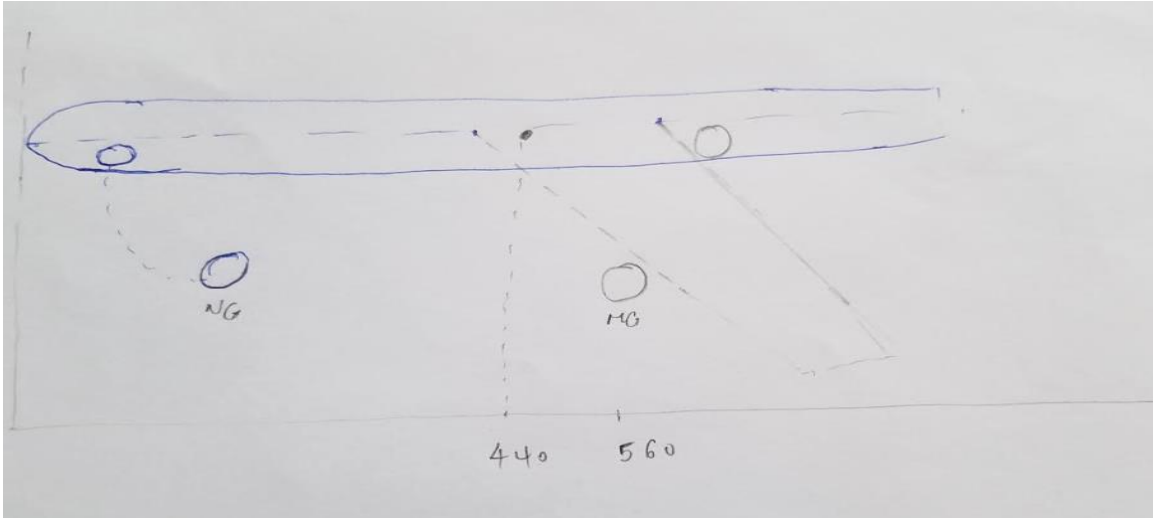


Figure 8.3: Tip-over criteria and landing gear retraction.

Since the most aft cg is very important to determine the loading on the struts, we can determine static load on each strut as follow.

$$\Rightarrow \text{Nose wheel strut: } P_n = \frac{W_{TO}l_m}{l_m+l_n} = 14,512lb$$

$$\Rightarrow \text{Main landing gear: } P_m = \frac{W_{TO}l_n}{l_m+l_n} = 21,163lb$$

Based on this static loading one nose wheel gear is good enough. We can compute the ratio of static loading to takeoff weight for the nose wheel and main landing gears.

$$\Rightarrow \frac{P_n}{W_{TO}} = 0.12 \text{ which implies 2 nose wheel struts.}$$

$$\Rightarrow \frac{n_s P_m}{W_{TO}} = 0.8, \text{ which implies 2 main landing gears.}$$

From typical landing gear data, the tire size can be selected as follow.

$$\Rightarrow \text{Main gear: } D_t \times b_t = 34 \times 12$$

$$\Rightarrow \text{Nose gear: } D_t \times b_t = 24 \times 8$$

8.4 Discussion

Figures 8.2 and 8.3 show the airplane with the landing gears and the retraction of the landing gear. In this work, the weight and balance analysis was done along with the design of the landing gear to satisfy the weight and balance conditions. It is clear that the aircraft satisfies the tip-over and ground clearance criterion. To reiterate figure 8.2 can be incorporated here.

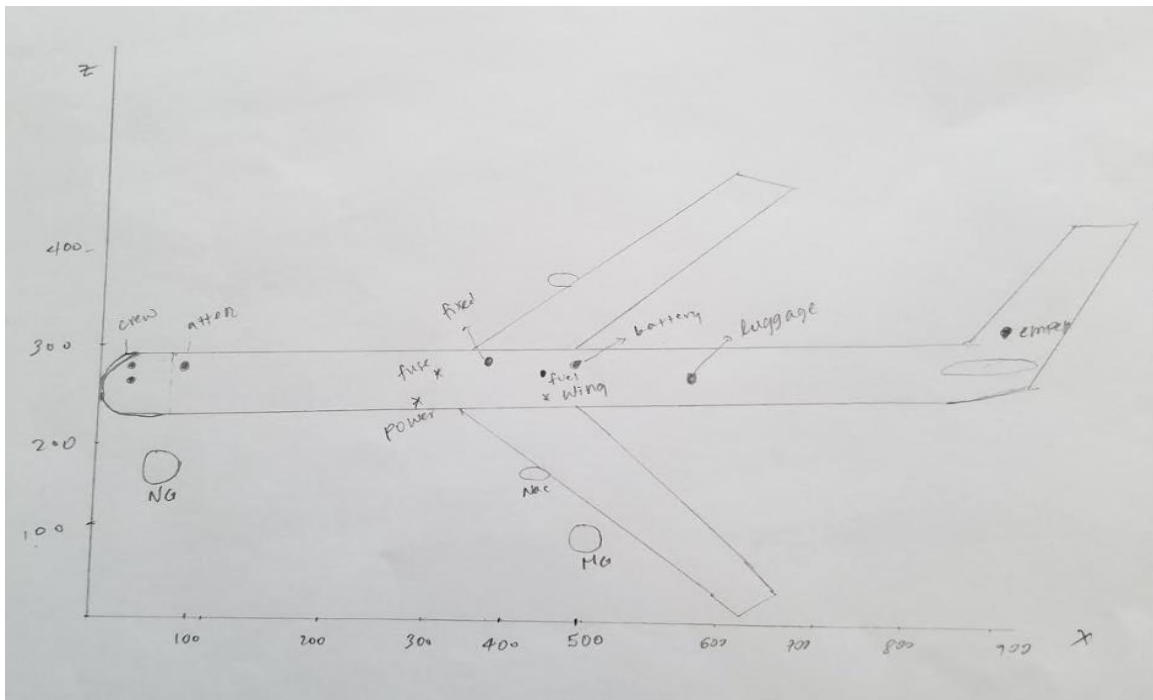


Figure 8.4: The complete airplane with cg of different components and the landing gear.

8.5 Conclusion

In this work the weights of the main components and the cg for each component is determined. The landing gear is also designed to satisfy the tip-over criteria. The potato curve is also the most important part of this work. It shows how much cg can shift for different loading scenarios. The two interesting points are the most aft and the most forward position of cg. If the most aft cg goes behind the main landing gear, the tip-over criteria is endangered. However, the hybrid electric aircraft has the

main landing gear behind the cg for the most aft case. As a result, at this stage of the preliminary design, the hybrid electric aircraft satisfies this condition.

CHAPTER 9---STABILITY AND CONTRL ANALYSIS /WEIGHT AND BALANCE- STABILITY AND CONTROL CHECK

9.1 Introduction

In the process of empennage design the sizes of the horizontal stabilizer and the vertical tail for the proposed hybrid-electric aircraft were determined from comparable aircraft data and by applying tail volume method. Based on the sizes of the horizontal and vertical stabilizers the weight of the empennage was determined during landing gear design. Other parameters such as aspect ratio and span for the horizontal stabilizer and the vertical stabilizer were also determined. The empennage contributes to the structural weight of the aircraft and any change in the weight of the empennage shifts both the aerodynamic center and the center of gravity of the aircraft. However, the aerodynamic center and the center of gravity shift must happen without destabilizing the aircraft both longitudinally and directionally. In this work the tradeoff between empennage weight and empennage size is covered. The sizes of the horizontal and vertical stabilizers determined in the empennage design will be assessed based on longitudinal and directional stability. This work also evaluates the one engine inoperative condition and the vertical tail size requirement in such a condition.

9.2 Static Longitudinal Stability

The change in the weight of the horizontal stabilizer shifts both the aerodynamic center and the center of gravity of the aircraft. In the design process, the weight and size of the horizontal stabilizer must be selected to satisfy a static margin requirement. To achieve this, the shifts in the most aft center of gravity and the aerodynamic center of the aircraft as the weight of the horizontal stabilizer is varied should be plotted and that plot is called the longitudinal X plot. For the hybrid electric aircraft being designed, from previous works, the most aft center of gravity was determined from the center of gravity excursion curve. The loading scenario that results the most aft cg is when the aircraft is at operating empty weight (Empty weight+crew+battery). The empennage weight is one of the components in this loading scenario and the shift in the aft center of gravity due to

the change in the empennage weight (horizontal stabilizer in this case shall be investigated).

From Landing Gear Design, the weight of the empennage (horizontal stabilizer and vertical stabilizer combined) was determined to be 1363lb. From geometry and the orientation of the horizontal stabilizer, the weight of the horizontal stabilizer alone can be determined as:

$$W_h = \frac{k_h S_h (3.81 S_h^{0.2} V_d)}{100 (\cos \Lambda)^{\frac{1}{2}}} \quad (9.1)$$

where k_h is given by

$$k_h = \frac{1 - \frac{h_h}{b}}{\frac{2l_h}{b}} = 0.744 \quad (9.2)$$

The values of the parameters in equations (9.1) and (9.2) above are given in Table 1 below.

Table 9.1: Values of Parameters Needed to Calculate Weight of Horizontal Stabilizer.

S_h	h_h	b	l_h	V_d	Λ
87.35ft ²	22ft	85ft	33ft	$\frac{800ft}{s}$	35°

Careful substitution of these values in equations (9.1) and (9.2) gives $W_h = 664lb$.

By using equations of similar nature and substitution of vertical stabilizer parameters given in Table 9.2 below the weight of the vertical stabilizer is 685lb.

Table 9.2: Parameters For Vertical Stabilizer Weight Calculation.

S_v	h_v	b	l_v	V_d	Λ
77.35	22ft	85ft	46ft	$\frac{880ft}{s}$	40°

Since the weight of the horizontal stabilizer for the area of the horizontal stabilizer determined from tail volume method is known the weight of the horizontal stabilizer for a given size of horizontal stabilizer can simply be determined from

$$W_h = \left(\frac{664}{87.36} \right) S_h = 7.6 S_h \quad (9.3)$$

By using results from Weight and Balance Analysis and the weight of the vertical stabilizer determined above, the most aft center of gravity of the aircraft as a function of W_h can be written as:

$$x_{cg} = \frac{18,945,970 + 75W_h}{44,032 + W_h} \quad (9.4)$$

The relationship between the size and the weight of the horizontal stabilizer and the most aft center of gravity is now prescribed. The most aft cg can be nondimensionalized by the predetermined aerodynamic chord of the wing ($\bar{c} = 46ft$ measured from the nose). The most aft cg for a range of W_h values are generated and tabulated below.

Table 9.3: Center of Gravity Shift Due to Size of Horizontal Stabilizer.

$S_h(ft^2)$	$W_h(lb)$	\bar{x}_{cg}
0	0	0.74671
20	152	0.74951
40	304	0.7523
60	456	0.75507
80	608	0.75781
100	760	0.76054
120	912	0.76325
140	1064	0.76594
160	1216	0.76862
180	1368	0.77127
200	1520	0.77391

The shift in the center of gravity of the aircraft due to the variation of the weight of the horizontal stabilizer is determined. Now the shift in the aerodynamic center of the aircraft has to be determined. For this reason the relationship between the aerodynamic center in fraction of the mean geometric chord of the aircraft and the size of the horizontal stabilizer can be written as:

$$\bar{x}_{acA} = \frac{(\bar{x}_{acwf} C_{L\alpha_{wf}} + \eta_h (1 + \frac{d\epsilon}{d\alpha}) (\frac{S_h}{S}) \bar{x}_{ach})}{C_{L\alpha}} \quad (9.5)$$

In equation (9.5) above $\bar{x}_{ac_{wf}} = \bar{x}_{ac_w} + \Delta\bar{x}_{ac_f}$ where $\Delta\bar{x}_{ac_f}$ is the shift in aerodynamic center caused by the addition of the fuselage to the wing.

The lift slope of the combination of the wing and the fuselage can be determined as

$$C_{L\alpha_{wf}} = k_{wf} C_{L\alpha_w} \quad (9.6)$$

The lift slope of the wing alone can be determined from the airfoil data and a lift slope data (figure A1). For the airfoil selected for the hybrid electric aircraft the wing lift slope is $\frac{0.075}{\text{degree}}$. Substituting this and $k_{wf} = 0.974$ for this aircraft, $C_{L\alpha_{wf}} =$

$$\frac{0.00561}{\text{degree}}. \text{ By the same token } C_{L\alpha_h} = \frac{0.070}{\text{degree}}.$$

Flow over the horizontal tail is affected by the downwash from the wing. That downwash gradient at the horizontal tail is given by

$$\frac{d\epsilon}{d\alpha} = [(K_A K_\lambda k_h (\cos \Lambda)^{0.5})^{1.19}] \frac{C_{L\alpha_w} \text{ at } M=0.93}{C_{L\alpha_w} \text{ at } M=0} \quad (9.6)$$

where

$$\Rightarrow K_A = \frac{1}{AR} - \frac{1}{1+A^{1.17}} = 0.0804$$

$$\Rightarrow K_\lambda = \frac{10-3\lambda}{7} = 1.32$$

$$\Rightarrow k_h = 0.744 \text{ from equation (9.2)}$$

Substituting the constants calculated previously in (9.6) gives $\frac{d\epsilon}{d\alpha} = 0.356$.

The shift in the aerodynamic center of the aircraft due to the addition of the fuselage can be calculated by dividing the fuselage into 13 bins of width w_i .

$$\Delta\bar{x}_{ac_f} = -\frac{dM/d\alpha}{\bar{q}S\bar{c}C_{L\alpha_w}} \quad (9.7)$$

where

$$\frac{dM}{d\alpha} = \frac{\bar{q}}{36.5} \left(\frac{C_{L\alpha_w}}{0.08} \right) \sum_{i=1}^{i=13} (w_{f_i})^2 \left(\frac{d\bar{\epsilon}}{d\alpha} \right)_i \Delta x_i \quad (9.8)$$

In Table 9.4 below the division of the fuselage into bins (Figure B1) and the corresponding parameters of the bins are presented.

Table 9.4: Cutting the Fuselage into 13 Sections of Different Width.

i	$w_i(ft)$	$x_i(ft)$	$\Delta x_i(ft)$	$(d\epsilon/d\alpha)_i$
1	5	29.5	6	1
2	6	23.25	6.5	1.1
3	7	17	6	1.15
4	8	11.25	6.5	1.2
5	9.8	5	7.5	1.25
6	9	3.5	7	0.0745
7	8.5	10	6	0.2129
8	7	15.25	5	0.3247
9	6	20.25	4.5	0.4311
10	4	24.5	4.0	0.5216
11	3	27.75	3.5	0.5908
12	2	30.75	2.5	0.6546
13	0.5	37.75	0.5	0.6919

Inserting the values in table 9.4 in equation (9.8) then in equation (9.7) gives

$$\Delta \bar{x}_{ac_f} = -0.197.$$

From previous works $\bar{x}_{ac_w} = 0.913$. From these two non-dimensional constants

$\bar{x}_{ac_{w_f}} = 0.716$. Since all the components of equation (9.5) are known the

aerodynamic center of the aircraft can be evaluated as a function of S_h .

$$\bar{x}_{ac_A} = \frac{0.0031 + 0.04508 \cdot 1.15 \left(\frac{S_h}{728}\right)}{0.0561 + 0.04508 \left(\frac{S_h}{728}\right)} \quad (9.9)$$

From equations (9.5) and (9.9) it is clear how the size of the horizontal stabilizer shifts both the aerodynamic center and the center of gravity. The difference between the center of gravity and the aerodynamic center at a given size of the horizontal stabilizer determines the static margin. For static margin of exactly 10%, the horizontal stabilizer area is $100ft^2$ (from figure 9.1 below).

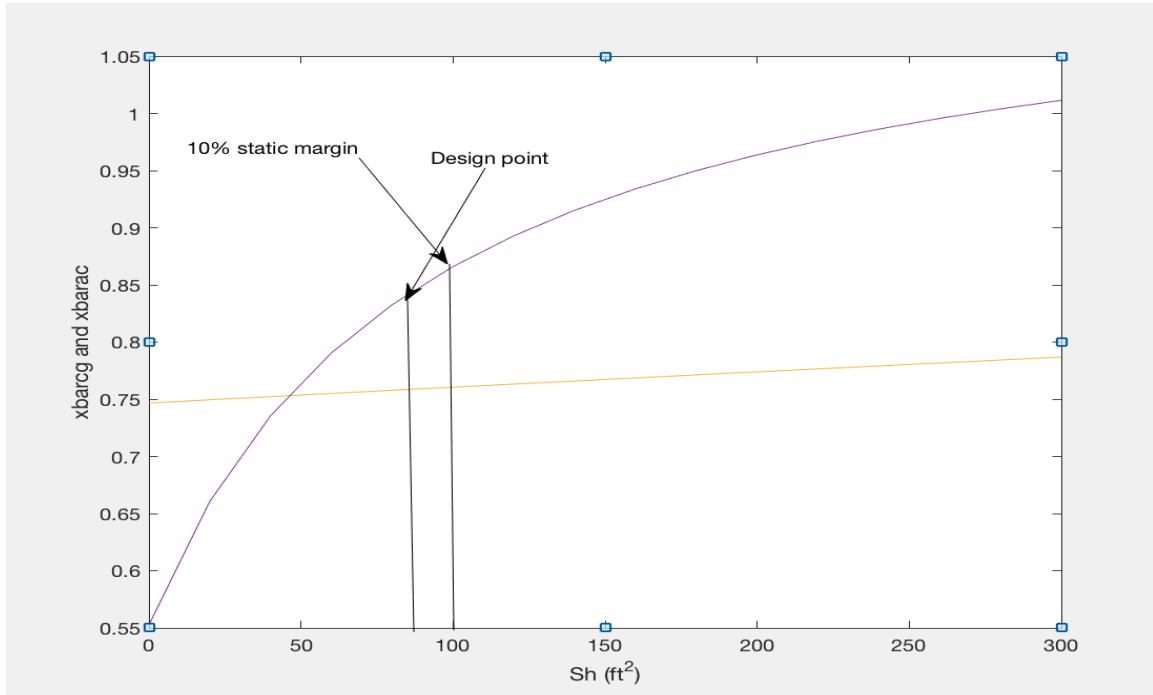


Figure 9.1: Longitudinal X Plot.

Since the horizontal tail area determined from the tail volume method is 87 ft^2 , it falls in the 10% static margin. As a result, the aircraft is longitudinally stable with the existing horizontal tail.

9.3 Static Directional Stability

The yawing moment due to sideslip derivative is given by

$$C_{n\beta} = C_{n\beta_w} + C_{n\beta_f} + C_{n\beta_v} \quad (9.10)$$

where the derivatives on the right-hand side are contributions from the wing, the fuselage, and the vertical stabilizer to the yawing moment. However, wing contribution to the yawing moment is important only at high angles of attack. As a result, for preliminary design purposes $C_{n\beta_w} = 0$. With this approximation the yawing moment due to sideslip becomes

$$C_{n\beta} = C_{n\beta_f} + C_{L\alpha_V} \frac{S_V x_V}{S b} \quad (9.11)$$

Contribution of the fuselage to the yawing moment is given by

$$C_{n\beta_f} = -\frac{57.3K_nK_R S_{B_s} l_f}{Sb} \quad (9.12)$$

Table 9.4: Values of Parameters and Constants in the Fuselage Contribution Equation (Figure A2 and A3 for Constants).

$S_{B_s}(ft^2)$	K_n	K_{RL}	$C_{L\alpha_v}(\frac{1}{degree})$
425	0.0015	2.2	0.264

Substituting the appropriate constants for the hybrid electric aircraft gives $C_{n\beta_f} = -0.0070$ which is destabilizing. The lift coefficient of the vertical stabilizer is $\frac{0.264}{degree}$ from airfoil data (Figure A1). The area and the distance from the center of gravity of the vertical stabilizer were estimated to be $77.35ft^2$ and $43ft$ respectively. By substituting these values equation (9.11) becomes:

$$C_{n\beta} = -0.0070 + 0.00012S_v \quad (9.13)$$

A simple relationship between the yawing moment due to sideslip angle derivative and the size of the vertical stabilizer is derived above. This result is plotted in figure 9.2 below.

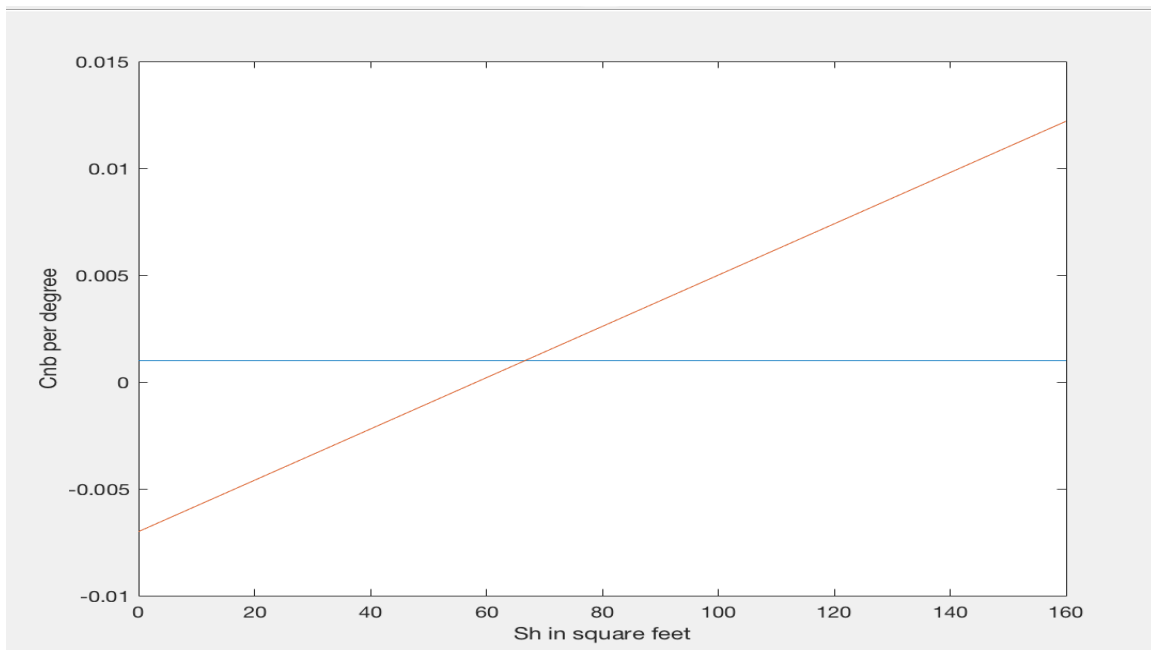


Figure 9.2: Directional Stability X Plot.

Since the hybrid-electric aircraft under design is required to be inherently stable, it is appropriate to assume $C_{n\beta} = \frac{0.0010}{degree}$. From the directional X plot, the size of the vertical stabilizer required for directional stability is $75ft^2$ which implies that the size of the vertical stabilizer determined from the tail volume method is reasonable to achieve directional stability.

9.4 Rudder Deflection to Hold One Engine Inoperative Condition

The rudder must have the authority to balance the critical engine out yawing moment. Yawing moment due to thrust of the operative engine in this critical condition about the center of gravity is given by:

$$N_{t_{crit}} = T_{Toe}y_t \quad (9.13)$$

where, from preliminary performance and landing gear design, $T_{Toe} = 13,916lbf$ and $y_t = 15ft$.

Substitution of these values in equation (9.13) gives a critical yawing moment of $N_{t_{crit}} = 208,740lbft$. There is also drag induced yawing moment due to the inoperative engine that the rudder has to compensate for. That drag induced yawing moment is given by:

$$N_D = 0.25N_{t_{crit}} = 52,185lb.ft \quad (9.14)$$

The rudder deflection to stabilize the aircraft during one engine out flight condition is given by

$$\delta_r = \frac{N_D + N_{t_{crit}}}{qSbC_{n\delta_r}} \quad (9.15)$$

The yawing moment coefficient due to the rudder deflection is in turn given by

$$C_{n\delta_r} = -\frac{C_{y\delta_r}}{b} (l_v \cos\alpha + z_v \sin\alpha) \quad (9.16)$$

From the detailed computation in Appendix B $C_{y\delta_r} = 0.116/degree$ and $C_{n\delta_r} = -\frac{0.0109}{degree}$. Substituting these values in equation (9.15), the rudder deflection needed to balance the total yawing moment is -10° .

9.5 Empennage Design- Weight and Balance- Landing Gear Design- Longitudinal Static Stability and Control Check

The sizes of the horizontal and the vertical stabilizers determined from the tail volume method are sufficient to give directional and longitudinal stability. The aerodynamic center and center of gravity shifts are in the range allowed for transport jet. The center of gravity shift due to the size of the horizontal stabilizer is not behind the main landing gear, which satisfies the tip-over criteria. As a result, iteration in weight and balance-landing gear design is not needed.

9.6 Discussion

The lateral stability of the hybrid electric aircraft was determined in the preliminary wing design. The aircraft also has to be stable both directionally and longitudinally. For this reason, the vertical and horizontal tails must be sized to provide the appropriate stability and control requirements. In this work, the horizontal stabilizer is sized to satisfy the 10% static margin. This is discussed in Longitudinal Stability section of this work. The vertical stabilizer is also sized to give an appropriate value of yawing moment due to sideslip derivative. That detail is presented in Directional Stability section of this work. It is also verified that the rudder can compensate for one engine inoperative condition with -10° deflection.

9.7 Conclusion

In this part of the design the longitudinal and directional stability of the hybrid electric aircraft is investigated. The longitudinal and directional stability of the aircraft is determined by preparing the longitudinal and directional X plots. From the Longitudinal X plot the shifts in aerodynamic center and the most aft center of gravity of the aircraft due to the size of the horizontal stabilizer is within 10% static margin. As a result, the aircraft is longitudinally stable with the predetermined horizontal stabilizer. Similarly, the directional stability of the hybrid electric aircraft under design is satisfied with the predetermined vertical stabilizer. Since both the vertical and horizontal tails provide the required stability requirements iteration between weight and balance, landing gear, and stability is not needed.

CHAPTER 10---DRAG POLAR ESTIMATION

10.1 Introduction

At this stage of the design the sizes of the main components of the hybrid-electric aircraft are determined. Parts of these components that are exposed to the free-stream flow contribute to drag. As a result, every time size of a component grows there is drag penalty that arises with the size increment. For this aircraft the wing, the fuselage, the empennage, and the nacelle contribute the most for the parasite drag of the aircraft. Knowing the wetted area of each of these components enables to determine the drag polar of the aircraft. The landing gear also contributes to the drag polar during landing and takeoff. In this work the overall drag polar of the aircraft will be determined as the sum of parasite drag, which is drag due to the size of the wetted area (also called zero lift drag), and lift induced drag, which is proportional to the square of the lift produced. This result will also be plotted to see the variation of drag on the aircraft during different phases of the flight as a function of lift produced during each flight condition.

10.2 Airplane Zero-Lift Drag

Components of the hybrid electric aircraft that contribute to the wetted area are :

- ⇒ The wing
- ⇒ The fuselage
- ⇒ The nacelle
- ⇒ The horizontal tail and
- ⇒ The vertical tail

To investigate the contributions of each component to the drag polar of the aircraft, the wetted area of each component should be calculated. Plan-form wetted area can most easily be found by

$$S_{wet_{plf}} = 2S_{ex} \left(1 + \frac{0.25 \left(\frac{t}{c} \right)_r (1 + \tau \lambda)}{1 + \lambda} \right) \quad (10.1)$$

In equation (10.1) S_{ex} is the exposed area of the component under consideration. Similarly, the wetted area of the fuselage is determined via:

$$S_{wet_{fuse}} = \pi D_f l_f \left(1 - \frac{2}{\lambda_f}\right)^{\frac{2}{3}} \left(1 + \frac{1}{\lambda_f^2}\right) \quad (10.2)$$

To determine the wetted area of the nacelle, the parameter method (1) can be employed. In determining the wetted area of the whole aircraft, the intersection of the wing and the fuselage has to be subtracted. The result of these calculations is summarized in table 10.1 below.

Table 10.1: Wetted Area Calculation of the Aircraft Components.

<i>Component</i>	<i>Area calculation method</i>	<i>Wetted Area (ft²)</i>
Wing	$S = 728ft^2, \left(\frac{t}{c}\right)_r = 0.12, \left(\frac{t}{c}\right)_t = 0.1$ $\tau = 1.2, \lambda = 0.25$ By (10.1)	1510
Wing and fuselage intersection	<i>Subtract the immersed wing area</i>	-56
Vertical Tail	$S_v = 77ft^2, \frac{t}{c} = 0.13, \lambda = 0.3$ By (10.2)	159
Horizontal Tail	$S_h = 87ft^2, \frac{t}{c} = 0.13, \lambda = 0.3$ By (10.2)	180
Nacelles	<i>Perimeter method</i>	200
Fuselage	$D_f = 9.8ft, l_f = 74ft, \lambda_f = 7.55$ By (10.2)	1361
Total	<i>Adding column 3</i>	3353

From figure 10.1 below for takeoff weight of $5.684 \times 10^4 lb$, the wetted area is $3500ft^2$ which has a 4.2% difference with the calculated wetted area. This difference is within 10% with the allowed wetted area from the wetted area correlation.

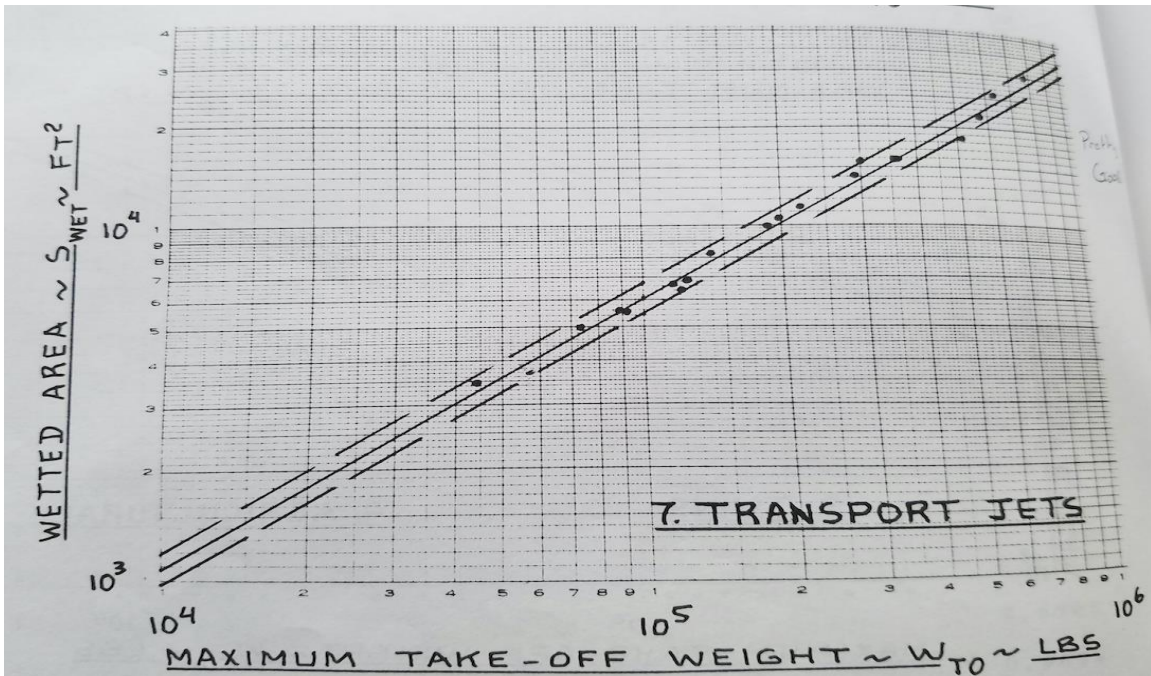


Figure 10.1: Take-off Weight versus Wetted area [1 p 124].

10.3 Low Speed Drag Increments

The zero-lift drag coefficient can be expressed as

$$C_{D0} = \frac{f}{S} \quad (10.3)$$

In equation (10.3) is the equivalent parasite drag area, which can be read from figure (10.2) below for the calculated wetted area.

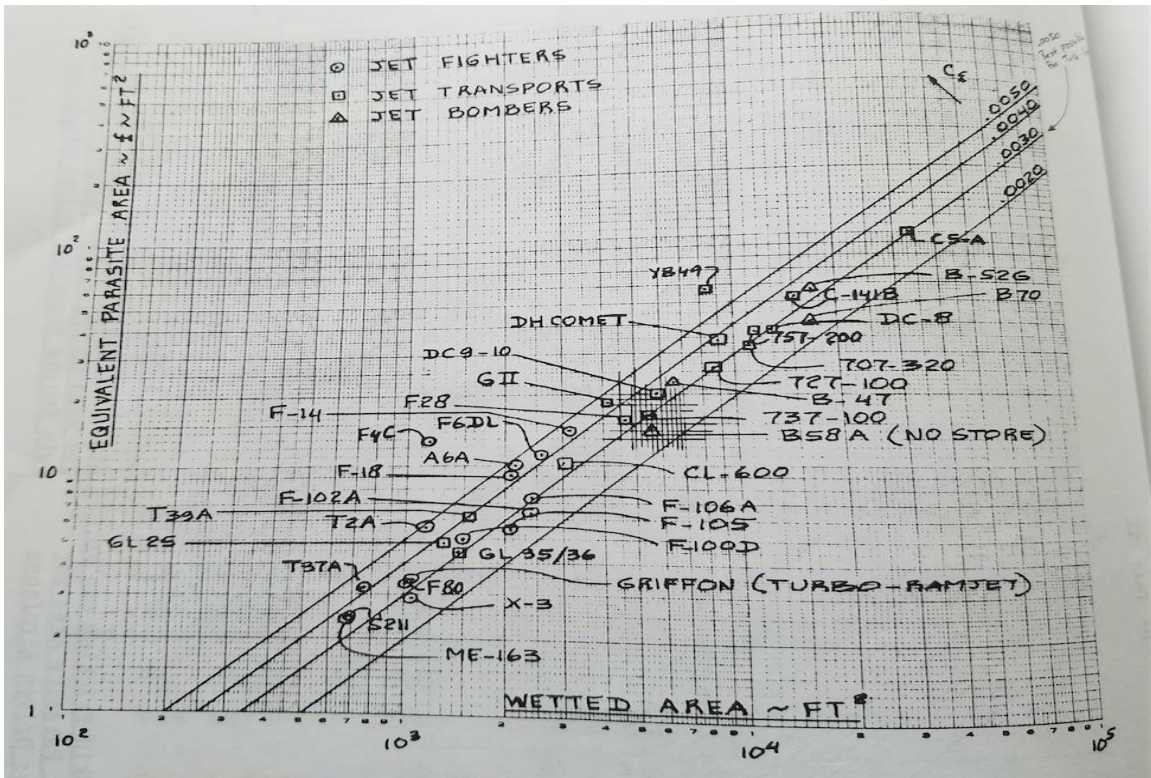


Figure 10.2: Equivalent Parasite Area for a given Wetted Area [1 p120].

The zero-lift drag coefficient of the hybrid-electric aircraft at low speed now follows from equation (10.3) and gives 0.02335 for $f = 17$.

10.4 Compressibility Drag

The compressibility drag for the hybrid electric aircraft from figure 10.3 below is 0.0003.

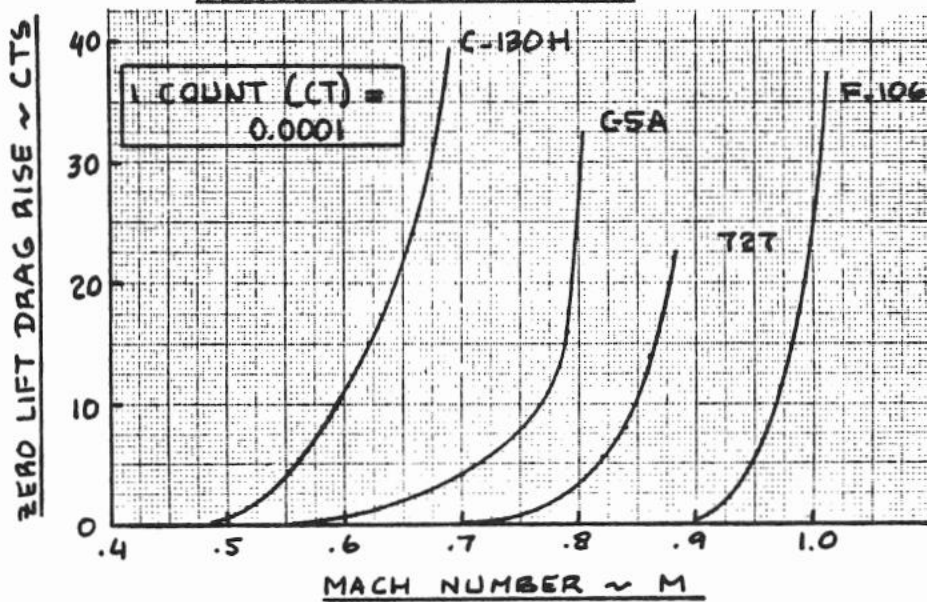


Figure 10.3: Compressibility drag [2, p286]

10.5 Airplane Drag Polar

Since the zero-lift drag and the compressibility drag increment are determined, it is possible to determine the drag polar. The cruise value of the zero-lift drag coefficient is now

$$C_{D_0} = 0.0003 + 0.02335 = 0.02365 \quad (10.4)$$

Adding the compressibility drag effect to the zero-lift drag coefficient found from performance sizing gives

$$C_{D_0} = 0.0003 + 0.002395 = 0.02425 \quad (10.5)$$

The results from the two equations above are very close to each other. As a result, $\frac{L}{D}$ does not have a big difference in these two cases.

Because the slight change in cruise drag has a negligible effect on takeoff and landing polar, these do not have to be re-evaluated.

It was stated that the high lift devices and the landing gear contribute to the drag of the aircraft and these values are included in takeoff and landing drag polar. Drag polar equations for different flight conditions are listed below.

$$\Rightarrow \text{Takeoff: } C_D = 0.03895 + 0.0398C_L^2$$

$$\Rightarrow \text{Cruise: } C_D = 0.02395 + 0.03747C_L^2$$

$$\Rightarrow \text{Landing: } C_D = 0.10095 + 0.04246C_L^2$$

Coefficient of drag relationships above can be plotted below.

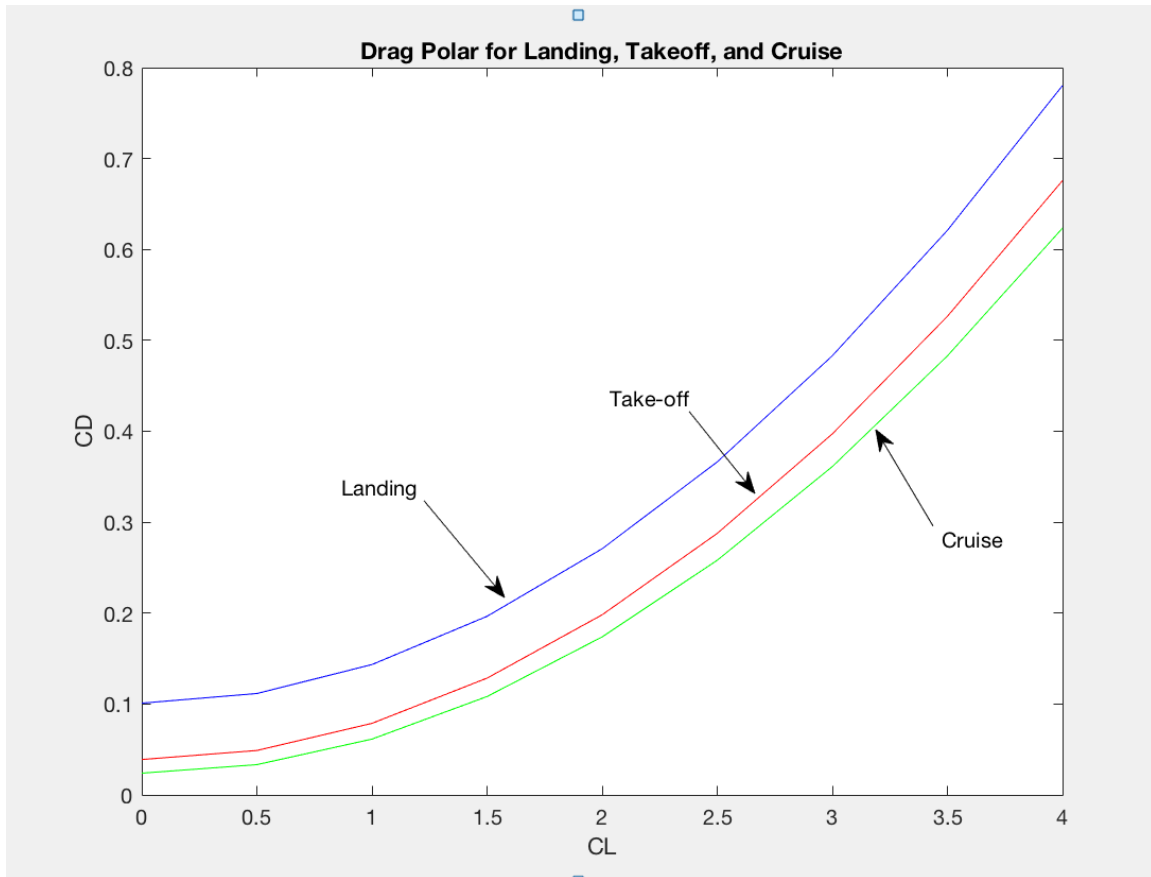


Figure 10.4: Drag Polar of the Hybrid-Electric Aircraft.

10.6 Discussion

Any surface of the aircraft that is exposed to the flow air contributes to the drag of the aircraft. The amount of drag a surface contributes to the drag polar is proportional to the size. For the hybrid-electric aircraft under design the main surfaces that contribute to the parasite drag are

- ⇒ The plan form which includes the wing and the empennage
- ⇒ The part of the fuselage that does not overlap with the wing and
- ⇒ The Nacelles.

The area of the surface that contributes to the drag polar is called wetted area, and the wetted area for each of the contributing surfaces is calculated and documented

in table 10.1. As the wing and the fuselage are larger than the other components of the aircraft, they contribute most of the wetted area towards the parasite drag calculation.

Drag of an aircraft has two main components, which are given in equation (10.6) below.

$$C_D = C_{D_0} + \frac{C_L^2}{\pi A e} \quad (10.6)$$

where C_{D_0} is the parasite drag and the second term on the right is the lift induced drag scaled by a constant. It is to the parasite drag that wetted area contributes. This contribution of all the surfaces is calculated by finding the wetted area. Even though the aircraft is designed to fly at subsonic speeds, compressibility drag is also possible and that is added to the parasite drag. Equations in the form of (10.6) are developed for takeoff with landing gear down, cruise speed, and landing with landing gear down and plotted in figure 10.4.

10.7 Conclusion

In this work the drag polar of the hybrid electric aircraft was determined for takeoff with landing gear up, cruise, and landing with landing gear up. This was done by determining the components of the aircraft that contribute to the drag. Then the wetted area of each component was determined to find the equivalent parasite area. From equivalent parasite area and the wing area, the low speed drag coefficient was determined. Adding the compressibility effect to the parasite drag and including the lift induced drag gives the cruise drag polar. Adding flap and landing gear contribution the drag polar for takeoff and landing was determined. Then the complete drag polar for the mission was plotted as a function of lift.

Chapter 11---Construction of V-n Diagram

11.1 Introduction

The variation of center of gravity versus weight of the aircraft is one important parameter in the process of designing any aircraft. This relationship was termed as cg excursion diagram, and it was explicitly determined for this specific aircraft in the previous chapters. Another important concept is the relationship between load factor and airspeed. This relationship is inherently a result of other parameters such as gross weight, altitude and maximum lift. A minimum load factor prevents structural damage and a faster aircraft is desirable in terms of gaining maximum efficiency. However, all combinations of speed and load factor are not available due to conditions like stall and structural damage. The region made up of the allowed combinations of speed and load factor is called the envelope of the aircraft, and the diagram that made up of the collection of these combinations is called the V-n diagram. If the aircraft operates in the allowed region, it can maneuver safely. This safe maneuverable region must be determined from different factors, and this chapter is dedicated to determining the V-n diagram of the hybrid electric aircraft under design.

11.2 Background

The flight operating strength of any aircraft is represented on a graph whose horizontal axis is airspeed (V) and vertical axis load factor (n). Load factor generally can be given by

$$n = \frac{L}{W} \quad (11.1)$$

where L is lift and W is the weight of the aircraft.

To establish the desired relationship between load factor and airspeed, equation (11.1) above can be written as follows.

$$n = \frac{\frac{1}{2}\rho_{\infty}V_{\infty}^2 C_L S}{W} \quad (11.2)$$

By rewriting the above equation, the maximum load factor can be given as follows.

$$n_{max} = \frac{\frac{1}{2}\rho_{\infty}V_{\infty}^2 C_{Lm}}{W/S} \quad (11.3)$$

The quadratic V-n relationship given by equation (11.3) above produces a single maximum load factor value of a given velocity at a maximum lift coefficient. A typical graphical representation is given by line AB in figure 12.1. below. If the aircraft represented by the V-n diagram in figure 11.1 is flying at V_1 with $C_L < C_{Lm}$, the load factor is the point represented by point 1. If C_L is now increased to C_{Lm} , point 2 represents the airspeed-load factor combination. Any further increase of C_L is impossible and would result stall. As a result, the point represented by 3 and the whole region above the curve is unobtainable. To increase the load factor the velocity must increase. However, indefinite increase in load factor is impossible since structural damage is highly likely after a critical point as given by point B. The corner velocity where this happens can be given by

$$V = \sqrt{\frac{2n_{max}}{\rho_{\infty}C_{Lmax}}} \frac{W}{S} \quad (11.4)$$

The velocity cannot also increase without bound since a structural damage might happen due to a higher dynamic buildup. The region that is inside these limits is the allowable region for the aircraft.

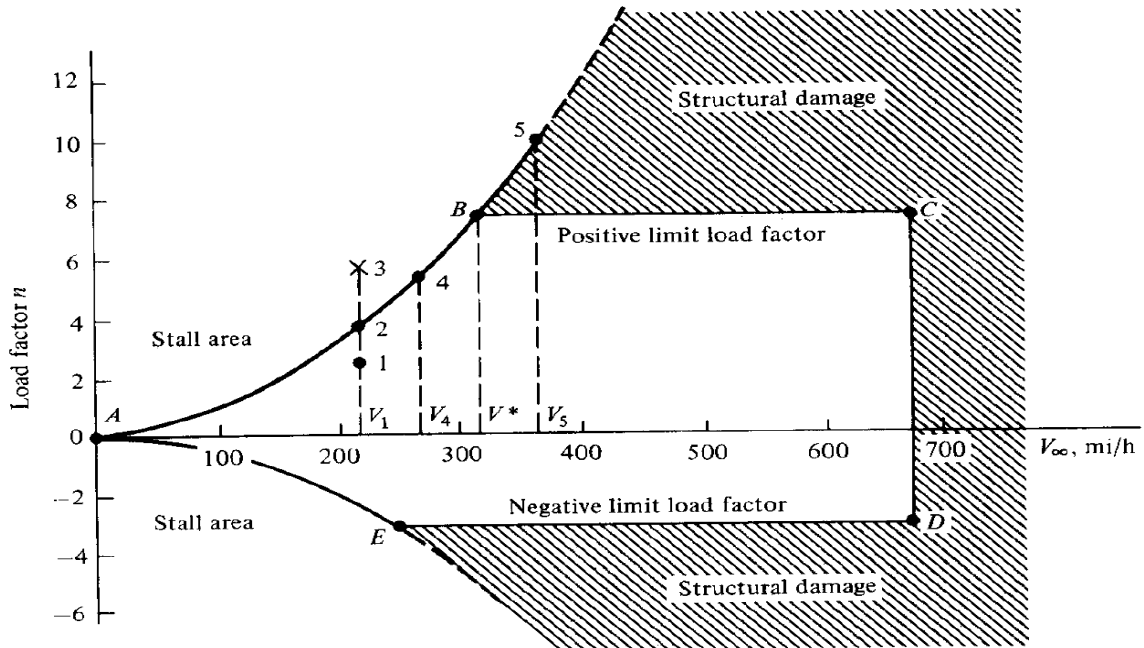


Figure 11.1: General representation of V-n diagram.

11.3 Method of V-n Diagram Construction

11.3.1 V-n Diagrams for FAR 25 Certified Airplanes

To construct V-n diagram, the following parameters must be prescribed.

- V_{s1} : +1g stall speed of the minimum steady flight speed which is possible.
- V_C : design cruising speed
- V_D : Design diving speed
- V_A : Design maneuvering speed
- V_B : Design speed for maximum gust intensity

11.3.2 Determination of Parameters and Critical Points

11.3.2.1 Determination of +1g Stall Speed

The minimum achievable steady flight speed for FAR 25 certified airplanes is given by

$$V_{s1} = \sqrt{\frac{\frac{2W_t}{S}}{\rho C_{n_{max}}}} \quad (11.5)$$

where

- W_t is gross takeoff weight in lbs determined from preliminary weight sizing
- S is wing area in ft^2
- ρ is air density in $slugs/ft^3$
- $C_{n_{max}}$ is the maximum normal force coefficient

The maximum normal force coefficient is given by

$$C_{n_{max}} = \sqrt{C_{L_{max}}^2 + C_{D_{max}}^2} \quad (11.6)$$

It is also acceptable to use

$$C_{n_{maxi}} = 1.1C_{L_{max}} \quad (11.7)$$

Table 11.1 below is a record of the parameters from preliminary design that are important to calculate minimum steady flight speed for the hybrid electric aircraft under design.

Table 11.1: Parameters for the calculation of minimum flight speed.

$W_t(lbs)$	$\rho(slug/ft^3)$	C_{Lmax}	$S(ft^2)$	C_{nmax}
56,800	0.002378	1.6	728	1.76

Using the parameters in table 11.1 and equation (11.5)

$$V_{s1} = \sqrt{\frac{2(78.022)}{0.002378(1.76)}} = 193ft/s = 114knots$$

11.3.2.2 Determination of Design Limit Load Factor (n_{lim})

The positive limit maneuvering load factor can be determined from

$$n_{lim+} \geq 2.1 + \frac{24,000}{W+10,000} \quad (11.8)$$

with the following exceptions.

- $n_{lim+} \geq 2.5$ at all times.
- $n_{lim+} \leq 3.8$ at take-off weight.

The positive limit load factor at take-off weight for the hybrid electric aircraft is

$$n_{lim+} \geq 2.1 + \frac{24,000}{56,800 + 10,000} = 2.459 < 3.8$$

So, it is reasonable to assume $n_{lim+} = 2.5$.

The negative design limit load factor is determined from $n_{lim-} \geq -1$ up to V_C and varies linearly from the value at V_C to 0 at V_D where the values of V_C and V_D are yet to be determined.

11.3.2.3 Determination of Design Maneuvering Speed

The design maneuvering speed (the corner speed) is given by the following equation.

$$V_A = V_{s1}(n_{lim+})^{\frac{1}{2}} \quad (11.9)$$

Using equation (11.9), the lower limit of design maneuvering speed is

$$V_A = 114(2.5)^{1/2} = 180knots$$

11.3.2.4 Construction of Gust Load Factor Lines

The design load limit factor for the construction of gust load factor lines is given by

$$n_{lim} = 1 + \frac{K_g U_{de} V C_{L\alpha}}{498 \left(\frac{W_t}{S}\right)} \quad (11.10)$$

where K_g is gust alleviation factor given by

$$K_g = \frac{0.88\mu_g}{5.3 + \mu_g} \quad (11.11)$$

where μ_g is the aircraft mass ratio defined by

$$\mu_g = \frac{2 \left(\frac{W_t}{S}\right)}{\rho c g C_{L\alpha}} \quad (11.12)$$

The parameters in equation (11.12) are given as follows.

- c : mean aerodynamic chord length = $5.95 ft$
- $C_{L\alpha}$: change of lift coefficient with respect to angle of attack = $4.33 rad^{-1}$
- g : gravity $g = 32.174 ft/s^2$
- ρ : Air density at sea level = $0.002377 slugs/ft^3$

Using these values in equation (11.12) gives $\mu_g = 79$ and using this in equation (11.11) gives $K_g = 0.823$.

The derived gust velocities U_{de} in FAR 25 (at $24,000 ft$) are the following.

- ✓ For gust line marked V_B : $U_{de} = 84.7 - 0.000933h = 63 fps$
- ✓ For gust line marked V_C : $U_{de} = 66.67 - 0.00083h = 47 fps$
- ✓ For gust line marked V_D : $U_{de} = 33.34 - 0.000417h = 24 fps$

Using the design load limit factor equation given by (11.10) along with the determined values, the gust line equations become the following.

$$\checkmark V_B \text{ gust line: } n_{lim} = 1 + 0.00577V \quad (11.13)$$

$$\checkmark V_C \text{ gust line: } n_{lim} = 1 + 0.0043V \quad (11.14)$$

$$\checkmark V_D \text{ gust line: } n_{lim} = 1 + 0.0022V \quad (11.15)$$

Plotting these lines along with the x-axis reflections of these equations gives the V-n gust load factor lines. The V-n gust lines plot for the hybrid electric aircraft under design is given in figure 11.2 below.

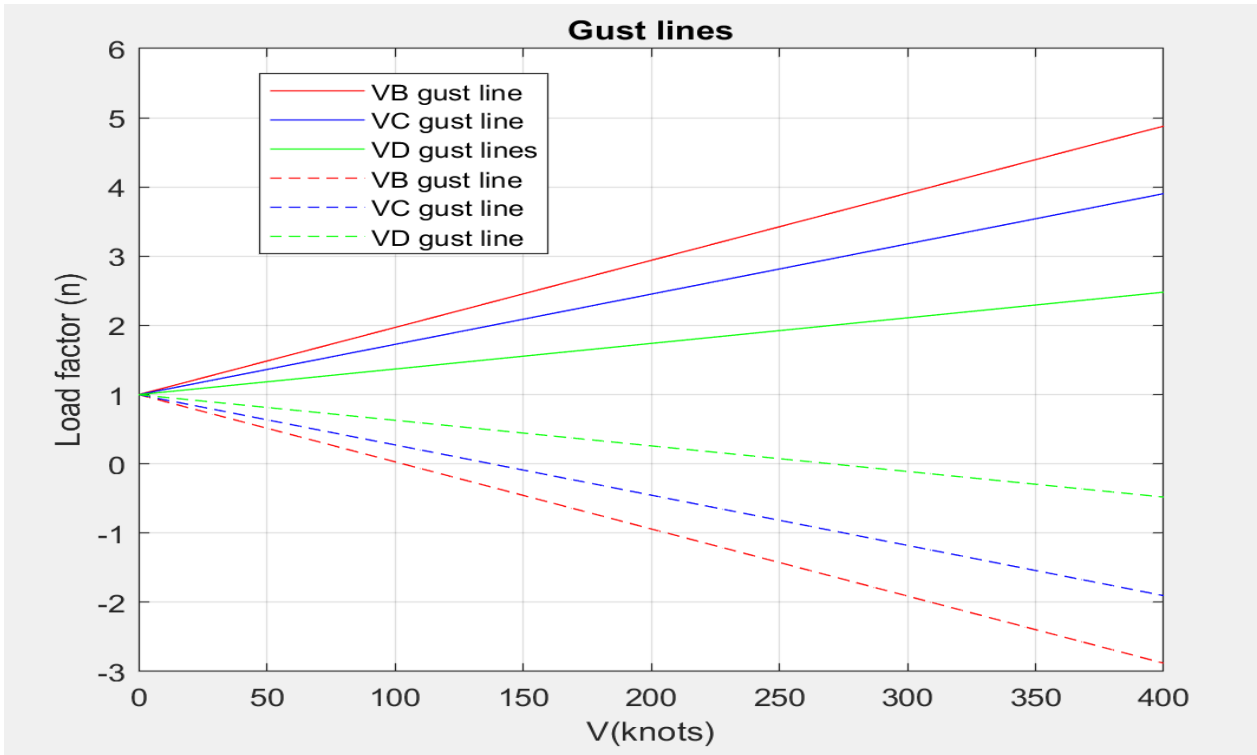


Figure 11.2: Gust load factor lines for the hybrid electric aircraft.

11.3.2.5 Determination Design Speed for Maximum Gust Intensity (V_B)

V_B follows from the intersection of the $+1g$ stall line and the V_B gust line. From figure 11.3 below, the intersection of $+1g$ stall line and V_B gust line is $V_B = 191 \text{ knots}$.

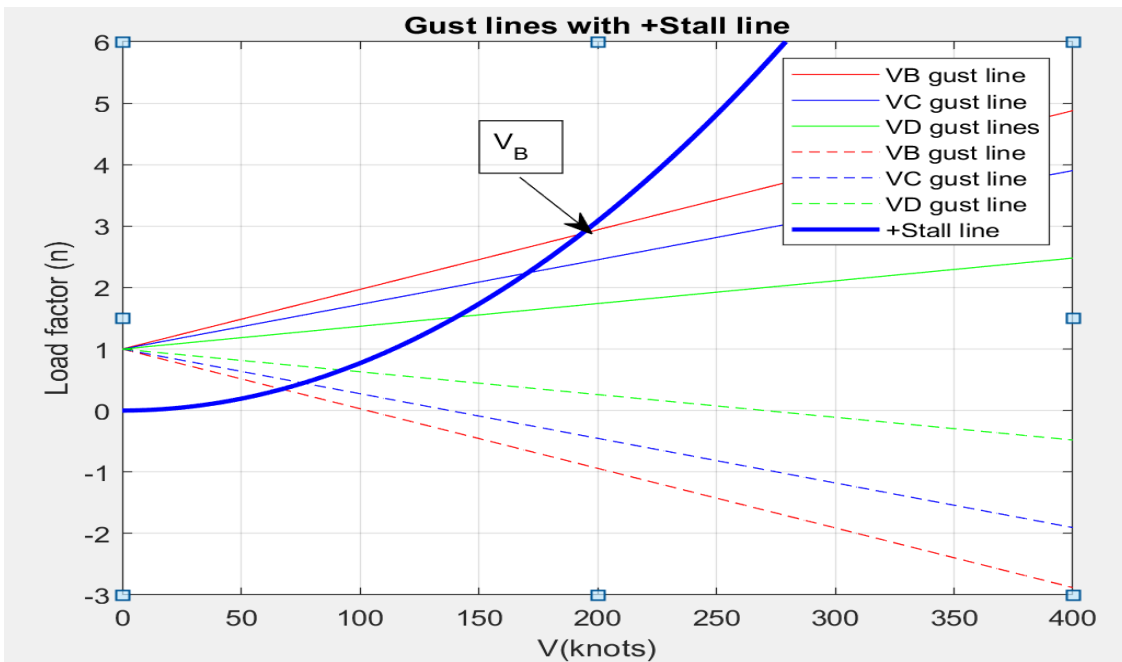


Figure 11.3: Gust load factor lines with positive stall line.

11.3.2.6 Determination of Design Cruising Speed

V_C must be sufficiently larger than V_B to provide for inadvertent speed increase likely to occur as a result of severe atmospheric turbulence. The design cruising speed is commonly given as follows.

$$V_C = V_B + 43 = 234 \text{knots}. \quad (11.16)$$

11.3.2.7 Determination of Design Diving Speed

The design diving speed V_D is given by

$$V_D = 1.2V_C \quad (11.17)$$

where V_C is the design cruising speed calculated in the previous section.

$$V_D = 1.2(234) = 280 \text{knots}$$

11.3.2.8 Determination of Negative Stall Speed Line

The negative stall speed line can be given by equation (11.5). It is reasonable to assume $C_{L_{max}} = -1$. The maximum negative normal force coefficient is given by $C_{N_{max}} = 1.1(-1) = -1.1$. It is also fairly reasonable to set $n_{neg} = -1$. With these assumptions, the negative stall speed is $V_{s_{neg}} = 145 \text{knots}$. The negative stall line also can be given by

$$n_{neg} = -0.000048V_{s_{neg}}^2 \quad (11.18)$$

The negative stall line along with the gust load factor line is shown in figure 11.4 below.

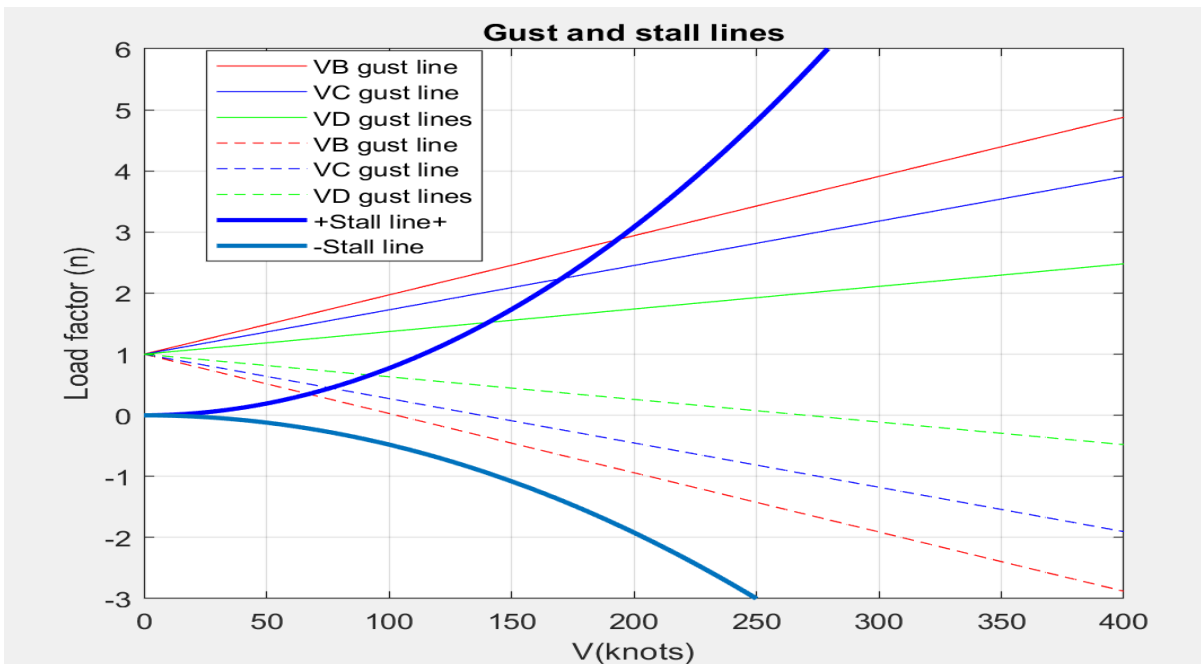


Figure 11.4: Negative stall line with gust load factor and positive stall lines.

11.3.2.9 V-n Diagram

Combining the results from the previous sections, the V-n Diagram of the hybrid electric airplane under design becomes the envelope in figure 11.5.

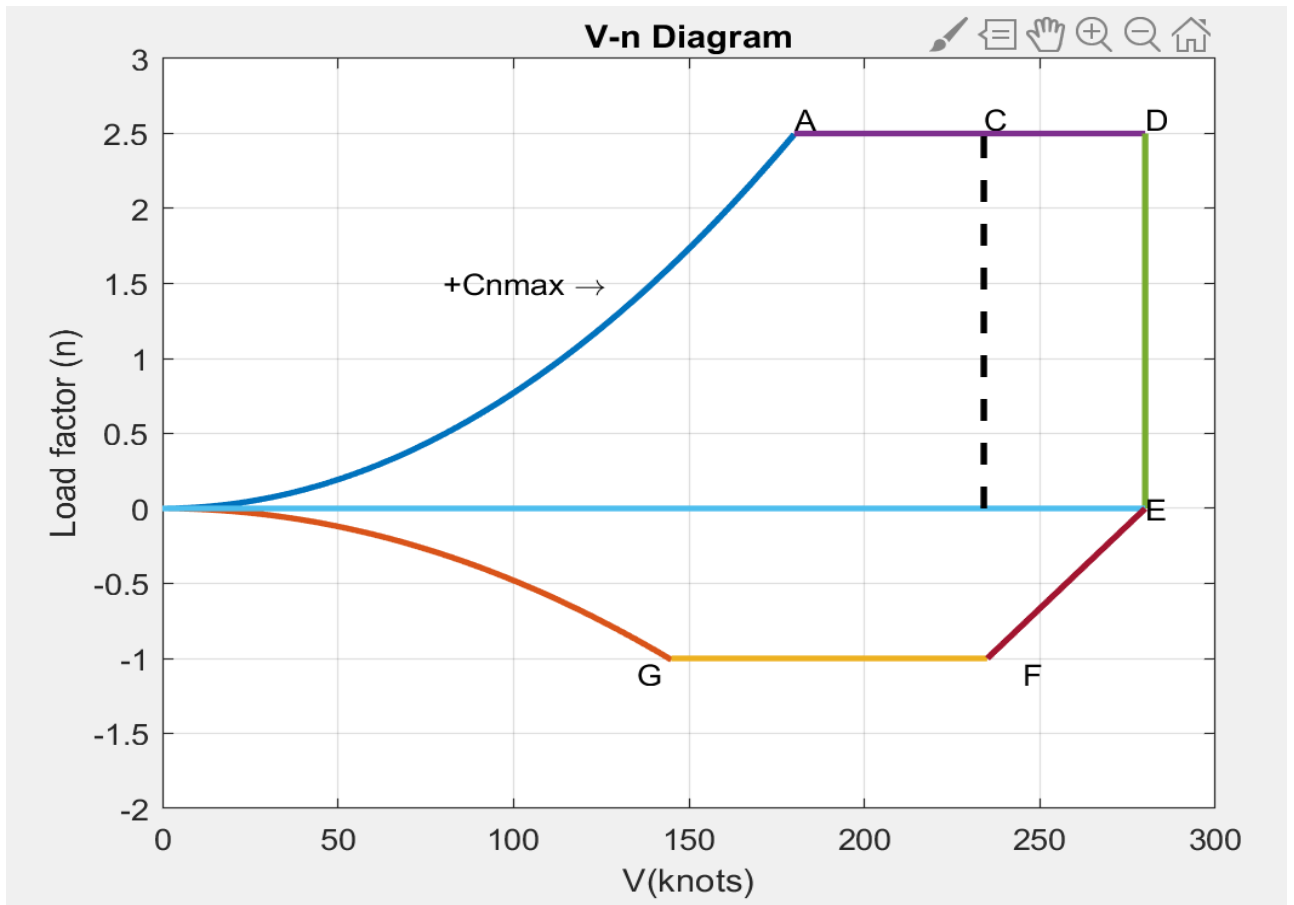


Figure 11.5: V-n diagram of the hybrid electric transport jet.

11.4 Discussion

The V-n diagram given in figure 11.5 differentiates the allowable combination of airspeed and load factor from the forbidden regions of all the combinations of speed and load factor. The envelope is bounded by the following primary factors.

- ✓ Load factor
- ✓ Maximum lift coefficient
- ✓ Maximum airspeed

The region bounded between the maximum positive load factor and the minimum positive load factor is allowable load factor region. This region of allowable load factor for the hybrid electric aircraft is given in figure 11.6 below. Any load factor greater than $+n_{max}$ and less than $-n_{max}$ is unobtainable region. The region out of the allowable region is highly likely to cause structural damage to the airframe.

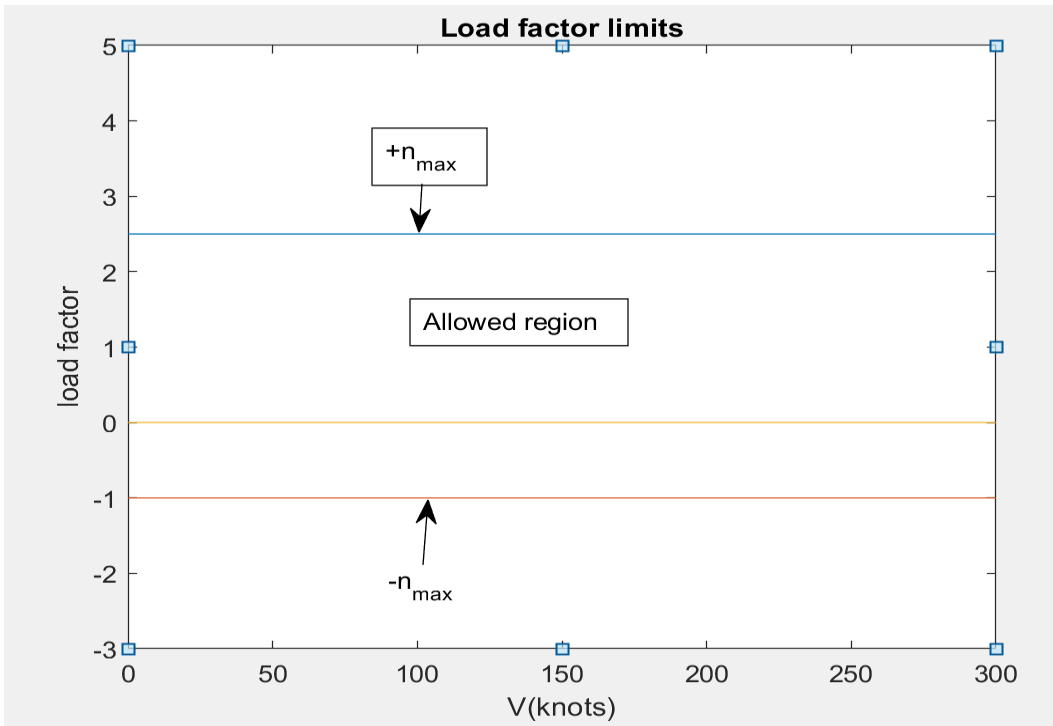


Figure 11.6: Allowed load factor region.

Infinite lift is impossible. As a result, any lift coefficient less than the maximum lift coefficient obtainable results stall. The line traced by the maximum lift coefficient shows that some part of the allowable load factor region is inaccessible. This fact is shown in figure 11.7 below. Anything between the stall lines is accessible if the load factor remains less than the maximum load factor.

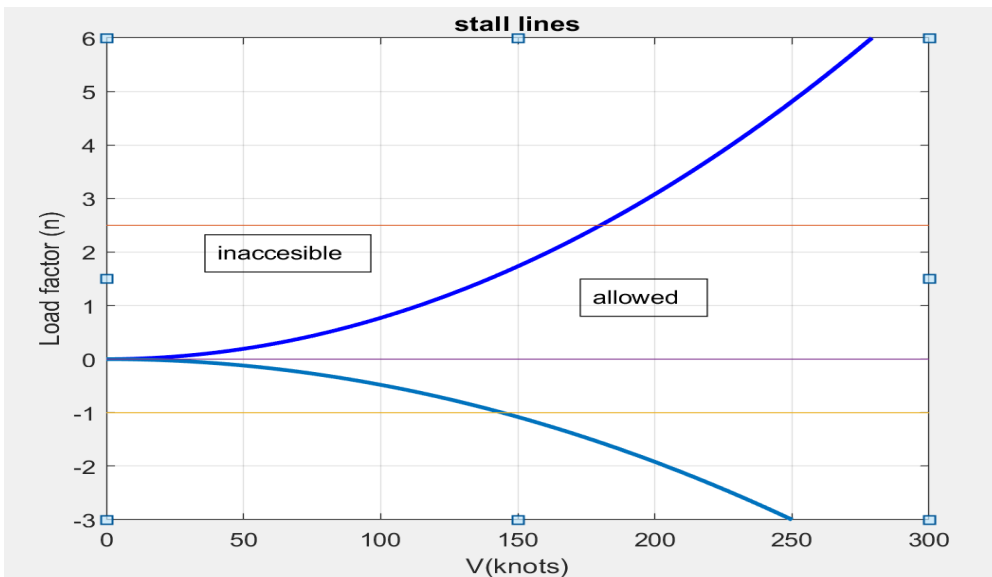


Figure 11.7: Inaccessible load factor regions.

The airspeed cannot grow indefinitely. Consequently, line DE in figure 11.5 sets the maximum airspeed limit. These allowable regions of speed and load factor close the allowable flight envelope of the hybrid electric aircraft.

11.5 Conclusion

There are a certain number of flight envelopes that flight need to follow when flying an aircraft. One of the most important flight envelopes is the V-n diagram. This diagram outlines the allowable combination of the load factor the airplane can handle and the airspeed at which the airplane must fly. In this work, the V-n diagram of the aircraft under design is constructed. The three most important regions which are the stall, the structural damage, and the allowable regions are determined based on the maximum lift, altitude and maximum lift coefficient.

Chapter 12----- Class II Method for Estimating Airplane Component Weights

12.1 Introduction

The weight of the aircraft was determined from preliminary design process. However, the estimated weight from class I was group weight. In this work, a detailed component weight estimation will be done. This accounts for details such as takeoff weight, wing and empennage design characteristics, load factor and design cruise and dive speed from V-n diagram, fuselage design and requirements, powerplant installation, landing gear design and disposition, system requirements and preliminary structural arrangements. In the preliminary design process the takeoff weight of the aircraft was estimated from four main components namely empty weight, payload weight, fuel weight, and crew weight. In this work, component empty weight which is composed of structural weight, powerplant weight, and fixed equipment weight will be estimated, and the detailed step-by-step process will be presented.

12.2 Structural Weight Estimation

From mission specifications and preliminary design process, the payload weight, crew weight, fuel weight and trapped fuel and oil weight is known. The structural weight of the airplane includes

- Wing weight (W_w)
- Empennage weight (W_{emp})
- Landing gear weight (W_g)
- Nacelles weight (W_n)

Hence, weight of the structure is given by the following equation.

$$W_{struc} = W_w + W_{emp} + W_g + W_n \quad (12.1)$$

12.2.1 Wing Weight Estimation

Wing weight for transport aircraft is given by

$$W_w = 0.0017W_{mzf} \left(\frac{b}{\cos\Lambda} \right)^{0.75} \left[1 + \left\{ \frac{6.3\cos\Lambda}{b} \right\}^{0.5} \right] n_{ult}^{0.55} \left(\frac{bs}{t_r W_{mzf} \cos\Lambda} \right)^{0.30} \quad (12.2)$$

where $W_{mzf} = W_{to} - W_f = 56,840 - 2,500 = 54,340\text{lbs}$, $\Lambda = 32^\circ$, $n_{ult} = 2.5$, $t_r = 2$, $S = 728\text{ft}^2$. Substituting these values in equation (12.2) above gives

$$W_w = 5,375\text{lbs}$$

12.2.2 Empennage Weight Estimation

Weight of the empennage is given by

$$W_{emp} = W_h + W_v \quad (12.3)$$

where W_h is weight of the horizontal stabilizer and W_v is weight of vertical stabilizer.

Since the design dive speed of the hybrid transport jet under design is greater than 250kts the equation below can be used to estimate the weight of the horizontal stabilizer.

$$W_h = K_h S_h \left[\frac{3.81(S_h)^{0.2} V_D}{1000(\cos\Lambda)^{0.5}} - 0.287 \right] \quad (12.4)$$

where $K_h = 1$ for fixed incidence stabilizer, $S_h = 87.36\text{ft}^2$, $\Lambda = 35^\circ$, $V_D = 280\text{kts}$.

Substituting these values in equation (12.4) above gives

$$W_h = 400\text{lbs}$$

In similar manner, weight of the vertical stabilizer is given by

$$W_v = K_v S_v \left[\frac{3.81(S_v)^{0.2} V_D}{1000(\cos\Lambda)^{0.5}} - 0.287 \right] \quad (12.5)$$

where $K_v = 1$, $S_v = 77\text{ft}^2$, $\Lambda = 40^\circ$.

Using these values in equation (12.5) above, the weight of the vertical stabilizer is

$$W_v = 357\text{lbs}$$

12.2.3 Fuselage Weight Estimation

The following equation applies to transport airplanes and to business jets with design dive speeds above 280kts to estimate the weight of the fuselage.

$$W_f = 0.021 K_f \left(\frac{V_D l_h}{w_f + h_f} \right)^{0.5} S_f^{1.2} \quad (12.6)$$

where

- $K_f = 1.08$ for a pressurized fuselage
- $l_h = \text{distance from wing root to horizontal tail root} = 25\text{ft}$
- $w_f = 9.8\text{ft}, h_f = 8\text{ft}$
- $S_{f_{gs}} = 1,600\text{ft}^2$ (fuselage gross shell area).

Substituting these values in equation (12.6) gives $W_v = 3,288\text{lbs}$.

12.2.4 Nacelle Weight Estimation

The weight of the nacelle is given by

$$W_n = 0.055T_{TO} \quad (12.7)$$

where $T_{TO} = 27,832\text{lbs}$ (total required takeoff thrust)

The weight of the nacelle is then $W_n = 1,530\text{lbs}$.

12.2.5 Landing Gear Weight Estimation

The weight of the landing gear is given by

$$W_g = K_{gr} \left(A_g + B_g(W_{TO})^{\frac{3}{4}} + C_g W_{TO} + D_g W_{TO}^{\frac{3}{2}} \right) \quad (12.8)$$

where $K_{gr} = 1$ for low wing airplanes. The constants A_g, B_g, C_g, D_g are taken from table 12.1 [1] for both the main and nose gears.

Table 12.1 Constants in Landing Gear Weight Equation.

```

=====
Airplane      Gear   Gear   Ag   Bg   Cg   Dg
Type          Type  Comp.
Jet Trainers  Retr.  Main   33.0   0.04   0.021  0.0
and Business  Retr.  Nose   12.0   0.06   0.0    0.0
Jets
Other civil   Fixed  Main   20.0   0.10   0.019  0.0
airplanes    Fixed  Nose   25.0   0.0    0.0024 0.0
              Fixed  Tail   9      0.0    0.0024 0.0
              Retr.  Main   40.0   0.16   0.019  1.5x10-5
              Retr.  Nose   20.0   0.10   0.0    2.0x10-6
              Retr.  Tail   5.0    0.0    0.0031 0.0

```

Using the constants from other civil airplanes (retractable) section of the table, the weight of the landing gear for the hybrid electric aircraft becomes $W_g = 2,327\text{lbs}$.

The task of estimating the structural weight is completed, and a summary of the results and comparison with Class I (summarized in table 8.3) sizing is presented in table 12.2 below.

Table 12.2: Structural Weight Comparison.

Type	Class I (lbs)	Class II (lbs)	Average
Wing	7,100	5,375	6,237
Empennage	1,363	757	1,060
Fuselage	6,418	3288	4,853
Landing Gear	2,272	2327	2,322
Nacelles	965	1530	1,248
Total			15,720

12.3 Class II Method for estimating Powerplant Weight

The airplane powerplant weight consists of the following components.

- Engines
- Air induction system
- Fuel system
- Propulsion installation

The powerplant weight is, therefore, given by

$$W_{pwr} = W_e + W_{ai} + W_{fs} + W_p \quad (12.9)$$

12.3.1 Weight of Engines

The weight of engines for the hybrid electric airplane under design is given by the following equation

$$W_e = N_e W_{eng} \quad (12.10)$$

where N_e is the number of engines and W_{eng} is weight per engine. Weight per engine is a function of the thrust the engine must provide. The thrust per engine for the hybrid electric aircraft, as determined from previous works, is $T_{TO} = 13,916lb$. Figure 12.1 [1]

below presents the weight per engine versus thrust. Reading the dry weight for the takeoff thrust given, weight per engine is 1,600lbs.

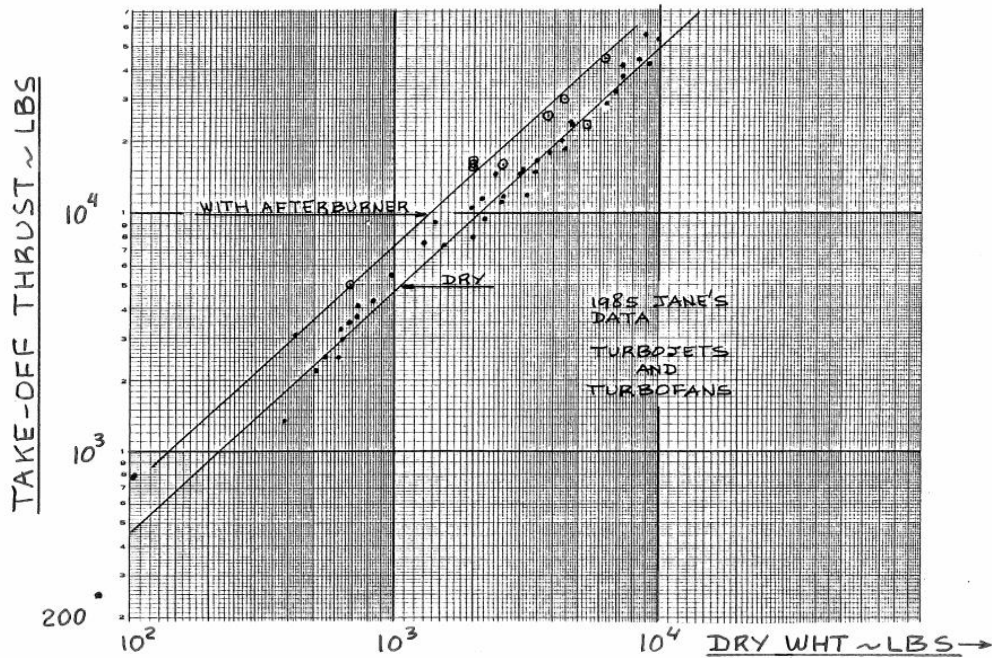


Figure 12.1: Takeoff Thrust versus Weight per Engine for Turbofan Engines [1].

Using equation (12.10) along with the value read from figure (12.1), the weight of the engines become

$$W_e = 2(1600) = 3,200\text{lbs}$$

12.3.2 Fuel System Weight Estimation

The following equation gives the weight of the fuel system for airplanes equipped with integral fuel tanks.

$$W_{fs} = 80(N_e + N_t - 1) + 15N_t^{0.5} \left(\frac{W_f}{K_{fsp}} \right)^{0.333} \quad (12.11)$$

In equation (12.11), $N_t = 2$, $W_f = 2,256\text{lbs}$, $K_{fsp} = 6.55 \text{ lb/gal (Jet propellant)}$,

Using these values in equation (12.11), the fuel system weight of the hybrid electric airplane becomes $W_{fs} = 390\text{lbs}$.

12.3.3 Estimation of Propulsion System Weight

The propulsion system weight is given by

$$W_p = W_{ec} + W_{ess} + W_{tr} + W_{osc} \quad (12.12)$$

where

- W_{ec} = Weight of Engine controls
- W_{ess} = Weight of engine starting system
- W_{tr} = Weight of thrust reverser
- W_{osc} = Weight of oil system and oil cooler.

Engine Controls:

For wing mounted jet engines, weight of engine controls is given by

$$W_{ec} = 88.46 \left\{ \frac{(l_f + b)N_e}{100} \right\}^{0.294} \quad (12.13)$$

where

- l_f = length of fuselage = 74ft
- b = wing span = 85ft

Using these values in equation (12.13) above gives $W_{ec} = 124lbs$.

Engine Starting System:

For airplanes with jet engines using electric starting system, weight of the engine starting system is given by

$$W_{ess} = 38.93 \left(\frac{W_e}{1000} \right)^{0.541} = 73lbs \quad (12.14)$$

Thrust Reversers:

Even though weight of thrust reversers is included in estimating engine weights, to make a better estimate and to improve the effect on cg due to thrust reversers, the following equation can be used to estimate the weight of thrust reversers.

$$W_{tr} = 0.1W_e = 3,200lbs \quad (12.15)$$

Oil System and Oil Cooler:

Weight of oil system and oil cooler, designated by, W_{osc} , is directly proportional to the weight of the engines as given by equation (12.16) below.

$$W = K_{osc}W_e \quad (12.16)$$

However, K_{osc} for jet engines is 0 which implies that the weight of the oil system and oil cooler is included in the weight of the engine.

This completes the task of class II powerplant weight estimation. Table 12.3 below presents comparison with class I sizing presented in table 8.3.

Table 12.3: Comparison of Powerplant Weights from Class I and Class II.

	Class I (lbs)	Class II (lbs)	Average
Powerplant	5,396	4,107	4,751

12.4 Class II Method for Estimating Fixed Equipment Weight

Fixed equipment for the proposed aircraft includes

1. Flight control system
2. Hydraulic and pneumatic system
3. Electrical system
4. Instrumentation, avionics, and electronics
5. Air conditioning, pressurizing, anti-icing and de-icing
6. Oxygen system
7. Auxiliary power unit (APU)
8. Furnishings
9. Baggage and cargo handling
10. Paint

Weight of fixed equipment is, therefore, given by

$$W_{feq} = W_{fc} + W_{hps} + W_{els} + W_{iae} + W_{api} + W_{ox} + W_{apu} + W_{fur} + W_{bc} + W_{pt} \quad (12.17)$$

where each term is the weight of the components listed above respectively. The step by step process of estimating the weight of each component is outlined below.

12.4.1 Flight Control System Weight Estimation

Weight of flight control system is given by

$$W_{fc} = K_{fc} W_{TO}^{\frac{2}{3}} \quad (12.18)$$

where $K_{fc} = 0.64$ for airplanes with powered flight control.

Substituting the takeoff weight, the weight of the flight control system is $946lbs$.

12.4.2 Hydraulic and/or Pneumatic System Weight Estimation

For commercial transports, the weight of hydraulic system is given by

$$W_{hps} = 0.008 W_{TO} = 450lbs \quad (12.19)$$

12.4.3 Electrical System Weight Estimation

For jet transport, the weight of the electrical system is given by

$$W_{els} = 10.8(V_{pax})^{0.7} (1 - 0.018V_{pax}^{0.35}) = 2000lbs \quad (12.20)$$

12.4.4 Instrumentation, Avionics, and Electronics Weight

The following equation gives the instrumentation, avionics, and electronics weight.

$$W_{iae} = 0.575(W_e)^{0.556}(R)^{0.25} = 253lbs \quad (12.21)$$

12.4.5 Weight Estimation for Air-conditioning, Pressurization, Anti&Deicing Systems

For pressurized jets, this is given by

$$W_{api} = 6.75(l_{pax})^{1.28} \quad (12.22)$$

where l_{pax} is the length of passenger cabin in feet which is $40ft$ for this aircraft.

Using this value in equation (12.22), $W_{api} = 758lbs$.

12.4.6 Oxygen System Weight Estimation

$$W_{ox} = 20 + 0.5N_{pax} = 40lbs \quad (12.23)$$

12.4.7 Auxiliary Power Unit Weight Estimation

$$W_{apu} = 0.005W_{TO} = 284lbs \quad (12.24)$$

12.4.8 Furnishings Weight Estimation

This category includes

- Seats
- Soundproofing
- Insulation
- Lavatory and associated systems
- Overhead luggage containers
- Firefighting equipment etc.

The weight of furnishings varies considerably with airplane type and with airplane mission since this category is a considerable fraction of the takeoff weight. The weight of furnishings for this aircraft is

$$W_{fur} = 0.211(W_{TO} - W_F)^{0.91} = 4,317lbs \quad (12.25)$$

12.4.9 Weight Estimation of Baggage and Cargo Handling Equipment

This is given by

$$W_{bc} = 3S_{ff} \quad (12.26)$$

In the equation above, S_{ff} is freight floor area in ft^2 .

The corresponding weight for freight area of $88 \times 125in$ is $262lbs$. Using this in equation (12.26) gives, $W_{bc} = 786lbs$.

12.4.10 Paint Weight Estimation

The weight of paint for this airplane is given by

$$W_{pt} = 0.003W_{TO} = 170lbs \quad (12.27)$$

This completes the task of estimating fixed equipment weight. Table 12.4 below presents comparison between fixed equipment weight from Class I and Class II sizing.

Table 12.4: Fixed Equipment Weight Comparison from Classes I and II.

	Class I (lbs)	Class I (lbs)	Average
Fixed Equipment	8,633	10,004	9,318

12.5 Class II Empty Weight Calculation

Empty weight of the airplane is given by

$$W_E = W_{stru} + W_{pwr} + W_{feq} \quad (12.28)$$

Since each term in equation (12.28) is determined, the empty weight of the airplane is now *29,789lbs*. Comparison of empty weight from Class I and Class II is given in table 12.5 below.

Table 12.5: Comparison of Empty Weight.

	Class I	Class II	Difference
Empty Weight (lbs)	32,147	29,789	7%

The battery handling and power generator weight is not included in the empty weight. Assuming battery handling and power generator weight to be *1,800lbs*, the difference is now 1.7% which is in the allowable range. In conclusion, class II empty weight is now *31,589lbs*.

12.6 Weight and Balance

Table 12.6 below presents weights of the airplane and coordinate of cg of each component.

Table 12.6: Coordinates of Each Weight.

	Weight (lb)	x(in)	Wx(lb-in)	y(in)	Wy(lb-in)	z(in)	Wz(lb-in)
Wing	6,237	500	3,118,500	0	0	220	1,372,140
Empennage	1,060	900	954,000	0	0	260	275,600
Fuselage	4,853	355	1,722,815	0	0	250	1,213,250
Nacelles	1248	510	636,480	0	0	150	187,200
Landing NG	415	90	37,350	0	0	120	49,800
Landing MG	1,892	560	1,059,520	0	0	95	179,740
Power plant	4,751	400	1,900,400	0	0	205	973,955
Fixed equip	9,318	570	5,311,260	0	0	270	2,515,860
Empty weight	29,774	500	14,887,000	0	0	220	6,550,280
Trapped fuel and oil	200	400	80,000	0	0	200	40,000
Fuel	2,256	510	1,150,560	0	0	200	451,200
Pilots	350	90	31,500	0	0	260	91,000
Passengers	8600	360	3,096,000	0	0	80	688,000
Attendant	300	120	36,000	0	0	260	78,000
Luggage	2,000	580	1,160,000	0	0	230	460,000
Battery	13,360	510	6,813,600	0	0	250	3,340,000
Takeoff weight	56,840	505	28,704,200	0	0	255	14,494,200

The crucial step in this analysis is finding the most forward and the most aft cg location and proving that the range stays in the acceptable region for the aircraft under design. The airplane maybe at different loading scenarios at any given time. For instance, the aircraft might have to fly with its Operating Empty Weight (OEW) only or it might have to fly with half passengers. Given that the airplane operates on fuel during takeoff and climb and then immediately switch to battery power, the airplane will have to takeoff with fuel and land with less or no fuel. This implies that the airplane goes through different loading phases in one given flight. For this reason, cg locations for different

loading scenarios should be investigated. The longitudinal cg location for different loading scenario is given by

$$x_{cg} = \frac{\sum Wx}{W} \quad (12.29)$$

Table 12.7 below shows the cg locations for different loading scenarios. This is also plotted in figure 12.2 to clearly show the most forward and the most aft cg locations and the range. In figure 12.3, the most forward cg location is 465in and the most aft cg location is 500in and these are at Empty weight + passengers and Empty weight respectively.

Table 12.7: Loading scenarios and their cg locations.

Loading Scenario	Weight	cg
Operating Empty Weight	46,240	494.2038
OEW+Passengers	54,840	473.158
OEW+Passengers+baggage	56,840	476.9174
Empty Weight	29,774	495.0737
Empty weight+passengers	38,374	464.8023
EW+passengers+battery	51,734	476.4744
EW+half passengers	34074	478.028
OEW with no fuel	54,384	478.5249
Empty Weight	29,774	500

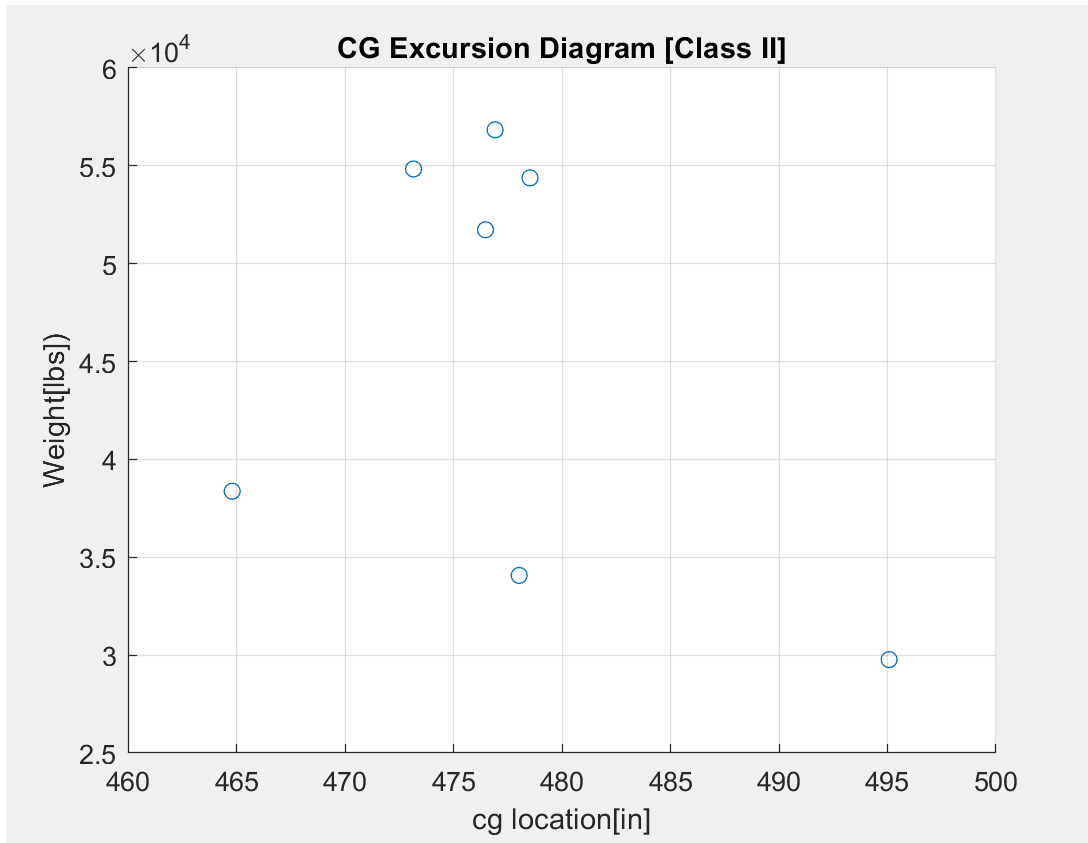


Figure 12.3: Cg excursion diagram.

12.7 Discussion

The group weight of components and preliminary weight and balance analysis was established in the previous chapters. However, weight and balance analysis is a crucial step in airplane design, and, as such, the a detailed component weight estimation, and, thus, a reliable weight and balance analysis must be established. This work goes beyond estimating group weight based similar aircraft data and estimates the weight of each component for a better and further understanding of how the aircraft behaves under various loading scenarios. This is done by estimating

- Structural weight
- Powerplant weight and
- Fixed equipment weight

These group weights include different components in them and a detailed weight estimation for each component is outlined in the previous section.

Along with the component weight estimation, a weight and balance of the aircraft is established. From the cg excursion diagram presented in figure 12.3, the range of cg variation under different loading scenarios is in range for the aircraft under design.

CHAPTER 13----Final Design Report-Environmental/Economic Tradeoffs; Safety/Economic Tradeoffs.

13.1 Introduction

The preliminary design of the hybrid electric aircraft is completed, and the details are given in previous works. In this work, the most important design parameters will be revisited and summarized. The overall design of the hybrid electric aircraft will also be evaluated in lights of economic, environmental, and safety issues.

Solutions to these issues that were proposed before and that are being considered now will be stated, and the designer will propose solutions to the issues involved with the design of a hybrid-electric aircraft such as this one. The aircraft under design will be compared with other aircraft of similar natures to show that how friendly the aircraft under design is in terms of the needs of the environment and passengers.

13.2 Summary of Most Important Design Parameters

Most of the parameters for the hybrid-electric aircraft under design are determined in the preliminary design, and the results of the calculations and the choices are stated in the previous successive preliminary design works. The most important parameters of this aircraft that are out of the previous works are summarized in table 13.1 below.

Table 13.1: Most Important Design Parameters of the Hybrid-Electric Aircraft.

<i>Parameter</i>	<i>Value</i>
<i>Fuselage length (l)</i>	74ft
<i>Fuselage diameter(D_f)</i>	9.8ft
<i>Wing area(S)</i>	728ft ²
<i>Wing span(b)</i>	85ft
<i>Wing aspect ratio(A)</i>	10
<i>Horizontal tail area(S_h)</i>	87ft ²
<i>Vertical tail area(S_v)</i>	77ft ²
<i>Takeoff weight(W_{to})</i>	56,840lb
<i>Battery weight($W_{battery}$)</i>	11,360lb
<i>Number of passengers</i>	40
<i>Payload weight(W_{pl})</i>	9,215lb
<i>Empty weight (W_E)</i>	34,000lb
<i>Crew</i>	3
<i>Wing sweep</i>	32°
<i>Mach number(M)</i>	0.93
<i>Cruise Altitude(h)</i>	24,000ft
<i>Fuel weight(W_f)</i>	2256lb

13.3 Recommendations

For the last century people in the aircraft design business have been in search of a way to transform the propulsion system of aircraft from fossil fuel driven propulsion system to hybrid-electric propulsion system. To achieve this, different types of batteries have been tried. However, the energy densities of existing batteries, in fact increasing dramatically over time, have limited the pace of the transformation. Even though it has been proved that hybrid-electric propulsion mechanisms are highly efficient compared to fossil fuel driven propulsive systems, the energy densities of the available batteries are nowhere close to the energy density of aviation gasoline. Since the battery technology has been showing progress

in achieving higher energy density, there still is hope that the transportation to hybrid-electric propulsion system is possible. Momentarily, the highest energy density of the Lithium-ion battery is 365Wh/kg. However, the design of the hybrid electric aircraft assumed battery energy density of 1400Wh/kg, which is very far away from the current energy density of the energetic battery. As a result, it is the designer's recommendation to keep an eye on the progress of battery technology to have aircraft of this type buzzing around the sky with less emission of Green House Gases and with minimal amount of noise.

13.4 Environmental/Economic Tradeoffs

The consumption of fossil fuel for transportation purposes is increasing these days than ever before (as shown in table 13.2) though the efficiency of the conversion of the energy from the fossil fuel to useful work is poor. On top of that, the combustion process releases Green House Gases, which extremely pollute the atmosphere. As a result, an efficient and environment friendly propulsive system is required to drive aircraft. The only efficient and effective substitute is using batteries. In the past decade, researchers have worked so hard to use batteries to propel airplanes with batteries. However, the amount of energy that a battery could provide, even though doubling every ten years as it is shown in table 13.3 below, has never been satisfactory. Since the use of batteries to drive airplanes is environment friendly and very efficient compared to the use of aviation gasoline, researchers are pushing the horizon of battery energy density.

Table 13.2: Fossil Fuel Usage by Country [2].

Net importer	Weight (10⁶ tons)
United States	564
Japan	199
P. R. China	175
India	128
Korea	116
Germany	106
Italy	88
France	83
Spain	61
Netherlands	57
Others	514
Total	2090

Table 13.3: Energy Densities and Efficiencies of Different Batteries [1]

Battery Type	Cost \$ per Wh	Wh/kg	Wh/kg Deliverable
Lead-acid	\$0.10 -0.17	25-41	22-37
NiMH	\$0.99	95	85
NiCad	\$1.50	39	35
Lithium-ion	\$.25 – 1.00	120 -185	115-135
Tesla		185	166
Next gen Li		365	328
Theory max (Li)		5,200	4700
Av gas	\$0.14	14,000	3800

From table 13.3, the current energy density of Lithium-ion battery has a long way to go to battle aviation gasoline. However, the data reveals that Lithium-ion battery is three times efficient compared to aviation gasoline. One problem is that there is a theoretical maximum energy density for lithium-ion battery. But if the battery technology reaches that theoretical maximum, the efficiency of the lithium-ion battery is greater than the efficiency of the aviation gasoline. With this progress, aviation gasoline will be replaced by more efficient lithium-ion battery.

Another tradeoff is the cost of batteries versus efficiency. It is an absolute fact that batteries are more efficient than aviation gasoline. But the price of batteries is very high compared to aviation gasoline, and that seems to impede the progress.

However, David Ullman states that “the price of Li batteries has been very high, but is falling rapidly.” This indicates that Li batteries will replace aviation gasoline, and hybrid-electric airplanes like the one under design will be able to fly around achieving higher efficiency and without polluting the environment.

13.5 Safety/Economic Tradeoffs

Being able to fly with electric propulsion system is very safe both for passengers and for the environment. It is safe to the passengers because the propulsion system is distributed, and the probability of failure is very low. The battery-propelled aircraft is also less noisy that it keeps the passengers comfortable. It is also clear that battery-propelled aircraft release less or no GHG to the environment, which reduces atmospheric pollution tremendously. However, with the current state of the art and with the design of the hybrid electric aircraft, cost of the battery and weight of the battery are problematic. The battery in the hybrid electric aircraft whose preliminary design is completed is only used for cruise and landing which means the rest of the mission is accomplished with aviation gasoline. Upon comparing the weights of the battery and the fuel, the battery is five times heavier than the fuel. Any increase in weight has a penalty for any air-based transport. As a result, the weight of the aircraft will increase with this propulsion system. On top of that a

small battery is more expensive than a gallon of fuel. While working on electric cars David Ullman states his observation of how batteries are expensive saying *The battery pack consisted of 100 Lithium-ion batteries. Each battery is 3.2volts so the total is 320 volts. These batteries weight 7lbs each for a total weight of 700lbs(320kg). They have energy density of 140wh/kg, so there is a total of 45kwh. This battery pack in an electric car is equivalent to about 1.2 gallons of gas at 100% efficiency or 6 gallons realistically. It is also worth noting that the batteries used in this example cost \$150 each, a total of \$15,000.*

The weight of the battery of the hybrid electric aircraft is 11,360lbs and supposes that the Lithium-ion batteries are connected to each other to provide the propulsion system for the hybrid-electric aircraft. The amount of batteries needed for this design would be 1,623. If by any chance, price has depreciated to \$100 each since the time this study was conducted, it would cost \$162,300 to make this propulsion system without considering the weight issue. Based on this analysis, the hybrid electric aircraft is impossible economically. However, hoping that batteries will depreciate, the hybrid electric aircraft will become a reality.

13.6 Conclusions

The preliminary design of the hybrid electric aircraft is completed. The aircraft is proved to be both friendly to the environment and safe to the passengers. However, the aircraft is cannot be feasible with the battery technology available at the time. If the aircraft is to be produced now, it is ineffective economically aside from the battery technology limitations. The design process is conducted assuming battery energy four times bigger than the current state of the art. Expecting that battery energy density doubles every ten years, the designer hopes that he will be in his hybrid electric aircraft in the next thirty to forty years.

References

- Anderson, J. (1989). *Introduction to Flight (3rd ed.)*. San Francisco, CA: McGraw-Hill.
- Bradley, M. K. (2015). *Subsonic Ultra Green Aircraft Research: Phase 2 - Volume 2 - Hybrid Electric Design Exploration*. Huntington Beach: NASA.
- David, U. (2009). *The Electric Powered Aircraft: Technical Challenges*. Retrieved from https://www.researchgate.net/publication/335824196_The_Electric_Powered_Aircraft_Technical_Challenges.
- Hepperle, M. (2012). *Electric Flight - Potential and Limitations*. NATO Science and Technology Organization.
- Knapp, M. (2018). Zunum Aero's Hybrid Electric Airplane Aims to Rejuvenate Regional Travel. Retrieved from IEEE Spectrum: URL: <https://spectrum.ieee.org/aerospace/aviation/zunum-aeros-hybrid-electric-airplane-aimsto-rejuvenate-regional-travel>.
- List of aircraft by date and usage category - Wikipedia. (n.d.). Retrieved from: https://en.wikipedia.org/wiki/List_of_aircraft_by_date_and_usage_category
- List of large aircraft - Wikipedia. (n.d.). Retrieved from https://en.wikipedia.org/wiki/List_of_large_aircraft
- Magnus Aircraft America. (n.d.). Retrieved from <https://www.magnusaircraftinc.com/fusion-212.html>
- Nansi, X. (2014). *Design and Optimization of Lithium-Ion Batteries for Electric-Vehicle Applications*. Retrieved from <https://deepblue.lib.umich.edu/handle/2027.42/107299>
- Nicolai, L. M. (1975). *Fundamentals of aircraft design*. San Jose, CA: METS.
- Operating Flight Strength (V-g / V-n Diagrams ... (n.d.). Retrieved from <http://www.aviationchief.com/operating-flight-strength-v-g--v-n-diagrams.html>
- Palt, K. (2017). *CASA C-295 - Specifications - Technical Data/Description*. Retrieved from Flugzeug info.net: URL: http://www.flugzeuginfo.net/acdata_php/acdata_c295_en.php

Riboldi, F. G. (2016). *An integrated approach to the preliminary weight sizing of small electric aircraft*. Aerospace Science and Technology.

Roskam, D. J. (2005). *Airplane Design: Parts I - VIII*. Lawrence, Kansas: DARcorporation.

Sadraey, M. (2009). *Aircraft performance analysis*. Saarbrücken, Germany: VDM Verlag Dr. Müller.

The More Electric Aircraft: Technology and challenges ... (n.d.). Retrieved from <https://ieeexplore.ieee.org/document/7008830/>.

Volta Volaré's futuristic GT4 e-hybrid airplane available ... (n.d.). Retrieved from <https://newatlas.com/volta-volare-gt4-hybrid-airplane/22416/>

Appendix A

In the iteration of calculating W_{TO} we have $\frac{W_{battery}}{W_{TO}} = 0.2$ and $W_F = 0.044 * W_{TO}$. Relationship between empty weight and take-off weight is given by

$$W_E = invlog\left(\frac{(\log(W_{TO}) - A)}{B}\right)$$

where $A = -0.1242$ and $B = 1.0774$. Tentative empty weight can be given as

$$W_{E_{tent}} = W_{TO} - W_{battery} - W_F - W_{PL}$$

where $W_{PL} = 9,215lb$. Estimating $W_{TO} = 56,500lb$,

$$W_E = 33,369lb$$

and

$$W_{E_{tent}} = 33,499lb$$

W_E and $W_{E_{tent}}$ are with in 2% so another iteration is needed. Estimating $W_{TO} = 57,500lb$,

$$W_E = 34,120lb$$

$$W_{E_{tent}} = 34,255lb$$

W_E and $W_{E_{tent}}$ are with in 5%. Estimating $W_{TO} = 56,800lb$

$$W_{E_{tent}} = 33,726lb$$

$$W_E = 33,734lb$$

W_E and $W_{E_{tent}}$ are within 5%. Therefore $W_{TO} = 56,800lb$ is a good estimate.

```
1 - A=-0.1242;
2 - B=1.0774;
3 - Wpl=9215;
4 - delta_min=1000000;
5 - min_at_i = 0;
6 - for i=56700:10:56900
7 -     Wetent=i-0.044*i-0.2*i-Wpl;
8 -     We=10^((log10(i)-A)/B);
9 -     delta=abs(Wetent-We)/Wetent;
10 -     if delta < delta_min
11 -         delta_min=delta;
12 -         min_at_i = i;
13 -     end
14 - end
15
16 - disp(delta_min);
17 - disp(min_at_i);
18
```

```
>> wto
    1.7463e-05

    56840
```

Appendix B

Appendix -B

Sensitivities of W_{TO} to c_j and $\frac{L}{D}$ can be calculated as

$$\frac{\partial W_{TO}}{\partial \frac{L}{D}} = -FEc_j \left(\frac{L}{D}\right)^{-1} = -145lb$$

$$\frac{\partial W_{TO}}{\partial c_j} = \frac{FE}{\frac{L}{D}} = 2,330lb.hr$$

Appendix C

Below is the code used to generate all the plots used in the body of the text.

```
%V-n Diagram
%Drawing the gustlines
V=0:400;
VB=1+0.0097*V;
VC=1+0.00726*V;
VD=1+0.0037*V;
VBn=1-0.0097*V;
VCn=1-0.00726*V;
VDn=1-0.0037*V;
Vs=0.000077*V.^2;
Vneg=-0.000048*V.^2;
figure()
plot(V,VB,'r')
hold on
plot(V,VC,'b')
hold on
plot(V,VD,'g')
hold on
plot(V,VBn,'r--')
hold on
plot(V,VCn,'b--')
hold on
plot(V,VDn,'g--')
hold off
figure()
```

```

plot(V,Vs,'b','LineWidth',2)
hold on
plot(V,Vneg,'LineWidth',2)
plot([0 300],[2.5 2.5])
hold on
plot([0 300],[-1 -1])
hold on
plot([0 300],[0 0])
hold off
ylim([-3 6])
grid on
title('stall lines')
xlabel('V(knots)')
ylabel('Load factor (n)')
%Plot the V-n diagram from the combination of the above points.
%Define the limits and equations
V1=0:145;
V2=0:180;
V3=235:280;
Vneg1=-0.000048*V1.^2;
Vs1=0.000077*V2.^2;
Vcd=(1/45)*V3-(280/45);
%Plot the V-n diagram
figure()
plot(V2,Vs1,'LineWidth',2)
hold on
plot(V1,Vneg1,'LineWidth',2)
hold on
plot([145 235],[-1 -1],'LineWidth',2)
hold on
plot([180 280],[2.5 2.5],'LineWidth',2)
hold on
plot([280 280],[0 2.5],'LineWidth',2)
hold on
plot([0 280],[0 0],'LineWidth',2)
hold on
plot(V3,Vcd,'LineWidth',2)
hold on
plot([234 234],[0 2.5],'k--','LineWidth',2)
hold off
title('V-n Diagram')
text(280, 2.6,'D')
text(234, 2.6,'C')
text(180, 2.6,'A')
text(135, -1.1,'G')
text(245, -1.1,'F')
text(280, 0,'E')
text(80,1.5,'+Cnmax \rightarrow ')
ylim([-2 3])
title('V-n Diagram')
xlabel('V(knots)')

```

```
ylabel('Load factor (n)')
grid on
figure()
plot([0 300],[2.5 2.5])
hold on
plot([0 300],[-1 -1])
hold on
plot([0 300],[0 0])
hold off
xlabel('V(knots)')
ylabel('load factor')
title('Load factor limits')

ylim([-3 5])
```